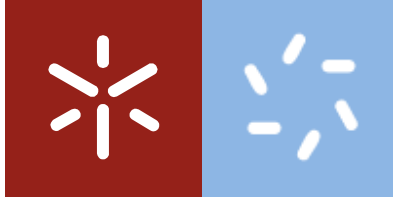




Universidade do Minho
Escola de Ciências

Patricia Daniela Cabral da Silva

**Nanobiosensors based in Graphene Field
Effect Transistors for biomarkers detection**



Universidade do Minho

Escola de Ciências

Patrícia Daniela Cabral da Silva

**Nanobiosensors based in Graphene Field
Effect Transistors for biomarkers detection**

Tese de Mestrado
Mestrado em Biofísica e Bionanossistemas

Trabalho efetuado sob a orientação do
Professor Doutor Pedro Alpuim

Anexo 3

DECLARAÇÃO

Nome: Patrícia Daniela Cabral da Silva

Endereço eletrónico: patriciadcsilva@hotmail.com Telefone: 916386643

Número do Bilhete de Identidade: 14313004 8 ZZ4

Título dissertação /tese :

Nanobiosensors based in Graphene Field Effect Transistors for biomarkers detection

Orientador(es): João Pedro dos Santos Hall de Agorreta de Alpuim

Ano de conclusão: 2016

Designação do Mestrado ou do Ramo de Conhecimento do Doutoramento: Mestrado em Biofísica e Bionanossistemas

Nos exemplares das teses de doutoramento ou de mestrado ou de outros trabalhos entregues para prestação de provas públicas nas universidades ou outros estabelecimentos de ensino, e dos quais é obrigatoriamente enviado um exemplar para depósito legal na Biblioteca Nacional e, pelo menos outro para a biblioteca da universidade respetiva, deve constar uma das seguintes declarações:

3. DE ACORDO COM A LEGISLAÇÃO EM VIGOR, NÃO É PERMITIDA A REPRODUÇÃO DE QUALQUER PARTE DESTA TESE/TRABALHO

Universidade do Minho 29/08/2016

Assinatura: Patrícia Daniela Cabral da Silva

ACKNOWLEDGMENTS

I would like to acknowledge all the team that worked with me at INL, making possible the achievement of this master thesis.

To my supervisor, Pedro Alpuim, who always accompanied the project development and was available to help me every time needed and for the help in acquiring the electrical measurements.

To Elisabete Fernandes, from the Nanomedicine group, for all the support in the development of the functionalization strategy and for the motivation.

To Fátima Cerqueira, for all the help and lessons on Raman spectroscopy.

To George Machado Jr. and Jérôme Borme for the fabrication of the EG-GFETs and graphene substrates.

To Rui Campos for the fruitful discussions on gold blocking approaches.

To Claudia Sousa for the support to acquire the SEM images.

And to all the INL members who trained me to allow the autonomous development of the project.

ABSTRACT

Ischemic stroke is one of the leading causes of death and morbidity in the world. The only FDA (U.S. Food and Drug Administration) approved therapy for ischemic stroke victims is the thrombolytic therapy, which increases the risk of hemorrhagic transformation, i. e., the transformation of an ischemic stroke into a hemorrhagic one. A large number of proteins have been identified as predictive biomarkers of this event. Therefore, biosensing applications are at development to achieve fast, sensitive and specific detection of the identified blood biomarkers.

Recently a new approach to graphene field effect transistors was proposed by Vieira et al., with polarization via electrolyte/solution, Electrolyte-Gated Graphene Field Effect Transistors (EG-GFETs). The developed architecture holds a concentric, in plane circular gate, allowing easy fabrication upscaling of the complete devices, and the transistor channel is exposed which is only possible due to the use of graphene as the channel material, since it is chemically very stable. The high sensitivity of graphene to electric charges and fields can thus be explored for biosensing applications, since changes in the electrolyte near graphene will translate into changes in the transistors electrical characteristics, in particular in the transfer curves. However, the problem for graphene is the lack of specificity, since the EG-GFETs will respond to any charged molecule present in the graphene neighbourhood, irrespectively of the chemical structure that contains it.

This way, the proposed project aimed to functionalize graphene to create a specific detection interface for biosensing applications, in particular for the detection of ischemic stroke related biomarkers. The graphene functionalization was studied for the detection of one of the biomarkers that help predict hemorrhagic transformation, MMP-9 (Matrix Metalloproteinase 9). In a first phase of the project, it was used graphene on top of Si/SiO₂ wafers. The functionalization strategy was studied, and a non-covalent functionalization of graphene was achieved by using a pyrene derivative. It was obtained a specific detection of MMP-9, with efficient blocking of the areas without antibodies. The studied strategy was then applied to EG-GFETs and the influence of the functionalization agents (buffer, biomolecules, ...) on the transistors characteristics was studied. We found that the functionalization had no significant effect on the devices electrical characteristics. MMP-9 at different concentrations was then added to functionalized devices and the transfer curves showed an evident shift of the Dirac point to lower gate voltages, related with the MMP-9 detection by graphene.

The successful functionalization of graphene with a target specific detection showed promising results from the electrical detection platform to future biosensing applications.

RESUMO

O AVC (acidente vascular cerebral) isquémico é uma das maiores causas de morte e incapacidade a longo prazo no mundo. No entanto, o tratamento dos pacientes com AVC isquémico é muito restrito, existindo apenas um tratamento clinicamente aprovado, a terapia trombolítica. No entanto, a aplicação desta terapia em pacientes com AVC isquémico aumenta o risco de transformação hemorrágica, ou seja, o AVC isquémico transforma-se num AVC hemorrágico. Nos últimos anos, um grande número de proteínas tem sido associado com o desenvolvimento da transformação hemorrágica, permitindo prever este acontecimento. Mas para que essas proteínas, biomarcadores, possam funcionar para a prevenção deste efeito é necessário desenvolver sistemas de deteção rápidos, sensíveis e específicos.

Uma nova configuração de transístores de efeito de campo de grafeno polarizados via eletrólito/solução, os EG-GFETs, foi desenvolvida recentemente. Esta nova arquitetura de transístores é completamente integrada no mesmo plano, com uma porta concêntrica e no plano do restante dispositivo, permitindo a produção em grande escala, e com o canal de grafeno exposto ao ambiente, o que só é possível devido à sua estabilidade química. Com o grafeno exposto, a sua elevada sensibilidade a cargas elétricas pode então ser explorada para aplicações em biossensores, uma vez que mudanças na composição do eletrólito junto do grafeno, serão traduzidas em alterações nas características elétricas dos transístores, nomeadamente nas curvas de transferência. No entanto, o grafeno apresenta falta de especificidade, provocando alterações no sinal dos EG-GFETs na presença de qualquer carga elétrica, independentemente da sua estrutura química.

Assim sendo, o que foi proposto neste projeto foi a funcionalização do grafeno para a criação de uma interface de deteção específica para aplicação a biossensores, em particular para a deteção de biomarcadores relacionados com o AVC isquémico/Transformação Hemorrágica. Foi então estudada a funcionalização de grafeno para a deteção de um dos biomarcadores preditores da transformação hemorrágica, MMP-9. Na primeira fase do projeto foram estudados substratos de grafeno. A estratégia de funcionalização foi estudada e conseguiu-se alcançar a funcionalização não-covalente do grafeno através do uso de um derivativo de pireno. Também se obteve a deteção específica de MMP-9, com um bloqueio eficiente das áreas sem anticorpos específicos. Esta estratégia foi então aplicada aos EG-GFETs e verificou-se que os agentes de funcionalização (buffer, biomoléculas, ...) não afetava significativamente as suas características elétricas, mas que quando expostos ao biomarcador, MMP-9, em diferentes concentrações, havia um evidente desvio do ponto de Dirac para voltagens de gate mais baixas, desvio relacionado com a interação entre a MMP-9 e o grafeno. Foi alcançada a funcionalização do grafeno, com deteção específica do biomarcador, e com resultados muito promissores relativamente aos EG-GFETs como uma futura plataforma deteção para biossensores.

Index

1. INTRODUCTION.....	1
2. MOTIVATION.....	2
Part I – STATE OF THE ART.....	2
3. GRAPHENE.....	2
3.1. Properties.....	3
3.2. Production.....	7
3.3. Applications.....	13
4. ELECTROLYTE-GATED GRAPHENE FIELD EFFECT TRANSISTORS.....	21
5. ISCHEMIC STROKE.....	23
5.1. Hemorrhagic Transformation.....	23
Part II – Project Development.....	26
6. METHODS.....	26
6.1. Materials.....	27
6.2. Methods.....	29
7. RESULTS.....	51
7.1. Experiment 1.1.....	51
7.2. Experiment 1.2.....	57
7.3. Experiment 1.3.....	59
7.4. Experiment 1.4.....	60
7.5. Experiment 1.5.....	62
7.6. Experiment 1.6.....	63
7.7. Experiment 1.7.....	64
7.8. Experiment 1.8.....	66
7.9. Experiment 1.9.....	69
7.10. Experiment 2.1.....	70
8. DISCUSSION.....	75
9. CONCLUSIONS.....	77
BIBLIOGRAPHY.....	79
APPENDIX I.....	84
Experiment 1.1 – Complementary Calculus, MNPs proportions.....	84
APPENDIX II.....	86
Experiment 2.1 – Complementary Results.....	86

ABBREVIATIONS LIST

PB – Phosphate Buffer; PBS – Phosphate Buffered Saline; DMF – N,N-Dimethylformamide; PBSE – 1-Pyrenebutanoic acid succinimidyl ester; Sulfo-LC-SPDP – Sulfosuccinimidyl 6-(3'-(2-pyridyldithio)propionamido)hexanoate; MMP-9 – Matrix Metalloproteinase; cFn – cellular Fibronectin; PDGF-CC – Platelet-Derived Growth Factor-CC; MNPs – Streptavidin coated Magnetic Nanoparticles; FET – Field Effect Transistor; EG-GFETs – Electrolyte-Gated Graphene FETs.

FIGURES INDEX

Figure 1: Graphene as the precursor of all graphitic materials.	3
Figure 2: Honeycomb lattice of graphene and triangular sub-lattices.	4
Figure 3: Electronic band structure of graphene.	4
Figure 4: Raman spectra of monolayer graphene.	5
Figure 5: Influence of temperature, flux and pressure on graphene domain size.	10
Figure 6: Graphene production by Molecular Beam Deposition.	11
Figure 7: Raman Spectra of obtained GO and rGO flakes.	12
Figure 8: Graphene as a fluorescence quencher.	15
Figure 9: Computational simulation of glucose oxidase immobilization onto the graphene surface using a bi-functional linker, PBSE (orange).	15
Figure 10: Field Effect Transistors typical configuration and transfer curve.	16
Figure 11: Devices electrical measurements, Drain-Source Current - Gate Voltage ($I_{DS}-V_G$), after each functionalization step and exposure to naltrexone.	18
Figure 12: AFM and electrical results from graphene modification with aptamers and IgE detection.	19
Figure 13: Transfer curves obtained for different concentrations of PSA-ACT and results correlation with solution pH.	20
Figure 14: Functionalization scheme with Antigen-binding fragments and detection of HSP.	21
Figure 15: Detection scheme for graphene FETs and influence on the device electrical signal.	22
Figure 16: Schematics of the experimental steps of the functionalization/detection process used in E 1.1.	35
Figure 17: Functionalization scheme for Experiment 1.2.	39
Figure 18: Stereomicroscope results.	52
Figure 19: Raman spectra obtained in different regions of the samples from Experiment 1.1.	53
Figure 20: Positive control region of the sample A59 after functionalization and detection of MMP-9.	54
Figure 21: Raman spectra obtained for each substance used in bio-functionalization of graphene.	55

Figure 22: Lorentzian fits done to the Raman spectra of the compounds with signature in the region of interest (2900 – 3000 cm ⁻¹).	56
Figure 23: Optical and Raman spectroscopy results from Experiment 1.2.	58
Figure 24: Optical and Raman spectroscopy results from Experiment 1.3.	60
Figure 25: Optical images of the samples after functionalization and detection of MMP-9 and cFn.	61
Figure 26: Optical and Raman spectroscopy results from Experiment 1.5.	63
Figure 27: Optical microscopy images of the samples A50 and A52 from Experiment 1.6.	64
Figure 28: SEM images from samples of Experiment 1.7.	65
Figure 29: SEM images from samples of Experiment 1.7.	66
Figure 30: SEM images from samples of Experiment 1.8.	67
Figure 31: Linkers used for functionalization of gold (A) and graphene (C), and the blocking agent used in Experiment 1.8, ethanolamine (B).	68
Figure 32: SEM images of the samples from Experiment 1.9.	70
Figure 33: Measuring setup and transfer curves from clean EG-GFETs.	71
Figure 34: Averaged transfer curves after each functionalization step, with the standard deviation bars, PBSE surface modification (red), antibodies anchoring (blue) and ethanolamine blocking (green).	72
Figure 35: Comparison of the transfer curves obtained after PBSE surface modification and after MMP-9 detection, for each concentration tested.	74
Figure 36: Transfer curves obtained for each EG-GFET after the cleaning process.	86
Figure 37: Transfer curves obtained for each EG-GFET after each functionalization/detection step.	87

TABLES INDEX

Table 1: Comparison of graphene production methods. The table shows the typical number of layers obtained, the highest dimension achieved and the maximum electrical mobility (in Si/SiO ₂ substrates) obtained by each method.	7
Table 2: Range of electrical mobility (μ) and minimum conductivity obtained in graphene transferred to different substrates.	7
Table 3: Control experiments performed to confirm if the sensor response derives from the specific binding of naltrexone to the μ -opioid receptor.	17
Table 4: Substrates used in the Experiment 1.1, divided by the modifications done on the graphene.	35
Table 5: Components measured with Confocal Raman Spectroscopy. The measurements were made in liquid drop, and also on dry substrates.	38

Table 6: Substrates used in the Experiment 1.3, divided by the modifications done on the graphene.	40
Table 7: Substrates used in the Experiment 1.4, classified according to the modifications done on the graphene.	41
Table 8: Substrates used in the Experiment 1.5, divided by the modifications done on the graphene.	42
Table 9: Substrates used in the Experiment 1.6, divided by the modifications done on the graphene.	43
Table 10: Substrates used in the Experiment 1.7, divided by the modifications done on the substrates.	44
Table 11: Substrates used in the Experiment 1.8, divided by the modifications done on the substrates.	45
Table 12: Substrates used in the Experiment 1.9, divided by the modifications done on the substrates.	46
Table 13: EG-GFETs used in the Experiment 2.1, divided by their origin (wafer and die).	49
Table 14: Summary of the results of percentage of coverage of the MNPs in the substrates.	65
Table 15: Summary of the results of percentage of coverage of the MNPs in the substrates.	67
Table 16: Dirac point and electrical mobility of the device, W14D18GFET2 after each functionalization step.	73
Table 17: Dirac point and electrical mobility of the averaged transfer curves shown in Figure 35.	74

1. INTRODUCTION

Biosensors have gained a special interest in medicine area for different health applications (prognosis and diagnosis of diseases, as well as for personalized treatment). A biosensing system should involve three main features: sensitivity, specificity and fastness, and the possibility of upscaling these devices make them a promising tool of work [1]. Biosensors based in graphene and graphene-like materials have made their way in the past years due to the extremely high sensitivity of this material to electric charges and fields [1, 2]. The possibility of using graphene in a FET (Field Effect Transistor) mode, where the devices can be easily produced in large-scale holds a great advantage for electronics and specifically for electronic sensing. However, to create a graphene-based device compatible with the specificity required for biosensing, requires a modification of the material, since it was already shown that graphene is influenced by any electrically charged molecule in its surroundings [3]. Taking it in account, some approaches have been explored, such as covalent modification of graphene-like materials (graphene oxide or reduced-graphene oxide) or non-covalent modification of graphene with the use of pyrene-derivatives [2]. The use of this non-covalent modification approaches has allowed to conjugate the specific detection needed with the electrical characteristics of graphene that would, otherwise, be compromised [2]. Therefore, it is proposed to make use of this non-covalent functionalization approaches to modify CVD (Chemical Vapour Deposition) grown graphene integrated in an electrolyte gated FET system. The use of an electrolyte gating instead of a solid one proposed by Vieira et al. [4] comes as a promising approach to lead this electronic system to the biosensing field, allowing a very stable environment for biomolecules, even during the electrical measures. Also, the proposed structure leaves the graphene channel exposed providing simple functionalization techniques.

Ischemic stroke is one of the leading causes of dead and long term disability [5], with severe side effects that can even be exacerbated/promoted by the clinical therapy at use (thrombolytic therapy), making of great importance the understanding of what is happening to the patient (in a biochemical perspective), that leads to such effects. The major problem related with ischemic stroke is the hemorrhagic transformation (HT), i.e., when the ischemic stroke turns into a hemorrhagic one [6], and the only FDA-approved therapy for ischemic stroke patient increases the risk of this transformation [6]. In past years a vast list of proteins has been related with this event [6-11], being considered predictive biomarkers of HT. Therefore, their early detection in ischemic stroke patients will allow a new approach for the patient treatment. What is then proposed is to apply the explored techniques for graphene functionalization for the specific detection of one of those biomarkers, MMP-9 (Matrix Metalloproteinase 9) [7], integrated in an electrolyte gated FET system, EG-GFETs, for electronic detection, i. e, development of a EG-GFET based biosensor.

2. MOTIVATION

Ischemic stroke is one of the leading causes of morbidity and mortality [5]. The only FDA approved therapy increases the risk of hemorrhagic transformation [6], leading to a worse outcome for the patient. The specific and fast detection of the biomarkers that are related with HT is required to prevent it.

EG-GFETs come as an option for biosensing due to the high sensitivity of graphene [4], and the use of a liquid environment that provides stability for the biomolecules during the measures. However, as graphene 'senses' any electric charge variation in its surroundings [3] it is important to create a specific detection mechanism on its surface. Therefore, the main goal of this project is to functionalize graphene to achieve specific detection of MMP-9, one of the biomarkers related with HT after ischemic stroke.

Before functionalizing directly EG-GFETs, graphene substrates that mimic the GFETs channel surface were tested for a complete study of the functionalization and specific recognition process. Only after the detection strategy was tested, the EG-GFETs channel was modified for electrical characterization of the functionalization and detection processes.

Considering the possibility of graphene functionalization showing lower binding capacity, an alternative proposed was the functionalization of gold, using already known and optimized approaches to apply on the EG-GFETs gold gate, which still allows the electrical characterization, but with a different approach. The binding efficiency on both surfaces was analysed in this work for that purpose.

Part I – STATE OF THE ART

3. GRAPHENE

Graphene is a 2D-material that was first isolated by Geim and Novoselov in 2004 [12]. The honeycomb sp² carbon structure of this material [13] allows extraordinary properties, from electric, to optical and mechanical, among others [14]. As a semiconductor, the charge carriers present in graphene can be of two types: electrons and holes [14]. However, contrary to regular semiconductors, the carrier concentration of any type can be changed (doping) just by the presence of an electric field (gating) [14]. This is due to the very particular structure of density of states (DOS) in graphene, in particular close to the singularities that arise at the points where the valence and conduction bands touch, the so-called Dirac points [14]. Close to each Dirac point a linear dispersion of the energy-momentum is observed, almost symmetrically into the valence and conduction bands, forming the well-known Dirac cones [13]. These features in the DOS are a consequence of the relativistic nature of the electrons in graphene, close to the Dirac points [13]. This shape

of the DOS allows the precise determination of the minimum conductivity point (also called Dirac point, for simplicity) using field-effect devices [13], like transistors. At room temperature and in graphene supported on dielectric substrates, a finite conductivity is always observed at the Dirac point due to two effects: the ambipolar transport from carriers that are thermally generated, and the carrier puddles that form at the graphene-substrate interface [14].

Graphene is the simplest of the graphitic materials [15], consisting of a single layer of carbon atoms arranged in the already mentioned honeycomb lattice [15], as shown in Figure 1. Therefore, graphene can be seen as the structural precursor of fullerenes, carbon nanotubes and graphite (which is no more than the overlap of several graphene sheets) [15].

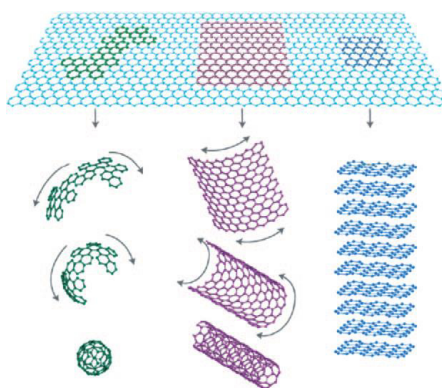


Figure 1: Graphene as the precursor of all graphitic materials. [15]

3.1. Properties

Before Geim and Novoselov first isolated graphene in 2004 [16], the existence of 2D materials was accepted as impossible due to the thermal instability of such system [17]. However, as graphene was isolated, it was shown possible the existence of such materials [17]. This was due to the small lattice and strong C-C interactions (sp^2), that prevented the destabilization of the material by thermal fluctuations [17].

Graphene has been considered as a wonder material, since it shows great promise in a large spectra of applications [18]. In dimensions, graphene is characterized by the honeycomb structure where the C-C bonds have 1.42 \AA [18] and the lattice parameter a is 2.42 \AA [18]. The lattice can be seen as the intercalation of two triangular lattices [18], as shown in Figure 2. The bonds between the carbon atoms in the lattice make use of σ orbitals leaving the π orbitals free, which are oriented perpendicularly to the atomic plan [12]. This free π orbitals allow the interaction of graphene with the surrounding environment, being responsible by the interaction between the several layers in graphite [18]. As σ - σ interactions

(covalent bonds) are more stable than π - π interactions (non-covalent interaction), this allows the separation of layers, property which led to the first procedure of graphene production [18].

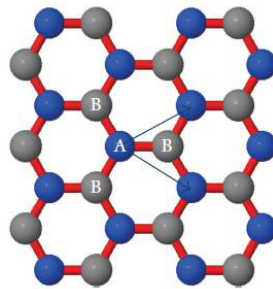


Figure 2: Honeycomb lattice of graphene and triangular sub-lattices. Each atom of a sub-lattice has three atoms of the other sub-lattice as the closest ones. [12]

3.1.1. Electronic

Unlike traditional semiconductors, graphene has a zero bandgap [12], which means that both valence and conduction band have the same energy on the Dirac point [12], as shown in Figure 3. This allows the study of graphene doping in a single sample, since the charge carriers change from electron to hole around the Dirac point, and vice-versa [12].

Graphene holds the record in electric mobility, reaching up to $10^6 \text{ cm}^2 \cdot \text{V}^{-1} \cdot \text{s}^{-1}$ [18], which is higher than the motilities reached with typical semiconductors as silicon [18]. This allows the fabrication of devices working at higher frequencies and with better performance [18].

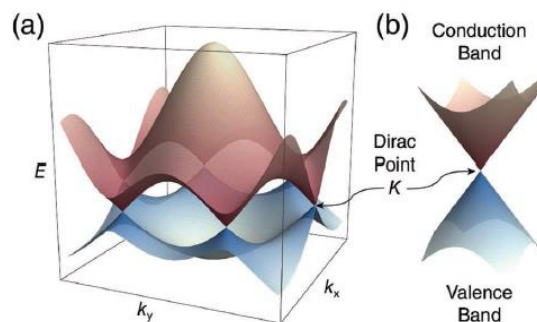


Figure 3: Electronic band structure of graphene. (a) Band structure of graphene. (b) The linear dispersion rate shows the mirrored Dirac cones, intersecting at the Fermi level, E_F (for un-doped graphene). [18]

3.1.2. Thermal

As graphene is composed by light atoms, but with strong intraplanar bonds, it is possible to achieve high sound speeds, near $20 \text{ km} \cdot \text{s}^{-1}$ [12]. This property is responsible by the high thermal conductivity of

graphene, which can go up to $5.2 \times 10^6 \text{ W.K}^{-1}$ at room temperature [12]. This characteristic increases the potential of graphene use in electrical circuits, since the high thermal conductivity eases the heat diffusion to the contacts, allowing the creation of more compact circuits [12].

3.1.3. Optical

Although graphene is only one atom thick it absorbs up to 2.3 % of the light [19], as consequence of its unique electronic structure. This means that, for every extra graphene layer, the absorbance increases by 2.3 %. However, this absorption is not enough to ‘see’ graphene at naked eye. This increment of absorbance allows the detection of 50 nm graphitic films [19], when transferred to a SiO_2 substrate since an optical path is added to the surface, creating a shift in the wavelength, which means that the wafer has a different colour [19]. For films bellow 1.5 nm thick is no longer possible to observe this shift [19], meaning that when monolayer to few-layer graphene is produced it is not detectable on the surface (only by high resolution SEM) [19].

Although graphene cannot be seen, it is possible to characterize it by the spectrum of inelastic dispersion, Raman dispersion, that comes from the interactions between phonons [12]. The typical spectrum of graphene is shown in Figure 4. The major characteristic of the spectra that defines if there is mono-layer or few-layer graphene is the ratio between the G and 2D peaks (2D peak must be more intense than G peak) [15]. The G peak, appear around 1600 cm^{-1} and is present for all graphitic materials [15]. However, the 2D peak, present around 2700 cm^{-1} , only appears for graphene materials (mono or few-layer) [15]. The other peaks are related with defects on the graphene sheet and they must have as low intensity as possible for high quality graphene [15].

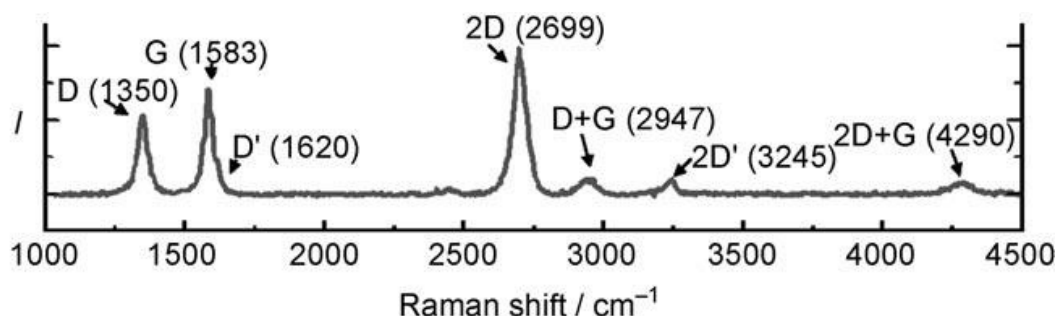


Figure 4: Raman spectra of monolayer graphene. Graphene prepared by mechanical exfoliation and analysed with a laser wavelength of $\lambda = 514.5 \text{ nm}$. [15]

3.1.4. Mechanical

Although graphene is only one atom thick, it can maintain high crystalline organization when suspended [20]. The most significant mechanical properties of this material are the high surface area, low density and high Young modulus [20]. The surface area of graphene is the largest of all known materials, achieving $2630 \text{ m}^2.\text{g}^{-1}$ [21]. This is due to the fact that graphene, as a monolayer, is completely exposed to the environment [21], creating a bigger area of interaction. This way, graphene comes as the ideal material for processes involving adsorption and surface reactions [21]. Besides, it comes as a support to anchor chemical functionalities or to create nanocomposites based in graphene [21]. This property of graphene makes it very sensitive to electric charges and fields in its vicinity at the same time it is chemically robust and bio inert [2]. The combination of surface reactions and sensitivity allows graphene to be applied to the sensing field, with applications in food safety, environment and medical diagnosis, among others [2].

Graphene is, to the moment, the strongest material ever discovered, since it holds pressures of 130 GPa [18], having a rupture resistance of 42 N.m^{-1} [18]. Besides, the honeycomb structure of graphene provides extraordinary elastic properties to the material, having a Young modulus of 1 TPa [18], a third order elastic rigidity of 2 TPa [18] and a shear modulus around 280 GPa [18]. One other interesting property is related with the free π orbitals, that contribute for the electrical conductivity as much as they contribute for the interplanar interaction. Although this van der Waals interactions are weak, when compared with the intraplanar covalent bonds, graphene is quite adhesive, having an adhesion of 0.45 J.m^{-2} [18] with SiO_2 and of 0.72 J.m^{-2} [18] with copper.

Finally, is important also to remember that graphene is a hydrophobic material [18], which means that water is repelled from the surface, having tendency to form droplets in it. This characteristic has implications in several areas such as biomedical devices/particles (possible toxicity) and anticorrosion coatings, were it can reduce the corrosion rate by 20 times [18].

3.1.5. Extrinsic

Although graphene as extraordinary properties associated, these characteristics depend on the quality of the graphene and the substrate that it has as support [12]. All of this will depend on the production method and on the material chosen as the substrate [12], as shown in Table 1 and Table 2.

Table 1: Comparison of graphene production methods. The table shows the typical number of layers obtained, the highest dimension achieved and the maximum electrical mobility (in Si/SiO₂ substrates) obtained by each method. [12]

Method	Layers	Dimensions (cm)	Electrical Mobility, μ ($\times 10^3 \text{ cm}^2 \cdot \text{V}^{-1} \cdot \text{s}^{-1}$)
Mechanical Exfoliation	1 a 10+	0,1	15
Thermal Decomposition (SiC)	1 a 4	50x10 ⁴	2
Ni-CVD	1 a 4	1	3.7
Cu-CVD	1	65	16

Table 2: Range of electrical mobility (μ) and minimum conductivity obtained in graphene transferred to different substrates. [12]

Substrate	Method	Electrical Mobility, μ ($\times 10^3 \text{ cm}^2 \cdot \text{V}^{-1} \cdot \text{s}^{-1}$)	Minimum conductivity, σ_{\min} ($\text{e}^2 \cdot \text{h}^{-1}$)
SiO ₂ /Si	Mechanical Exfoliation	10-15	4
Boron nitride	Mechanical Exfoliation	25-140	6
Suspended	Mechanical Exfoliation	120-200	1,7/ π
SiC	Thermal Decomposition	1-5	-
SiO ₂ /Si	Ni-CVD	2-5	-
SiO ₂ /Si	Cu-CVD	1-16	-

Looking at the data from Table 1 and Table 2 it is easy to see the importance of choosing the adequate method and substrate, according to the applications pretended. Comparing Mechanical Exfoliation method with Cu-CVD we can notice that the first tends to reach higher electrical mobility, for the same substrate material. However, Cu-CVD allows large area production, which is important for commercial applications. Also, suspended graphene can achieve higher mobility than when the material is deposited on a solid surface.

3.2. Production

The first time graphene was isolated, it was obtained by mechanical exfoliation, with a method known as Scotch Tape [16]. This is a top-down production method, and today several methods are based on this technique as thermal decomposition, among others. Along the years some bottom-up methods also emerged, such as Chemical Vapour Deposition (CVD) [12] and Molecular Beam Deposition [22]. In this chapter these techniques will be explored, since it is important to understand them and their final product to know what we are dealing with on devices.

3.2.1. Mechanical Exfoliation (Scotch Tape)

As said, the scotch tape method was developed by Geim and Novoselov in 2004 [16]. This is top-down process that starts with 1 mm thick HOPG (highly oriented pyrolytic graphite) [19].

Oxygen plasma is used to do dry erosion of the surface on the top graphite plates [19]. This surface is then pressed against a thick layer of photoresist (in glass substrate), which is then heated up to create adhesion between the photoresist and the graphite surface [19]. This allows the removal of this superficial layer from the remaining HOPG [19]. After that, scotch tape is used to separate the graphite flakes [19]. The flakes remaining on the photoresist are removed with acetone [19]. After observation and characterization of the graphite flakes, they are transferred to the desired substrate, as a Si/SiO₂ wafer [19]. For the transfer, the substrate is simply dipped in the solution where the flakes are floating to allow the adherence of the flakes to the substrate [19]. After, the substrate is clean using ultrasounds and isopropanol [19].

With this process it is shown that flakes that are less than 10 nm thick stay strongly attached to the substrate due to van der Waals interactions and capillarity [19].

3.2.2. Thermal Decomposition (SiC)

Thermal decomposition of SiC is a simple method, based on the heating of the SiC substrate in ultra-high vacuum (UHV) to temperatures around 1000 °C to 1500 °C [12]. This heating process causes the sublimation of silicon, leaving a carbon rich surface [12]. The study of the material with electronic microscopy reveals that the carbon layer obtained is of graphitic nature [23], which indicates the potential to apply the technique to produce graphene.

Published work from Berger [24] shows few-layer graphene production based on this method. In this work the Si side of a 6H-SiC crystal was prepared by oxidation/erosion with H₂ to increase the quality of the

surface [24]. The substrate was then heated by an electron beam in UHV up to 1000 °C to remove the oxidised layer [24]. After the removal of this layer, the substrate was heated up to 1250-1450 °C, forming thin graphitic layers [24]. The number of layers obtained was dependent on the temperature used on the second heating step, having obtained between 1 to 3 graphene layers, with electrical mobility up to 1100 cm².V⁻¹.s⁻¹ [24].

However, Emtsev refers that heating the SiC substrate in a 900 mbar atmosphere instead of UHV it was possible to reduce the surface roughness and produce bigger continuous graphene layers up to 50 µm long [25]. Applying this method, Emtsev was able to produce graphene with electrical mobility up to 2000 cm².V⁻¹.s⁻¹ [25].

As this method allows graphene production at wafer scale, it has potential to the semiconductors industry [12]. However, some problems are associated with this method, such as the control of the number of layers, the reproducibility for large area growth and the effects of the interface with the SiC substrate [12].

3.2.3. Chemical Vapour Deposition (CVD)

Unlike thermal decomposition, where the carbon is already on the surface, in the chemical vapour deposition carbon is obtained by a gaseous precursor (such as CH₄, methane) and a transition metal is used as the catalyst for the graphene growth [12].

Nickel (Ni-CVD)

Graphene growth in polycrystalline nickel foils is reported by Yu et al. [26]. In this work Ni was first tempered with a H₂ atmosphere and then exposed to an atmosphere with CH₄, Ar and H₂, at atmospheric pressure and a temperature of 1000 °C, for 20 minutes [26]. After this process, the substrates were cooled down at different cooling rates, from 20 °C.s⁻¹ to 0.1 °C.s⁻¹ [26]. It was concluded that the number of graphene layers obtained was dependent on this cooling rate, with few-layer graphene (3-4 layers) being obtained with the cooling rate of 10 °C.s⁻¹ [26].

Copper (Cu-CVD)

The method of graphene growth in copper substrates is very similar to the previous one, since the major change is the catalyst used. Li et al. [27] reports the use of 25 µm thick copper foils that were first heated up to 1000 °C under a H₂ flux of 2 sccm (standard cubic centimetres per minute) at low pressure [27]. After the foil was exposed to a CH₄ flux (carbon precursor) of 35 sccm with a 500 mTorr pressure [27]. The

analysis of the sample with Raman spectroscopy and SEM confirmed that the graphene obtained was mostly monolayer, independently of the growth time [27]. This results are indicative that the process of graphene growth on copper is auto-limitative and surface mediated [27]. The graphene obtained with this process reached electrical mobility up to $4050 \text{ cm}^2 \cdot \text{V}^{-1} \cdot \text{s}^{-1}$ [27]. Another paper from the same group studies the dependence of graphene domain size with temperature and gas flux and pressure [28], as shown in the results of Figure 5. Growing graphene at $1035 \text{ }^\circ\text{C}$, with a CH_4 flux of 7 sccm and a pressure of 16 mTorr, bigger graphene domains were obtained, with average areas of $142 \text{ } \mu\text{m}^2$ [28]. Using a two-step growth method, to fill the regions between domains, the group was able to produce graphene with electrical mobility reaching $16000 \text{ cm}^2 \cdot \text{V}^{-1} \cdot \text{s}^{-1}$ [28].

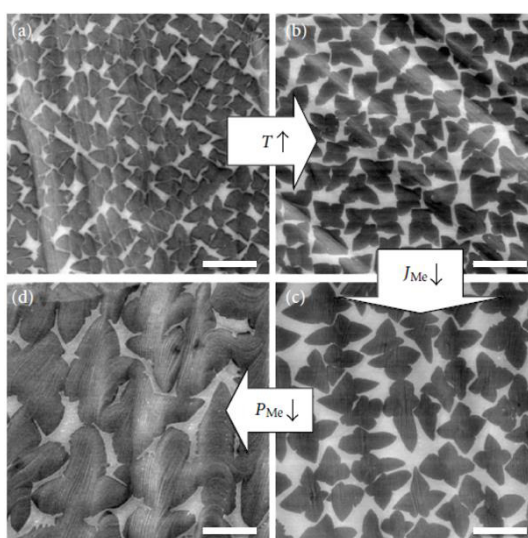


Figure 5: Influence of temperature, flux and pressure on graphene domain size. Scale bars are 10 μm .

Adapted from [28].

3.2.4. Molecular Beam Deposition

Molecular beam deposition was reported by Zhan et al. [22] to grow graphene layer-by-layer. Starting with ethylene as a gas source, the carbon precursor was break down with thermal cracker, as shown in Figure 6, and carbon was deposited on a nickel substrate [22]. For temperatures higher than $800 \text{ }^\circ\text{C}$ were obtained high quality, large area graphene layers [22]. With this method it is possible to produce one or more layer of graphene, and the number of layers as shown to be independent of the cooling rate, indicating that carbon is not absorbed by the nickel catalyst [22], as it happens in the CVD method.

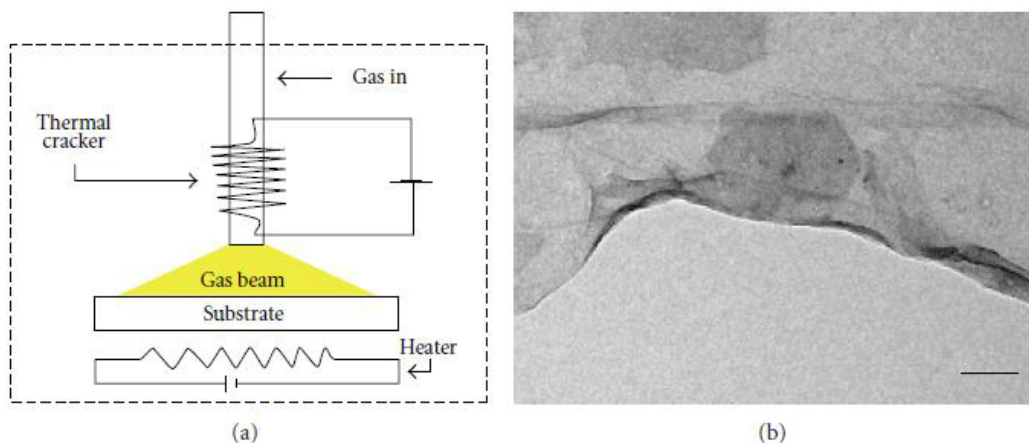


Figure 6: Graphene production by Molecular Beam Deposition. (a) Diagram of the deposition system setup. (b) TEM picture of a graphene film obtained by this process. Scale bar is 100 nm. [22]

3.2.5. Carbon Nanotubes Unzipping

Graphene nano-ribbons production is reported by Kosynkin et al. [29] by the unzipping of carbon nanotubes (CNTs).

The longitudinal opening of the CNTs was done in a suspension with sulphuric acid (H_2SO_4) and potassium permanganate ($KMnO_4$) [29]. With this process graphene oxide nano-ribbons were obtained, and were subsequently chemically reduced [29]. The nanoribbons obtained showed conductive properties, however inferior to large scale graphene, due to the oxygen defect points [29].

3.2.6. Reduced Graphene Oxide (rGO)

Although some of the methods described (mechanical exfoliation, CVD, etc.) are able to produce high quality graphene, they are very expensive [30]. Reduction of graphene oxide comes as a cheap solution, since the precursor, graphene oxide, is cheap to produce [30].

Larisika et al. [30] reports an improved method of graphene production based on graphene oxide. The process starts with natural graphite flakes, with 3-5 mm of average size [30]. The exfoliation of the graphite flakes is done by a chemical method, modified Hummer's method, that has as a final product, graphene oxide [30]. The graphite flakes are mixed with H_2SO_4 and stirred at 80 °C for 4-5h [30]. After the solution cools down, the flakes are sonicated 1h, diluted with DI water (Deionized water) and left overnight [30]. After, the solution is filtered (0.2 mm porous filter) to obtain a pre-oxidised graphite powder [30]. The product is dried and then added slowly to a concentrated solution of H_2SO_4 and $KMnO_4$ [30]. The solution is

left stirring 2h at room temperature and then DI water is added [30]. The solution is left stirring in an ice-bath for another 2h before a final dilution with DI water [30]. After this process, hydrogen peroxide (H_2O_2) is added to the solution and left overnight [30]. The upper portion (supernatant) of the solution was collected, filtered and washed with HCl, to remove any metal ions, and then with DI water to remove the acid [30]. The resulting solution was left stirring in DI water, overnight, to obtain a stock solution of Graphene Oxide (GO) [30]. The final solution was then centrifuged for 3 minutes (at 5000 g) and purified by dialysis for 1 week [30]. Finally, the product was dried [30].

Only after graphene oxide was produced, the reduction process took place. The substrate, Si, is first cleaned and treated with APTES ((3-Aminopropyl)triethoxysilane) to enhance to adsorption of graphene oxide on the surface [30]. The substrate was then dipped in a graphite oxide solution (1.3 mg/mL) for 1h, followed by rinsing with DI water and drying with N_2 gun [30]. The reduction process is done by hydrazine vapour reduction: the samples are put into glass petri dishes and 98% Hydrazine Monohydrate is added on the edges of the dishes [30]. The samples are then kept in the sealed dishes at 70 °C for 16h. With this method, were obtained flakes of rGO with an average size of 700 μm^2 and thickness of 0.8 nm [30]. However, Raman spectroscopy characterization shows low quality graphene, as seen in Figure 7.

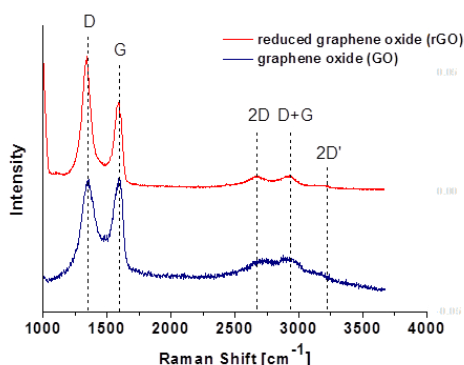


Figure 7: Raman Spectra of obtained GO and rGO flakes. [30]

This low quality of rGO when compared with typical graphene is due to the polar groups, O and OH generated during the graphite oxidation process [21]. Although this oxidation process makes the graphite hydrophilic, allowing chemical exfoliation, the reduction process cannot remove entirely this groups from the GO flakes [21]. This makes the rGO flakes rich in lattice defects and oxygen residues, which creates significant differences between this material and pristine graphene [21].

3.3.Applications

Graphene and graphene-like materials have been studied for an enormous range of applications, from electronics, to environmental and biomedical devices [18].

Flexible electronics is a field of great interest, since this kind of devices tends to be more versatile. As the optical transmittance of mono and few-layer graphene is higher than ITO (Indium tin oxide), the most used material in this area, and other emerging materials, and its resistance is comparable to the referred material, graphene shows promise in the flexible electronics [31]. Graphene has been already used in a variety of applications on flexible electronics as a transparent electrode, including touch-screen sensors [32], organic light-emitting diodes (oLEDs) [33] and organic photovoltaic devices [34].

Conductive inks have shown promise for radiofrequency identification tags, light emitting diodes (LEDs), batteries and transistors, which can be built by printing liquid-dispersed functional materials, such as organic polymers or nanoparticles [35]. Several techniques have been applied to build this devices, at low cost, however the performance of the printed devices is dependent on the quality of the materials of the ink, and how they are arranged on the target substrate [35]. Graphene, and other 2D materials, come as an option, since they are solution-processable and have very useful physical and chemical properties [35]. Graphene can meet most of the requirements needed for conductive inks, thanks to the high carrier mobility, mechanical strength, stability and potential for low cost production [35]. By now, devices produced by conductive inks are at study, combining graphene and other 2D materials (as MoS₂, WS₂ or Boron Nitride), such as photodetectors and transistors [35].

Graphene as also shown potential to improve different electrochemical energy storage devices. Properties such the high surface area, electrical conductivity and mechanical strength, and the potential for low cost production are very promising to achieve high capacity and energy density, and fast charge and discharge rates for energy storage [36]. Graphene has been studied mainly for two important devices in energy storage: electrochemical capacitors and batteries [36].

Corrosion is one of the biggest challenges faced by the steel industry [37]. Robust and long-lasting solutions are required to overcome this problem and until recently corrosion protection was based on zinc and chromium coatings [37]. However, the adverse effects of chromium in human health and environment have led to restrictions in the use of this coatings in Europe [37]. Therefore, there is a need for more effective, environmental friendly and cheaper coatings. As the electrical properties of graphene are of great interest for several applications, its impermeability to all gases and salts make this material an excellent candidate for anticorrosion coatings [37]. Graphene electrical conductivity and high surface area play a critical role in the

anticorrosion mechanism, mainly for metal substrates coatings, as it provides an alternative path for electrons, so that they do not reach the cathodic side (the metal substrate) [37]. Also the non-permeability of pristine graphene acts as an excellent barrier for water, oxygen and other corrosive agents [37].

Graphene and graphene-like materials offer a huge range of unique, versatile and tunable properties that can be applied for biomedical purposes. The 2D flat surface of graphene can be functionalized to achieve a hydrophilic surface contrary to the hydrophobic nature of graphene which may be associated with toxic effects [38]. The versatility for chemical functionalization together with a handful of properties of graphene reveal the potential of this material for biomedical applications such as highly sensitive biosensors, molecular transporters, coatings or substrates for tissue engineering, gene sequencing, among others. [39]

3.3.1 Biosensors

The biosensing field is of supreme importance to improve the quality of human life whether by point of care diagnosis of diseases, security applications or environmental safety [1]. Graphene's properties make it an attractive option for the construction of biosensing devices as a transduction platform, be it electrical, electrochemical or optical [1].

Graphene has been explored as a quencher for fluorescence-based detection schemes. Chang et al. labelled an aptamer specific for thrombin with a fluorescent dye and used graphene as a substrate for non-specific adsorption of the aptamer [40]. In this configuration, all the fluorescence was quenched due to the transfer of the fluorescence resonance energy to the substrate [41], as shown in Figure 8. The addition of thrombin resulted in the formation of a complex with low affinity with graphene, causing changes in conformation which led to a configuration where the fluorescent dye was no longer in contact with graphene, allowing fluorescence emission [47]. The scheme presented was very sensitive, achieving detection limits around 30 pM. Similar schemes have been applied for DNA detection, based on the hybridization of complementary strands, which allowed the multiple detection of three different strands [41].

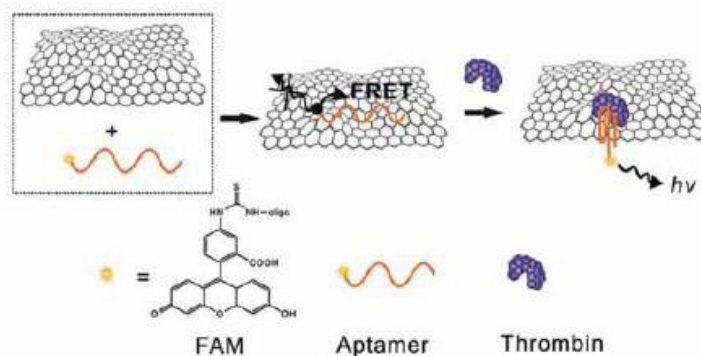


Figure 8: Graphene as a fluorescence quencher. The fluorescence of the dye-labelled aptamer is quenched when the aptamer 'binds' to graphene. When thrombin combines with the aptamers, the fluorescent signal is recovered. [40]

Electrochemical detection is a highly sensitive method of detection and it also offers selectivity since different molecules can have different oxidation/reduction potentials [1]. Viswanathan et al. reports the use of graphene for enzymatic detection of glucose [42]. CVD grown graphene was modified with a bi-functional linker, 1-Pyrenebutanoic acid succinimidyl ester (PBSE), that binds to graphene by non-covalent π - π interaction in one end and to the enzyme, glucose oxidase, by a covalent amide bond with the linker [42], as shown in Figure 9. The detection of glucose is then based on the reaction between the enzyme and glucose, which leads to the production of hydrogen peroxide (H_2O_2), an electrochemical species [42]. The concentration of this molecules relates with glucose concentration in solution, allowing the determination of the analyte amount [42].

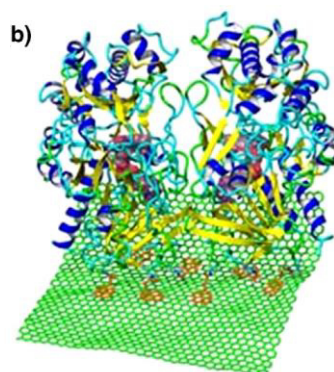


Figure 9: Computational simulation of glucose oxidase immobilization onto the graphene surface using a bi-functional linker, PBSE (orange). [42]

In terms of electrical transduction platforms, field-effect transistors (FETs) have gained great interest for biosensing devices, as they can provide electronic detection fully integrated into chips produced by the semiconductors industry [1]. Therefore, FETs attract not only the academics but also the industry. FET based biosensors rely on bio-recognition reactions happening in the gate of the device [1].

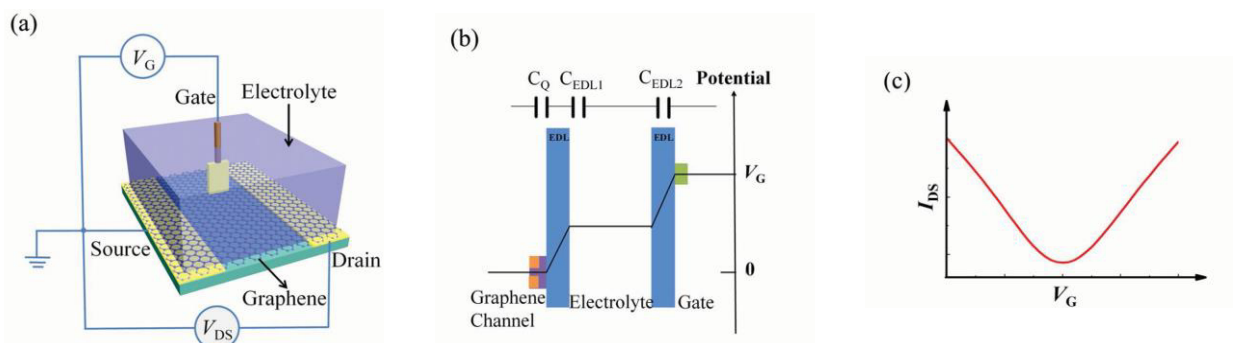


Figure 10: Field Effect Transistors typical configuration and transfer curve. (a) Typical configuration of a Solution-Gated Graphene Field Effect Transistor (SG-GFET). (b) Potential drop that occurs in a SG-GFET under a gate voltage V_g , where the blue bars represent the electrical double layers (EDLs) formed between the graphene and the electrolyte (EDL1) and between the electrolyte and the gate (EDL2). (c) Typical transfer curve of a SG-GFET at a constant drain voltage, V_{DS} . Adapted from [2].

Graphene FETs can be applied for different detection schemes. Dong et al. reports the use of Ni-CVD grown graphene for electrical detection of single nucleotide mismatch in DNA [43]. In this work graphene was decorated with gold nanoparticles that had the probe DNA attached [43]. When the complementary DNA was added, a shift to lower gate voltages was observed (at the minimum conductivity point, Dirac point), with the shift increasing with concentration up to 100 nM [43]. After that concentration the signal was stable, indicating saturation (all the DNA probes had complementary DNA bound) [43]. However, when single nucleotide mismatch DNA was added, the observed shift was smaller, meaning that the Dirac point ($V_{G, \min}$) was less sensitive to the mismatched DNA [44].

Cohen-Karni et al. reports the use of mechanically exfoliated graphene flakes in cell-based biosensors [44]. Spontaneously beating chicken cardiomyocytes were placed on the graphene and Si nanowires conjugated device [44]. The device output achieved well-defined extracellular conductance signals, with a signal-to-noise ratio of 4 [44]. They showed the dependence of the signal on the device size and demonstrated that the solution gated graphene transistors had a better performance than other planar devices, such as micro-electrode arrays, offering the unique capability of recording signals both on n- and p-type devices just by modulating the working gate voltage [44]. The work of this group and of others [45] suggests that the performance of SG-GFETs (Solution Gated Graphene Field Effect Transistors) together with the potential applications of graphene in flexible electronics can be developed to the field of bioelectronics, such as electrically functional neural prostheses [2].

Graphene field effect transistors have also been reported for the detection of naltrexone [46], a drug that reverses the effect of opioids since it is recognised by the same receptors: the μ -opioid receptors (MUR) [46]. In this work Lerner et al. modified the graphene channel with 4-carboxybenzenediazonium

tetrafluoroborate to produce carboxylic acid sites on the graphene and then immobilized EDC/s-NHS (1-ethyl-3-[3-(dimethylamino)propyl]-carbodiimide hydrochloride/sulfo-N hydroxysuccinimide) on those available sites [46]. A modified, soluble variant of MUR (with the same recognition abilities) was incubated and immobilized on the modified sites of graphene [46]. After that, the response of the devices was measured for different naltrexone known concentrations [46]. For each device only one concentration was used to avoid sample contamination along the trials [46]. The electrical characterization of devices was done for each functionalization step and for the several concentrations detected [46], as shown in Figure 11. It was shown a dependence between the Dirac point shift and the naltrexone concentration for the tested concentrations [46]. The mechanism that explains those Dirac shifts is the conformational changes that occur in the receptor when the recognition occurs [46]. The devices were also shown to be specific in the detection as the shifts obtained for other situations (without receptor, other analyte, etc.) was very different from what was obtained with the specific detection [46].

Table 3: Control experiments performed to confirm if the sensor response derives from the specific binding of naltrexone to the μ -opioid receptor. Adapted from [46].

Sample	Analyte	Average ΔV_{Dirac} (V)
<i>MUR-GFET</i>	Buffer (no naltrexone)	0.04 ± 0.38
<i>MUR-GFET</i>	Flumazenil, 10 $\mu\text{g}/\text{mL}$	-0.23 ± 0.43
<i>MUR omitted</i>	Naltrexone, 10 $\mu\text{g}/\text{mL}$	-0.25 ± 0.35
<i>Anti-HER2 scfv-GFET</i>	Naltrexone, 10 $\mu\text{g}/\text{mL}$	-0.31 ± 0.48
<i>MUR-GFET</i>	Naltrexone, 10 $\mu\text{g}/\text{mL}$	8.78 ± 0.55

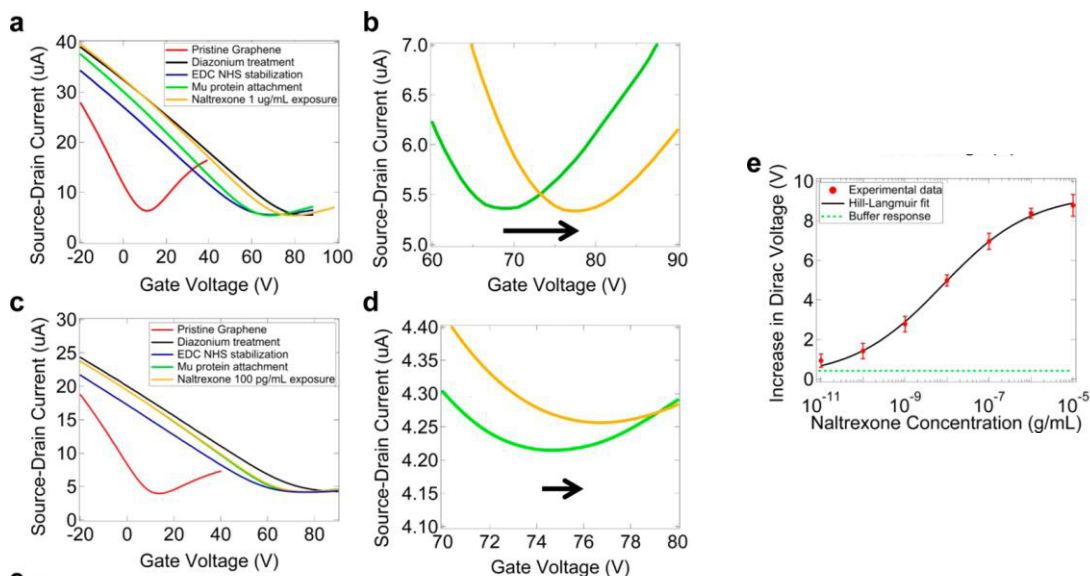


Figure 11: Devices electrical measurements, Drain-Source Current - Gate Voltage ($I_{DS}-V_G$), after each functionalization step and exposure to naltrexone. (a) $I_{SD}-V_G$ plot for each functionalization step and exposure to $1\mu\text{g/mL}$ of naltrexone (yellow plot). (b) Magnification of the shift in gate voltage between the final functionalization step (green) and the naltrexone recognition step (yellow), for $1\mu\text{g/mL}$. (c) $I_{SD}-V_G$ plot for each functionalization step and exposure to 100pg/mL of naltrexone (yellow plot). (d) Magnification of the shift in gate voltage between the final functionalization step (green) and the naltrexone recognition step (yellow), for 100pg/mL . (e) Device response (ΔV_{Dirac}) in function of naltrexone concentration. The data was fitted to a modified Hill-Langmuir model. Adapted from [46].

So far, graphene was reported in biosensing to study DNA, enzymatic and cell activity and drug detection. However, reports on immunosensing based on GFETs has been growing, with reports on the detection of several biomolecules, such as IgE (Immunoglobulin E) [47], IgG (Immunoglobulin G) [48], PSA-ACT (Prostate Specific Antigen/ α 1-Antichymotrypsin) [49] and HSP (Heat Shock Proteins) [50], among others.

In the case of IgE protein detection, Onho et al. reports the successful immobilization of IgE specific aptamers onto the graphene surface (graphene obtained by mechanical exfoliation), achieving specific detection of the protein [47]. The immobilization of the aptamers was achieved by non-covalent functionalization of the graphene surface with the bi-functional linker PBSE, with which the aptamers formed a stable amide bond [47]. As the dimensions of the aptamer were known (around 3 nm of height), AFM (Atomic Force Microscopy) was performed to confirm the successful functionalization [47], as shown in Figure 12.

To avoid unspecific reactions of IgE with PBSE, ethanolamine was used as a blocking agent to react with the remaining active groups of the linker [47], making the aptamer the only active region of the surface for reactions with IgE. After this, the specific detection was tested, using various analytes: IgE, BSA (bovine

serum albumin) and SA (streptavidin) [47]. Different concentrations of IgE were also tested [47]. The results showed that the Source-Drain current was stable when the device was exposed to non-target proteins (BSA and SA), but dropped when exposed to IgE (Figure 12) [47]. This drop in the source-drain current showed to increase with concentration, with relation fitted by a Hill-Langmuir model [47], as shown in Figure 12.

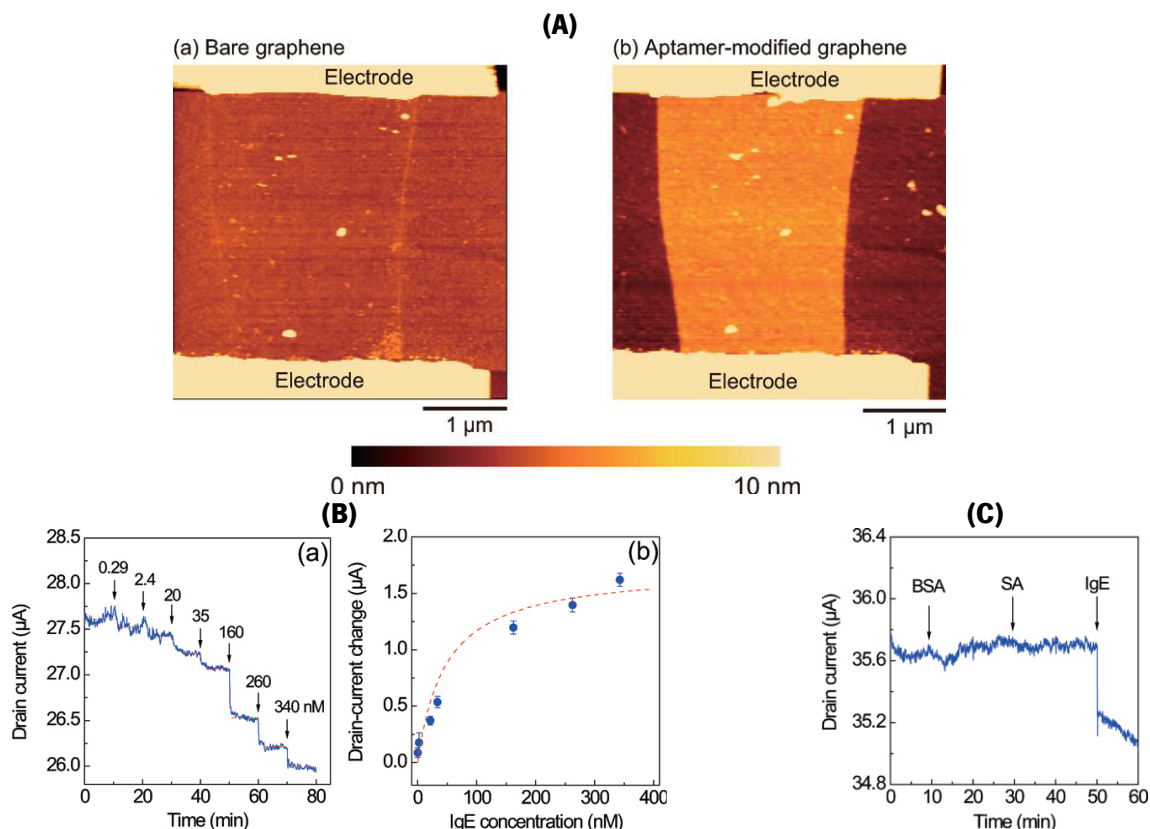


Figure 12: AFM and electrical results from graphene modification with aptamers and IgE detection.

(A) AFM pictures of the graphene channel before (A.a) and after modification with the aptamers (A.b). (B) Source-drain current variation with the increasing IgE concentration. (C) Source-drain current variation with non-target proteins (BSA and SA) and with the target protein (IgE). Adapted from [47]

The detection of IgG was reported by Mao et al. using a FET that combines TRGO (thermally reduced graphene oxide) with antibodies attached to gold nanoparticles (AuNPs) [48]. In this work, the surface modification for specific detection was simply made by adding the AuNPs with antibodies on the TRGO channel [48]. In this case the remaining surface was also blocked with an optimized blocking buffer composed of known blocking agents, as BSA and Tween 20 and fish gelatin [48]. It was verified that the IgG binding with the antibodies induced a significant change the resistance of the device, characteristic used as the sensor response. A detection limit of 0.2 ng.mL^{-1} was achieved with this method [48].

Kim et al. reports a highly sensitive rGO FET system for the detection of a prostate cancer biomarker, PSA-ACT (prostate specific antigen/ α 1-antichymotrypsin) [49]. The rGO channel was also modified with the bi-functional linker, PBSE, allowing the immobilization of the specific antibody for the recognition of PSA-ACT,

PSA mAb [49]. In this case, ethanolamine and sodium cyanoborohydride were used as blocking agents, reacting with remaining free sites of the linker [49]. The study of the devices response with different analyte concentrations was done considering the isoelectric point of the protein [49], as shown by the results in Figure 13. When using a solution with pH below the isoelectric point of PSA-ACT, the protein became positively charged causing a shift to higher gate voltages (in Drain-Source current – Gate Voltage plots), and when using the solution at a pH above the isoelectric point the effect was the opposite [49].

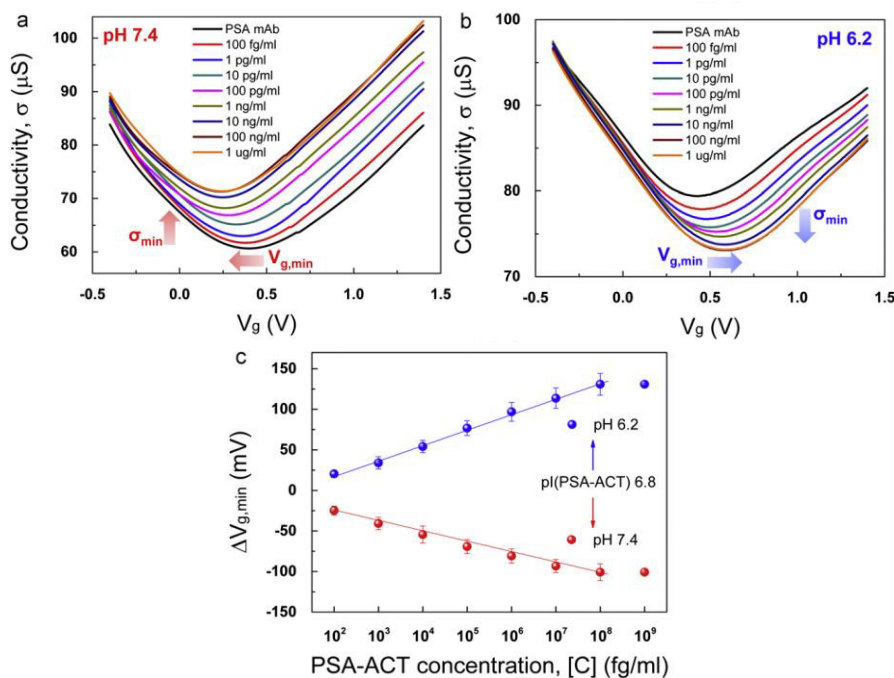


Figure 13: Transfer curves obtained for different concentrations of PSA-ACT and results correlation with solution pH. (a) Transfer curves obtained after functionalization (black) and for each PSA-ACT concentration tested, with a pH 7.4. (b) Transfer curves obtained after functionalization (black) and for each PSA-ACT concentration tested, with a pH 6.2. (c) Variation of Dirac point with PSA-ACT concentration, with the different solutions used. Adapted from [49].

Some authors refer that the use of antibodies as the recognition element can provide a poorer outcome due to the dimensions of the biomolecule, which can lead to less sensitivity, since the reaction between antibody-antigen can happen too far from the graphene surface (further than the Debye length) [47]. This way the approaches with aptamers [47] or antibodies fragments [50] also come as an option for the specific detection in graphene FETs. However, this approaches come with drawbacks. Aptamers, although very promising due to their small size, exist only in a few different types, limiting the antigens that can be detected [3], i.e., they cannot be applied for all biosensing systems.

Okamoto et al. reports a system that uses only the Antigen-Binding Fragment of the antibody (Fab), instead of the whole molecule [51]. The mechanically exfoliated graphene was functionalized by non-covalent functionalization using PBSE, like other mentioned authors [47, 49]. The antibody fragments were then

immobilized by reaction with the linker, followed by blocking of remaining linker sites with ethanolamine [50]. The fragments immobilized were specific for Heat Shock Proteins (HSP) and the device response was studied for several concentrations [50], as shown in Figure 14.

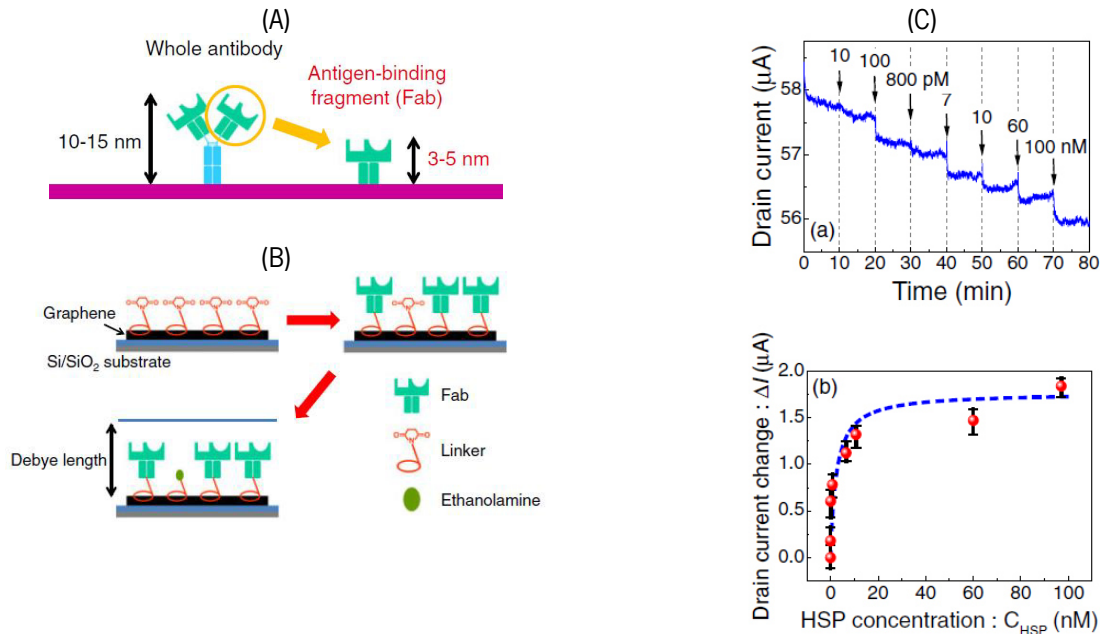


Figure 14: Functionalization scheme with Antigen-binding fragments and detection of HSP. (A) Scheme showing the difference between the use of the whole antibody and of the fragment, Fab. (B) Functionalization schematics. (C) Drain-source current variation with time and HSP concentration. Adapted from [50].

The results obtained show a sensitivity similar to the above reported systems, detection limit around 10 pM [50], giving no real indication if the use of smaller receptors such as Fab or aptamers is advantageous in comparison with the use of antibodies. However, all the systems reported show good specificity and high sensitivity which gives indication that solution/electrolyte gated graphene field effect transistors are a promising approach for the biosensing field with potential to easily reach the industry.

4. ELECTROLYTE-GATED GRAPHENE FIELD EFFECT TRANSISTORS

As reported above, graphene-based field effect transistors, with liquid gating, have been widely used for biosensing applications, as the transduction mechanism, which relies on the charge carriers on the graphene channel that are influenced by an external electrostatic perturbation [51]. Electrolyte-Gated Graphene Field Effect Transistors (EG-GFETs) work in a similar way to solid gate FETs, where the gate electrolyte modulates the Fermi energy in the channel material, creating variations in the channel current that are measured by the drain and source electrodes [51]. In the case of electrolyte gating, what gives rise to those Fermi energy variations is the charged molecules present in solution, as shown in Figure 15, where

the presence of negatively charged molecules changes the resistance measured at the channel (due to current variations) [51].

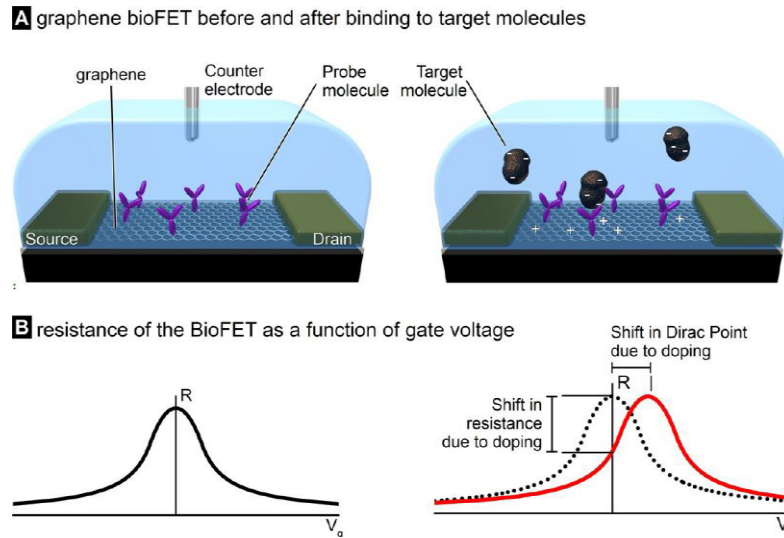


Figure 15: Detection scheme for graphene FETs and influence on the device electrical signal. (A) Schematics of a graphene BioFET before and after binding of the charged target molecule. (B) Shift in resistance observed as a consequence of the target molecule binding, that dopes the graphene. [51]

Therefore, it is important to always consider the electrolyte at use, since its electric charges will influence the doping of the graphene channel.

Several mechanisms have been suggested to explain this conduction perturbation caused by the electric charges in solution such, electrostatic gating, changes in gate coupling, carrier mobility changes and Schottky barrier effects [51]. However, Heller et al. [52] showed that only electrostatic gating and Schottky barrier effects are active in carbon nanotubes based FETs, although the extent of the effect seemed dependent of each individual device.

Conventional devices (solid dielectric) operating in the linear region, have the source-drain current (I_{SD}) sensitivity in the channel dependent on several geometric factors such as the oxide capacitance (C_{ox}), width (W) and length (L) of the channel, and carrier's mobility [52], with the dependence shown in Equation 1.

$$I_{SD} = \mu \cdot C_{ox} \cdot \frac{W}{L} \cdot \left[(V_{GS} - V_{th}) \cdot V_{DS} - \frac{V_{DS}^2}{2} \right] \quad (1)$$

Assuming the same dependence for electrolyte gated GFETs, the advantages of the use of graphene as the channel material are obvious, due to its high carrier mobility, stability in aqueous solutions (no oxides, so C_{ox} can be high) and 2D structure that can be shaped into any lateral dimensions [51]. With conventional semiconductors a robust and thin oxide layer is needed to protect the channel, which reduces the gating effect of charged molecules and the channel area [51].

In comparison with the solid dielectric devices, EG-GFETs work at much lower gate voltages, since almost all the voltage applied to the gate electrode drops in the electrical double layers (EDLs) formed at the gate/solution and solution/graphene interfaces, that are nanometer sized [4]. As a consequence, the electrostatic capacitance per unit of area is much higher than in conventional back gated structures, where the gate contact and the graphene are separated by hundreds of nanometers with the solid dielectric [4].

5. ISCHEMIC STROKE

Stroke is one of the leading causes of dead and long term disability [5] with more than 80 % of all strokes being ischemic ones [5]. An ischemic stroke occurs when there is an occlusion of a blood vessel due to a thrombus or an embolus [5]. This occlusion stops/reduces the blood flow creating a hypoxic region, causing the death of the brain cells supplied by the occluded vessel [53].

5.1. Hemorrhagic Transformation

The hemorrhagic transformation (HT) is a bleeding that occurs in the ischemic brain area after a stroke (ischemic stroke) [6]. It occurs in 10 % to 40 % of the patients with ischemic stroke, being associated with worse outcomes, since this event is related with increased stroke morbidity and mortality [6].

HT is usually divided into symptomatic and asymptomatic groups, based on the deterioration of the patient neurological status within the first 36h after stroke [6]. This clinical classification is very useful for larger hemorrhages, since those tend to be symptomatic and more likely to affect negatively the patient outcome [6], and so very important to prevent. However, the asymptomatic hemorrhages can worsen the outcome, particularly when cognition and neurologic functions are affected weeks or months after stroke [6]. This might be derived from the exacerbation of cerebral edema and other toxic effects of the blood from the HT [6]. Therefore, it is also important to reduce/prevent the smaller HTs to provide better outcomes for the patients, over time.

The HT happens when the cerebral blood flow is restored in the damaged vasculature [6]. This event itself is the key factor for the HT however, the administration of thrombolytic therapy, the only FDA-approved therapy for ischemic stroke, increases the risk of HT [6]. In the thrombolytic therapy, tissue Plasminogen Activator (tPA) is administrated to degrade fibrin-based blood clots [6]. However, tPA increases reperfusion and activates Matrix Metalloproteinases and signalling pathways that lead to HT [6]. Other thrombolytic agents, such as streptokinase and tenecteplase also promote HT [6]. Due to this effect of the therapy for ischemic

stroke, there is a need for a fast recognition of the factors that help promoting HT, to allow the prevention and early treatment of this effect.

Several factors are associated with HT [6] and can be used to detect or prevent it from happening. Within this factors we have clinical features, like age, stroke severity, body weight along others, blood biomarkers such as MMP-9 and PDGF-C and genetic factors, with several genes related with increased HT risk [6].

5.1.1. HT Biomarkers

As said, several blood biomarkers are related with HT and can help to predict the event, which allows to adjust the treatment of the patient with ischemic stroke, to diminish the gravity of HT or even prevent it from happening.

One of those biomarkers is Matrix Metalloproteinase 9, MMP-9, gelatinase B, 92 kDa type IV collagenase [7], which is an enzyme that targets other proteinases, proteinase inhibitors, clotting factor, growth factor-binding proteins, cell-cell adhesion molecules, almost all extra-cellular matrix proteins [7], among other targets. This makes MMP-9 a very versatile enzyme, with roles in many biological processes [7]. It is involved in embryonic development, reproduction, bone development, wound healing, cell migration and in brain learning and memory functions [7]. However, enhanced expression of this protein has also been associated with several pathological conditions, including neuropsychiatric disorders (Epilepsy, Autism, Bipolar disorders and Schizophrenia) [7] and central nervous system disorders (such as Alzheimer's, multiple sclerosis, brain tumors and ischemic stroke) [7]. Several studies confirm the critical role of MMP-9 during human stroke and reperfusion injury (injuries caused by the restoring of blood flow after an ischemic period) [7]. Those results are also correlated with several animal models which show an evident increase of MMP-9 expression in ischemic stroke [7]. MMP-9 is released in response to ischemic injury in neurons and neuroglial cell [7]. Also, the release of free radicals, tPA and other molecules have the capacity to activate MMP-9 [7]. The increased levels of this biomarkers are associated with several complications including excitotoxicity, neuronal damage, apoptosis, oxidative stress, and most importantly Blood Brain Barrier (BBB) disruption that lead to cerebral edema and hemorrhagic transformation after cerebral ischemia [7]. It has been proposed that the negative effects of tPA based therapy for ischemic stroke are derived from the tPA ability to activate MMP-9 [7]. Recent studies confirm the presence of high MMP-9 levels on infarct tissue and also in the peri-infract areas, indicating that MMP-9 is related with infract size growth [7]. Therefore, MMP-9 has been suggested as a marker for brain ischemia and as a predictor of HT in patients treated with tPA [7].

Angiopoietin, a cell-specific growth factor protein [54], is expressed by a variety of cells, such as endothelial cells, pericytes and neuronal cells [54]. Angiopoietin is reported to reduce the post-ischemic hyper permeability that is triggered after ischemic stroke and leads to blood brain barrier disruption [54]. However, the levels of this protein decrease after ischemic stroke, effect that increases with tPA administration, increasing the risk of BBB disruption and HT [54].

Cellular Fibronectin (cFn), an adhesive dimeric glycoprotein that promotes cell to cell and cell to matrix interactions [8], is another biomarker associated with HT [55]. As this protein is confined to the vascular endothelial cells, high plasma levels of cFn may indicate endothelial tissue damage [8]. In fact, it was already shown that hemorrhagic transformation after tPA administration is related with high cFn levels, in which levels above $3.6 \mu\text{g}\cdot\text{mL}^{-1}$ predict HT [8].

Tissue Plasminogen Activator, tPA, activates not only MMP-9, but also other proteins such as Platelet-Derived Growth Factor-CC (PDGF-CC) [9]. The activation of this protein leads to increased cerebrovascular permeability, compromising the integrity of the blood brain barrier [9]. It was shown that the blockage of the PDGF-CC receptor, PDGF- α , attenuates tPA associated complications in mice models of ischemic stroke [9]. Serum levels of PDGF-CC are associated with HT and severe brain edema, reaching its peak around 24h after ischemic stroke [9]. As PDGF-CC signalling cascade regulates the permeability of the BBB, its activation by tPA upregulates the PDGF-CC expression, leading to a prolonged activation of its receptor, PDGF- α , which leads to the deterioration of the BBB, leading to hemorrhagic transformation [9].

Neuroserpin is a serine protease inhibitor [10], produced at the neurons. In vitro studies show that neuroserpin acts as a tPA inhibitor, with potential to reduce the harmful effects of the thrombolytic therapy [10]. However, in contrast with some of the reported biomarkers, neuroserpin serum levels decrease in the first 24h after stroke [10], leaving space for the inflammatory and BBB disruption pathways, which are activated by tPA and lead to HT, to take place.

Another protein related with hemorrhagic transformation is S100 Calcium Binding Protein B, or S100B [11]. In normal conditions, the level of S100B is 40 times higher in the cerebrospinal fluid than it is in serum. However, the increased permeability that occurs due to tPA administration, creates a leakage of this protein to the serum [11]. This way, increased levels of S100B in serum are indicative of BBB damage after thrombolytic therapy in ischemic stroke, which is associated with HT [11].

The variety of identified biomarkers related with hemorrhagic transformation, with different behaviours and consequences, show the complexity of the signalling pathways occurring in the ischemic brain. Therefore,

the detection of only one of this biomarkers is not enough to predict HT, being necessary the multiple detection of biomarkers.

Part II – Project Development

6. METHODS

To achieve a biosensing system based on EG-GFETS, first it is needed to study the functionalization of the transducing active area of the biosensor: the graphene FET channel. Therefore, the functionalization of graphene was performed, firstly in graphene substrates (graphene transferred to SiO₂ substrates) and then in the devices (EG-GFETs).

To achieve the functionalization of graphene, experimental protocols were prepared based on published material concerning graphene and carbon nanotubes modification with pyrenes [42, 47, 49, 50], and on unpublished material concerning the modification of gold surfaces with specific antibodies.

All the experiments were performed at the facilities of International Iberian Nanotechnology Laboratory (INL). As graphene is chemically stable [15] and covalent modification of the material alters its electrical properties [2], a non-covalent method was used to modify graphene. Therefore, a pyrene-derivative, 1-Pyrenebutanoic acid succinimidyl ester (PBSE) was used to create an interface between graphene and the biosensing element. The pyrene group of PBSE establishes a very stable non-covalent interaction due to the similarity in the structure of this group with graphene (π - π interaction), and remains with a free ester group that will allow the reaction with the amine group of the sensing element, i.e., antibodies. This way, the antibodies will have a very stable bond with the linker, without affecting significantly the electronic properties of graphene, as will be shown below.

Knowing that after the immobilization of antibodies some free ester groups can remain active on the surface, it was necessary to study a blocking approach to prevent un-specific reactions of the biomarker with the linker. Two strategies were studied: BSA blocking, which is a very common protein used in blocking approaches [49], and Ethanolamine [47, 49, 50], which is a small molecule with an amine group in one extremity (to react with PBSE) and a hydroxyl group that blocks the reaction of the linker with proteins.

To study those processes in the graphene substrates, it was necessary to apply a tagging approach to allow the visualisation under the optical microscope of the reaction sites, resulting in specific recognition of the biomarker and evaluating the blocking approach. To perform the tagging, magnetic nanoparticles (MNPs) were used, since they allow the direct visualisation of the results and were immediately available for use (as they were in use by other groups). The use of this MNPs implied other experimental steps, as they needed modification to recognize the biomarker, MMP-9, in solution, before application to the substrates. The MNPs

were modified with biotin antibodies (specific for the protein to tag) that reacted with the MNPs surface by a biotin-streptavidin reaction, and were blocked with BSA.

In the second phase of the project, where electrical measurements were performed, the tagging was no longer needed since the modifications on the surface were studied by changes in the devices electrical characteristics. Unlike the first part, where the MMP-9 concentration was always the same and much higher than what was needed to saturate the antibodies (this way the distribution of the antibodies could be correctly analysed), in this second part several different concentrations, and much lower, were tested. The concentrations tested were 100 ng.mL^{-1} , 10 ng.mL^{-1} , 1 ng.mL^{-1} and 0.1 ng.mL^{-1} . These concentrations belong to the range of values reported for MMP-9 levels and level variation within the pathology at study.

6.1. Materials

For the execution of the experimental work, different equipment was used, software, lab materials and solutions, as listed below.

6.1.1. Equipment

Direct Write Laser Lithography System – Heidelberg, DWL2000

Broad Beam Ion Milling System – Nordiko, 7500

Dicing – DISCO DAD, 3350

CVD – FirstNano, EasyTube® 3000

HDMS Priming/Vapor Prime – Yield Engineering Systems, Inc.

Microspotter – Scenion, SciFlexArrayer S3

Magnetic Concentrator, Dynamag2 – Dynal-biotech

Keithley 2400 source-meter

Keithley 4687 picoammeter/Voltage source

Confocal Raman system, Witec Alpha 300R

Laser (for Raman) – Nd-Yag 532nm laser

Wide-Field Upright Fluorescence Microscope – Nikon, Ni-E

Stereomicroscope – Nikon SMZ 1500

Scanning Electron Microscope – FEI, Quanta 650 FEG

6.1.2. Software

WITec Project Plus

WITec Project FOUR+

Microsoft Office Excel 2016

Origin 9.0

Image J

6.1.3. Materials

Graphene substrates, 7x7 mm² (Si (100) wafers, B-doped, 8 – 30 Ω cm – LG Siltron; Copper 99.999 % – Alfa Aesar)

Gold substrates, 7x7 mm² (Si (100) wafers, B-doped, 8 – 30 Ω cm – LG Siltron; Chromium adhesive layer; Gold)

6.1.4. Reagents/Solutions

Acetone – Sigma Aldrich, product number 32201

Isopropanol (IPA) – Sigma Aldrich, product number 33539-R

Ethyl Acetate, anhydrous 99.8 % – Sigma Aldrich, product number 270989

N,N-Dimethylformamide, anhydrous 99.8 % (DMF) – Fisher Scientific, product number D/3841/17

Iron Chloride (FeCl₃) – Sigma-Aldrich, product number 157740

AZ 400K Developer 1:4 – AZ, product number 10063823163

1-Pyrenebutanoic acid succinimidyl ester (PBSE) – Sigma Aldrich, product number 1001553659

Phosphate Buffered Saline Tablets – Sigma Aldrich, product number P4417

Phosphate buffer (PB) – 100 mM NaH₂PO₄, 100 mM Na₂HPO₄, pH 7.2

Sulfosuccinimidyl 6-(3'-(2-pyridyl)dithio)propionamido)hexanoate (Sulfo-LC-SPDP) – Thermo Scientific, product number 21650

Bovine Serum Albumin (BSA) – Sigma-Aldrich, product number A9418

Ethanolamine, 98 % – Sigma-Aldrich, product number E9508

Tween 20 – Sigma-Aldrich, product number P9416

Glycerol – Sigma-Aldrich, product number G5516

Streptavidin coated Magnetic Nanoparticles, 250 nm, 4.9x10¹¹ particles.mL⁻¹ – Nanomag-D, Micromod, product number 09-19-252

Mercaptohexanol (MCH) – Sigma-Aldrich, product number 451088

Biotin Anti-Human Matrix Metalloproteinase 9, 0.5 mg.mL⁻¹, Immunostep

Biotin Purified Anti-Human Fibronectin, 7.9 mg.mL⁻¹, Immunostep
Purified Anti-Human Matrix Metalloproteinase 9, 0.92 mg.mL⁻¹, Immunostep
Purified Anti-Human Fibronectin, 4.8 mg.mL⁻¹, Immunostep
Purified Anti-Human Platelet-Derived Growth Factor C, 5 mg.mL⁻¹, Immunostep
Cellular Fibronectin (cFn), 1 mg.mL⁻¹, Immunostep
Matrix Metalloproteinase 9 (MMP-9), 1 mg.mL⁻¹, Immunostep

6.2. Methods

6.2.1. Solutions Preparation

6.2.1.1. PBS 10 mM

To prepare PBS buffer using tablets, the information given by the supplier is that 1 tablet in 200 mL of ultrapure water produces a buffer with 10 mM concentration. As it was desirable to prepare a bigger volume to store, 400 mL of PBS 10 mM were prepared.

- 2 PBS tablets (Sigma-Aldrich) were added to 400 mL of ultrapure water (MiliQ) in a graduated cylinder.
- A pH meter, the solution pH was calibrated according to the protocol for pH meter calibration, then the pH of the solution was measured, and a pH of 7.4 was confirmed;
- The solution was autoclaved during 2h on liquid cycle, and was stored at 4°C.

6.2.1.2. PBS 100mM

- 1 PBS tablet was diluted in 20 mL of ultrapure water to achieve PBS at 100 mM.
- The solution was mixed until the tablet was completely dissolved.
- The solution was stored at 4 °C.

6.2.1.3. PB 10 mM

PB buffer was also used in the experiments. It was used at the same concentration of the PBS buffer (6.2.1.1), 10 mM. It was obtained from a stock solution prepared previously to the lab work beginning.

- PB 10 mM was prepared by dilution of the stock solution of PB 100 mM (already existent) according to need.
- 5mL of PB 100 mM were diluted in 45 mL of ultrapure water, for a final volume of 50 mL and a final concentration of 10 mM.
- The pH of 7.2 (equal to the 100mM stock solution used) was confirmed using a pH meter.
- The solution was stored at 4 °C.

6.2.1.4. PBS-Tween 20 and PB-Tween 20

PBS-Tween 20 and PB-Tween 20 were used in the preparation of the MNPs and Proteins. Tween 20 was always used at 0.05%.

Independently from the base buffer, the solution was prepared using the same amounts:

- a. 5 μL of Tween 20 were added to PBS or PB for a final volume of 10 mL.
- b. The solution was stored at 4 $^{\circ}\text{C}$.

6.2.1.5. PBSE 10 mM

To prepare PBSE, its molecular weight was taken into account. As PBSE is not stable in aqueous solution [53], it has to be prepared in other solvents such as methanol or dimethylformamide (DMF) [53].

PBSE is often used as a fluorescent probe [53], meaning it is not stable when exposed to light. Therefore, the PBSE solution was prepared and stored in a dark glass bottle.

To prepare PBSE at the correct concentration (10mM) in DMF, some complementary calculus were made, taking into account the molecular weight and density of PBSE (data provided by the supplier, [54]).

- a. 38.5 mg of PBSE (powder) were weighted and transferred to a dark glass bottle.
- b. 10 mL of DMF were added to the bottle and the solution was mixed until PBSE was completely dissolved.
- c. The PBSE solution and powder were stored at room temperature.

6.2.1.6. Anti-MMP-9

Anti-MMP-9 was used as the specific antibody for the detection of MMP-9 (positive control). Depending on the reported experiment, Anti-MMP-9 was prepared in PBS 10 mM, PBS 100 mM, PB 100 mM or PB 10 mM. All Anti-MMP-9 solutions were prepared for a final concentration of 250 $\mu\text{g}\cdot\text{mL}^{-1}$ accordingly to the optimized concentration for an immobilization on gold surface [unpublished work].

- a. Anti-MMP-9 stock solution was added to PBS 10 mM, PBS 100 mM, PB 100 mM or PB 10 mM, according to the experiment, for a final concentration of 250 $\mu\text{g}\cdot\text{mL}^{-1}$.
- b. Until use the solution was maintained refrigerated.

6.2.1.7. Biotin Anti-MMP-9

Regarding the use of Magnetic Nanoparticles (MNPs), Biotinylated Anti-MMP-9 was used to modify the surface of the MNPs. MNPs were functionalized with biotinylated antibodies at 50 $\mu\text{g}\cdot\text{mL}^{-1}$ according to an established protocol that uses Magnetoresistive platforms on the detection of medical biomarkers at INL.

- a. Anti-MMP-9 biotinylated stock solution was added to PBS 10 mM for a final concentration of 50 $\mu\text{g}\cdot\text{mL}^{-1}$.

Anti-MMP-9 biotinylated was also prepared in PB 10mM buffer for other experiments, at the same final concentration.

6.2.1.8. Anti-PDGF-CC

Anti-PDGF-CC was used as a negative control in the first experiments to control the existence of reactions of MMP-9 with non-specific antibodies, negative control. All Anti-PDGF-CC solutions were prepared for a final concentration of $250 \mu\text{g.mL}^{-1}$ accordingly to the optimized concentration for a gold surface [unpublished work].

- Anti-PDGF-CC stock solution were added to PBS 10 mM, for a final concentration of $250 \mu\text{g.mL}^{-1}$.
- Until use the solution was maintained refrigerated.

6.2.1.9. Anti-cFn

Anti-cFn was used as a positive control for specific detection of cFn. All Anti-cFn solutions were prepared in PBS 10 mM or PB 10 mM, according to the experiment, for a final concentration of $250 \mu\text{g.mL}^{-1}$ accordingly to the optimized concentration for a gold surface [unpublished work].

- Anti-cFn stock solution was added to PBS 10 mM or PB 10 mM, for a final concentration of $250 \mu\text{g.mL}^{-1}$.
- Until use, the solution was maintained refrigerated.

6.2.1.10. Biotin Anti-cFn

Magnetic Nanoparticles (MNPs) were functionalized with biotinylated antibodies. The Anti-cFn biotinylated solution was prepared for a final concentration of $50 \mu\text{g.mL}^{-1}$ according to the protocol in use for magneto resistive detection platforms at use in INL. The solution was freshly prepared in the day of the experiment.

- $1.2 \mu\text{L}$ of Anti-cFn biotinylated stock solution was added to PB 10 mM for a final volume of $120 \mu\text{L}$.
- Until use, the solution was maintained refrigerated.

6.2.1.11. MMP-9 (protein)

MMP-9, the biomarker under study was prepared in different buffers (Tween 20 buffers) used at different concentrations according to the requirements of the experiment.

As MMP-9 stock solution comes at a concentration of 1 mg.mL^{-1} , the calculations were made to know the volume needed to prepare each solution:

$C_{\text{stock}} = 1 \text{ mg.mL}^{-1}$; $C_1 = 20 \mu\text{g.mL}^{-1}$; $C_2 = 2 \mu\text{g.mL}^{-1}$; $C_3 = 1 \mu\text{g.mL}^{-1}$; $C_4 = 100 \text{ ng.mL}^{-1}$; $C_5 = 10 \text{ ng.mL}^{-1}$; $C_6 = 1 \text{ ng.mL}^{-1}$; $C_7 = 0.1 \text{ ng.mL}^{-1}$

$C_x \times V_x = C_y \times V_y$, knowing how much volume was needed for each concentration (it varied between concentrations, since some solutions were used to prepare others), it was possible to calculate how much volume was needed to prepare the desired solution.

$$C_1: C_{\text{stock}} \times V_{\text{stock}} = C_1 \times V_1 \Leftrightarrow V_{\text{stock}} = (20 \times 0.1)/1000 \Leftrightarrow V_{\text{stock}} = \mathbf{0.002 \text{ mL} = 2 \mu\text{L}}$$

$$C_2: C_{\text{stock}} \times V_{\text{stock}} = C_2 \times V_2 \Leftrightarrow V_{\text{stock}} = (2 \times 0.5)/1000 \Leftrightarrow V_{\text{stock}} = 0.001 \text{ mL} = 1 \mu\text{L}$$

$$C_3: C_2 \times V_2 = C_3 \times V_3 \Leftrightarrow V_3 = (1 \times 0.5)/2 \Leftrightarrow V_3 = 0.25 \text{ mL} = 250 \mu\text{L}$$

$$C_4: C_2 \times V_2 = C_4 \times V_4 \Leftrightarrow V_4 = (100 \times 0.5)/2000 \Leftrightarrow V_4 = \mathbf{0.025 \text{ mL} = 25 \mu\text{L}}$$

$$C_5: C_3 \times V_3 = C_5 \times V_5 \Leftrightarrow V_5 = (10 \times 0.5)/1000 \Leftrightarrow V_5 = \mathbf{0.005 \text{ mL} = 5 \mu\text{L}}$$

$$C_6: C_5 \times V_5 = C_6 \times V_6 \Leftrightarrow V_6 = (1 \times 0.1)/10 \Leftrightarrow V_6 = \mathbf{0.01 \text{ mL} = 10 \mu\text{L}}$$

$$C_7: C_5 \times V_5 = C_7 \times V_7 \Leftrightarrow V_7 = (0.1 \times 0.1)/10 \Leftrightarrow V_7 = \mathbf{0.001 \text{ mL} = 1 \mu\text{L}}$$

For the first experimental phase, MMP-9 was prepared for a final concentration $C_1 = 20 \mu\text{g} \cdot \text{mL}^{-1}$.

In a second phase of the project, concentrations C_4 , C_5 , C_6 and C_7 were prepared:

- MMP-9 $2 \mu\text{g} \cdot \text{mL}^{-1}$ was added to PB-Tween 20 0.05% for a final concentration **C_4 , $100 \text{ ng} \cdot \text{mL}^{-1}$** .
- MMP-9 $1 \mu\text{g} \cdot \text{mL}^{-1}$ was added to PB-Tween 20 0.05% for a final concentration **C_5 , $10 \text{ ng} \cdot \text{mL}^{-1}$** .
- MMP-9 $10 \text{ ng} \cdot \text{mL}^{-1}$ was added to PB-Tween 20 0.05% for a final concentration **C_6 , $1 \text{ ng} \cdot \text{mL}^{-1}$** .
- MMP-9 $2 \mu\text{g} \cdot \text{mL}^{-1}$ was added to PB-Tween 20 0.05% for a final concentration **C_7 , $0.1 \text{ ng} \cdot \text{mL}^{-1}$** .

6.2.1.12. cFn (protein)

cFn was prepared in the different buffers (Tween 20 buffers) used and in different concentrations according to the requirements of the experiment. For the first experimental phase, MMP-9 was prepared for a final concentration of $20 \mu\text{g} \cdot \text{mL}^{-1}$. The calculations made for MMP-9 are also applicable to cFn, since the stock concentration is the same.

- cFn stock solution was prepared in the buffer solution (PBS-Tween 20 or PB-Tween 20) for a final concentration of $20 \mu\text{g} \cdot \text{mL}^{-1}$.
- Until use, the solution was maintained refrigerated.

6.2.1.13. BSA

BSA was used as a blocking agent for the modified substrates and for the MNPs. BSA was freshly prepared every week. For the substrates BSA 1 % was used and for MNPs was used BSA 5%. Both, were prepared in PBS or PB according to the experiment.

- The solutions were stored at $4 \text{ }^\circ\text{C}$.

6.2.1.14. Ethanolamine

Ethanolamine 100 mM was used as a blocking agent for the functionalized graphene surfaces. The concentration of ethanolamine prepared was based on reported work [47, 49, 50]. To determine the

volume of stock solution necessary, complementary calculation were made considering the molecular weight and density values [57] of ethanolamine.

- a. 242 μL of Ethanolamine stock solution were added to 30 mL of ultrapure water.
- b. The pH meter was calibrated according to the protocol for the equipment and the pH was adjusted to 7.0 with 1 M of HCl.
- c. Ultrapure water was then added to achieve 40 mL of final volume.
- d. The solution was then stored at 4 $^{\circ}\text{C}$.

6.2.1.15. Mercaptohexanol

Mercaptohexanol, MCH, was used as a blocking agent in bare gold surfaces, and was used at 20 mM.

6.2.1.16. Sulfo-LC-SPDP

Sulfo-LC-SPDP was used as the linker molecule for gold substrates. It was prepared for a final concentration of 1 $\text{mg}\cdot\text{mL}^{-1}$.

- a. 0.5 mg of Sulfo-LC-SPDP (powder) was weighted and diluted in 500 μL of PB 10 mM.
- b. The solution was stored at room temperature until used.

6.2.2. Experimental Procedures

6.2.2.1. Substrate Preparation

As said the first experimental part was made in graphene substrates, requiring a lot less time and cleanroom procedures. Single Layer Graphene was grown by chemical vapour deposition within a quartz tube in a 3-zone furnace, FirstNano EasyTube® 3000, in 99.999 % purity copper foils from Alfa Aesar, with 25 μm thickness and 25x25 mm^2 size. Methane (CH_4) was used as the carbon precursor with a flow of 50 sccm and hydrogen (H_2) was used with a flow of 300 sccm.

The deposition process began with the transfer of the copper foil (catalyst) to the reaction chamber. An initial heating of the copper was done at 1020 $^{\circ}\text{C}$ for 20 minutes in a H_2 atmosphere to clean, increase grain size and smooth the copper surface. Then the CH_4 gas flow was introduced, keeping the H_2 flow during 30 minutes, with a fixed temperature of 1020 $^{\circ}\text{C}$ and pressure of 0.5 Torr. Graphene grows on both sides of the foil. To allow the graphene transfer a temporary substrate PMMA, was used. PMMA was spin coated on the top side of the graphene/copper/graphene sample. Copper was then dissolved by immersing the sample in a solution of FeCl_3 0.5 M, for 2h. To remove any copper residues from the PMMA/graphene sample, it was cleaned in HCl 2% and deionized water, five times. Until the transfer to the Si/ SiO_2 substrate, the sample was stored in ultrapure water.

The substrate for graphene was a 200 mm Si wafer (B-doped, $8 - 30 \Omega \cdot \text{cm}^{-1}$, LG Siltron) with 200 nm of thermally oxidized SiO_2 . The wafer was pre-diced in $7 \times 7 \text{ mm}^2$ squares, i.e., the wafer was cut only until half of the wafer thickness (from the bottom) with a dicing saw, DISCO DAD 3350, allowing easy graphene transfer (larger transfer area) and posterior manual separation of the squares. After the pre-dicing the wafer was manually cut into half, as the graphene for transfer would only cover that amount. The wafer was washed in acetone and isopropanol (IPA) to remove the resist, and dried with nitrogen flow. To make the wafer surface more hydrophobic, thus enhancing the graphene adhesion, the surface was then treated with the HDMS Priming/Vapor Prime equipment. The PMMA/graphene samples were then manually transferred to the half-wafer until it was fully covered. N_2 gun was used to remove the excess water underneath the graphene films, followed by annealing at $180 \text{ }^\circ\text{C}$, for 7h, to complete the drying process. The PMMA was then removed with acetone and the quality of the transferred graphene and homogeneity was verified by optical images and confirmed by Confocal Raman Spectroscopy.

The wafer was then manually cut into the $7 \times 7 \text{ mm}^2$ squares. All of the squares were numbered sequentially (1,2, ...) in the bottom side, with identification of the graphene sample (A, B or C), using a diamond pen. Before being used in the experiments, the substrates needed were analysed in detail with optical images and Confocal Raman Spectroscopy to record the pre-functionalization state of them. The substrates were then freshly cleaned with a 2h ethyl acetate bath, followed by strong rinsing with ultrapure water and drying with N_2 gun.

6.2.2.2. Experiment 1.1

As the PBSE non-covalent interaction with graphene substrates has shown promising results for biomolecules attachment on the surface [42, 47, 49, 50], the first experiment intended exactly to confirm this evidence. Therefore, the graphene substrates were firstly modified with PBSE to allow the posterior anchoring of antibodies as the specific sensing part. The antibodies were added as spots on the substrate, with positive (specific antibodies, Anti-MMP-9) and negative (non-specific antibodies, Anti-PDGF-CC) control spots distributed on the surface, as shown in Figure 16. BSA was used to block the remaining groups of the linker and the biomarker, MMP-9, was tagged with MNPs to allow the direct visualization of the recognition process on the substrate.

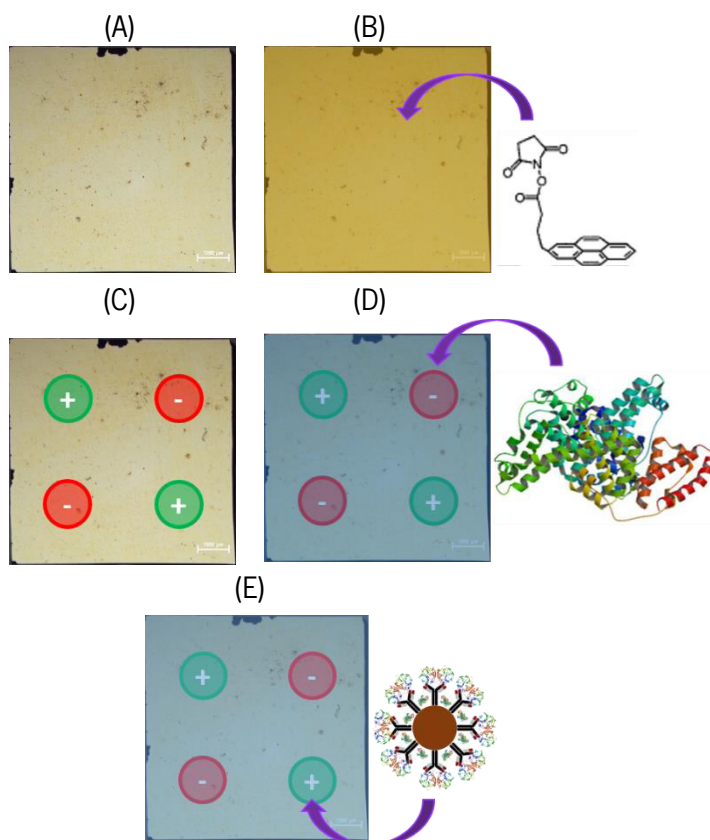


Figure 16: Schematics of the experimental steps of the functionalization/detection process used in E 1.1. (A) Optical microscopy image of a bare graphene substrate with 7x7 mm². (B) The linker, PBSE, was added to all the surface, creating a large-area interface for the biomolecules interaction. (C) Antibodies spots distribution on the modified graphene surface. The green spots correspond to the positive control, Anti-MMP-9, and the red ones correspond to the negative control, Anti-PDGF-CC. (D) The blocking with BSA was then applied over all the substrate to ensure it could reach all the free sites from PBSE. (E) The biomarker, MMP-9, was then tagged with MNPs (in brown) and added to the functionalized surface where it was expected to be detected by the specific antibodies, Anti-MMP-9.

The controls and substrates used for this experiment are shown in Table 4:

Table 4: Substrates used in the Experiment 1.1, divided by the modifications done on the graphene.

Controls	Substrates
	A7
	A9
PBSE + Antibodies + BSA + Tagged MMP-9	A59
	C3
PBSE + Antibodies	C7
PBSE	A29

Experimental Procedure

1. Surface Modification with PBSE

- a. PBSE 10mM was added to the graphene substrates, covering the whole surface;
- b. The substrates were kept in a humid atmosphere, incubating, at room temperature, for 2h;
- c. The substrates were then rinsed with DMF and ultrapure water, and dried with N₂ gun;
- d. The substrate A29 was stored in a plastic box until the measurements.

NOTES: As DMF can interact with the plastic of the micropipette tips, the addition of PBSE on the substrates always had to be quick and the tip changed for each substrate to avoid polystyrene residues in the solution. Due to the toxic and carcinogenic effects of DMF, this part of the experimental procedure was done in a fume hood.

2. Antibodies Immobilization

- a. Anti-MMP-9 at 250 $\mu\text{g}\cdot\text{mL}^{-1}$ in PBS 10 mM was spotted, as the positive control, on the substrates in 1 μL spots, according to the scheme of Figure 16(C);
- b. Anti-PDGF-CC at 250 $\mu\text{g}\cdot\text{mL}^{-1}$ in PBS 10 mM was spotted, as the negative control, on the substrates in 1 μL spots, according to the scheme of Figure 16(C);
- c. The substrates were kept in a humid atmosphere, incubating, at 4 °C, overnight;
- d. The substrates were then rinsed with PBS 10 mM;
- e. The substrate C7 was stored in a plastic box until the measurements.

3. Surface Blocking

- a. About 60 μL of BSA 1 % (in PBS 10 mM) was added to each substrate;
- b. The substrates were kept in a humid atmosphere, incubating, at room temperature, during 40 minutes;
- c. The substrates were then rinsed with PBS 10 mM.

4. Biomarker Detection

Before adding MMP-9 to the substrates, the biomarker was tagged with MNPs. To ensure all the MNPs get saturated, first with the biotinylated antibodies and then with the biomarker, some complementary theoretical calculations were made and are shown in Appendix I.

The proportion of antibodies to MNPs was kept as in the calculation (1 μL of MNPs to 30 μL of Antibodies at 50 $\mu\text{g}\cdot\text{mL}^{-1}$), but the proportion for MMP-9 was increased to ensure the saturation of the MNPs (1 μL of MNPs to 100 μL of MMP-9 at 20 $\mu\text{g}\cdot\text{mL}^{-1}$).

- a. 4.4 μL of MNPs (1 μL per substrate + 0.4 to amend for losses during the preparation process) were washed in 500 μL of PBS-Tween 20 10 mM;
- b. The eppendorf with the MNPs was placed in a magnetic concentrator (MG), to remove the wash solution. MNPs were concentrated in the wall of the eppendorf during \approx 2 minutes;
- c. The solution was discarded, and the MNPs were resuspended in 4 μL of PBS-Tween 20 10 mM;
- d. 120 μL of Biotin Anti-MMP-9 at 50 $\mu\text{g}/\text{mL}$ was added to the MNPs;
- e. The solution was left incubating for 1 h, stirring at 100 rpm;
- f. After this period, the MNPs were placed on the MG, 2 minutes, and the unbound antibodies were removed through the discarded solution;
- g. The MNPs were washed once with 120 μL of PBS-Tween 20 10 mM;
- h. 120 μL of BSA 5 % were added to the MNPs to block any remaining free sites in their surface;
- i. The solution was left incubating, 40 minutes, stirring at 100 rpm;
- j. Steps f. and g. were repeated;
- k. 400 μL of MMP-9 20 $\mu\text{g}\cdot\text{mL}^{-1}$ (in PBS-Tween 20 10 mM) were added to the modified MNPs;
- l. The solution was left incubating, 1 h, stirring at 100 rpm;
- m. Steps f. and g. were repeated;
- n. The tagged MMP-9 was resuspended in 80 μL (20 μL for 1 μL of MNPs) of PBS-Tween 20 10 mM;

MMP-9 was then ready for interaction with the functionalized substrate:

- o. 20 μL of tagged MMP-9 were added to each substrate;
- p. The substrates were left in a humid atmosphere, at room temperature, during 1h;
- q. The substrates were then rinsed with PBS-Tween 20 10 mM, PBS 10 mM and ultrapure water;
- r. The substrates were then left drying in air, i.e., each one in a separated plastic box.

5. Samples Analysis

The prepared substrates were analysed by Confocal Raman Spectroscopy and a Nikon SMZ 1500 Stereomicroscope.

6.2.2.3. Experiment 1.1 – Complementary Data

To understand the results obtained with Raman Spectroscopy (see RESULTS, Experiment 1.1), there was the need to identify which was the Raman signature of each component used on the graphene substrates. Therefore, the solutions were prepared and analysed.

Table 5: Components measured with Confocal Raman Spectroscopy. The measurements were made in liquid drop, and also on dry substrates.

Components	Measures		
	Wet	Dry	
	Si	Glass	Si
PBSE 10mM (in DMF)	✓		
PBSE (powder)			✓
Anti-MMP-9 250µg/mL (in PBS 10mM)		✓	✓
Anti-PDGF-CC 250µg/mL (in PBS 10mM)		✓	✓
BSA 1% (in PBS 10mM)		✓	✓
MMP-9 20µg/mL (in PBS-Tween 20 10mM)	✓	✓	✓
MNPs (in PBS-Tween 20 10mM, 4µL of MNPs in 120µL of buffer solution)		✓	✓
PBS 10mM			✓

The first approach was a wet measurement. For each component, a drop of solution was placed on top of a Si substrate and immediately measured. However, the heating caused by the laser was leading to drop evaporation and fast loss of focus, making the obtaining of the spectra difficult.

To solve this, glass substrates were then used, where the drop of solution was let dry at room temperature. With the dry samples it was possible to obtain the spectra, but it was verified that some of the components had peaks in the same region of glass, creating difficulties for posterior data treatment. Knowing that Si has a simpler spectrum and thus easier to filter, the dry measurements were repeated on Si substrates. The Raman signatures were then used to understand the data obtained in the Experiment 1.1.

6.2.2.4. Experiment 1.2

As some differences emerged in the Raman peaks obtained between the Experiment 1.1 and the complementary spectra of the isolated components, it was hypothesized that graphene could be the cause of such a difference (see RESULTS, Experiment 1.1). This way, the functionalization procedure was repeated on silica (SiO₂) and glass substrates to verify if the obtained peaks were organized in a more similar way with the isolated compounds spectra. The functionalization scheme used was the same shown in Figure 16.

Another hypothesis was that the MNPs could be interfering with the Raman signal, so in half of the substrates the biomarker, MMP-9, was not tagged, as shown by the scheme in Figure 17.

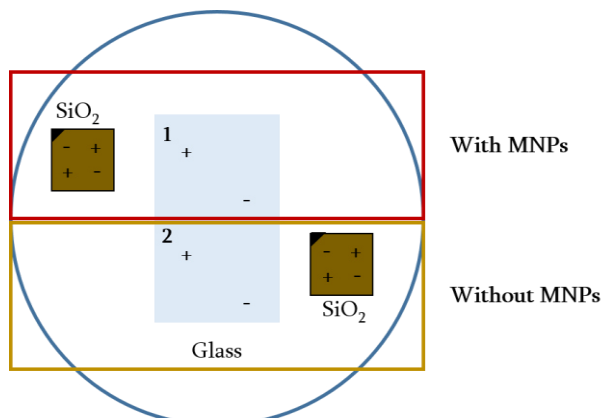


Figure 17: Functionalization scheme for Experiment 1.2. For one silica and one glass substrate, MMP-9 was tagged with MNPs. For one silica and one glass substrate, MMP-9 was not tagged. Positive (Anti-MMP-9, +) and negative (Anti-PDGF-CC, -) controls were used to confirm specific detection.

Experimental Procedure

For the steps 1 (surface modification with PBSE), 2 (antibodies immobilization) and 3 (surface blocking), of the functionalization protocol, it was used the same procedure of Experiment 1.1.

For the step 4 (biomarker detection), two different MMP-9 solutions were prepared: 1 with the nanoparticles tagging (equal to the Experiment 1.1 protocol) and 1 without any tagging (prepared according to Methods, Solutions Preparation, MMP-9 (protein)). Everything else was made according the procedure of Experiment 1.1.

The samples of Experiment 1.2 were analysed only using Confocal Raman Spectroscopy.

6.2.2.5. Experiment 1.3

As the results from Experiment 1.2 did not allow o take any conclusions about the hypothesis made, it was decided to repeat

Experiment 1.1 but without tagging MMP-9. This way it would be possible to verify if the differences in the Raman spectra were due to the MNPs or not. The controls and the samples used are listed in the Table 6.

Table 6: Substrates used in the Experiment 1.3, divided by the modifications done on the graphene.

Controls	Substrates
PBSE + Antibodies + BSA + MMP-9	A18
PBSE + Antibodies + BSA	A1
PBSE + Antibodies	A22
PBSE	C14

Experimental Procedure

For the steps 1 (surface modification with PBSE), 2 (antibodies immobilization) and 3 (surface blocking), of the functionalization protocol, it was used the same procedure of Experiment 1.1.

For the step 4 (biomarker detection), MMP-9 was prepared without MNPs tagging according to Methods, Solutions Preparation, MMP-9 (protein)). Everything else was made according the procedure of Experiment 1.1.

The samples of Experiment 1.3 were analysed only using Confocal Raman Spectroscopy.

6.2.2.6. Experiment 1.4

The Raman spectra obtained on the samples of Experiment 1.3 gave indication of possible contamination of the samples. Therefore, the experiment was repeated, this time with duplicates of each control. Some more substrates were also functionalized for the detection of cFn, since this protein is bigger and can be detected in AFM, as an alternative measurement to the Raman Spectroscopy. During the experiment doubts emerged about the stability of PBSE in solution. Therefore, a new PBSE 10 mM solution was prepared and used in 3 substrates. The controls and samples used are shown in Table 7.

Table 7: Substrates used in the Experiment 1.4, classified according to the modifications done on the graphene.

PBSE	Biomarker	Controls	Substrates
"old"	MMP-9	PBSE + Antibodies + BSA + MMP-9	A3; A12
		PBSE + Antibodies + BSA	A17; C11
		PBSE + Antibodies	A26; A24
		PBSE	A8; C1
	cFn	PBSE + Antibodies + BSA + cFn	A33
		PBSE + Antibodies + BSA	A36
PBSE + Antibodies		A5	
"new"	MMP-9	PBSE + Antibodies + BSA + MMP-9	A19
		PBSE + Antibodies + BSA	A34
		PBSE + Antibodies	C6

Experimental Procedure

For the step 1 (surface modification with PBSE), it was used the same procedure of Experiment 1.1.

In step 2 (antibodies immobilization) instead of the 4 antibodies spots scheme (used in the previous experiments) only 2 spots were made, with a bigger volume: 1 spot of the positive control antibody (Anti-MMP-9 or Anti cFn according to the sample) and 1 spot of the negative control antibody (Anti-PDGF-CC), with a 2 μ L volume for each spot.

The surface blocking step (step 3) was performed according to what is described on the procedure of Experiment 1.1.

For the step 4 (biomarker detection), MMP-9 and cFn were prepared without MNPs tagging according to Methods, Solutions Preparation, MMP-9 (protein) and cFn (protein)). Everything else was made according the procedure of Experiment 1.1.

The samples of Experiment 1.4 were analysed only using Confocal Raman Spectroscopy.

6.2.2.7. Experiment 1.5

The results from the previous experiments (see RESULTS, Experiment 1.4) showed the formation of aggregates on the samples with the complete assay. It was hypothesized that this aggregation was caused by the remaining sodium chloride salts (from the buffer) on the substrates during the drying of the samples. To verify this hypothesis, the solutions that were previously prepared with PBS buffer, were now prepared with PB buffer (does not contain sodium chloride). As all the experiments showed that the detection of MMP-9 is specific, i. e., there is no MMP-9 recognition in the negative control spot, this control was not used. From this experiment on, the control used for non-specific detection was only the blocked background of the substrates. The controls and samples used are presented in the Table 8.

Table 8: Substrates used in the Experiment 1.5, divided by the modifications done on the graphene.

Controls	Substrates
PBSE + Antibodies + BSA + MMP-9	A11
PBSE	C8
Bare graphene	A28

Experimental Procedure

For the steps 1 (surface modification with PBSE), 2 (antibodies immobilization) and 3 (surface blocking), of the functionalization protocol, it was used the same procedure of Experiment 1.1.

For the step 4 (biomarker detection), MMP-9 was prepared without MNPs tagging according to Methods, Solutions Preparation, MMP-9 (protein)). Everything else was made according the procedure of Experiment 1.1.

All the solutions that were prepared with PBS 10mM in previous experiments, were prepared with PB 100mM in Experiment 1.5.

The samples of Experiment 1.5 were analysed using Confocal Raman Spectroscopy and Optical Microscopy.

6.2.2.8. Experiment 1.6

In the Experiment 1.5, the buffer solution used had a different concentration (100 mM instead of 10 mM) from the buffer used in previous experiments. To verify if this was the causing difference in the

results obtained, in Experiment 1.6 the procedure was repeated but this time using the previous buffer, PBS, at the 100 mM concentration, and the new buffer, PB, at the correct concentration of 10 mM. The controls and samples used are presented in the Table 9.

Table 9: Substrates used in the Experiment 1.6, divided by the modifications done on the graphene.

Controls	Substrates
PBSE + Antibodies + BSA + Tagged MMP-9 (in PBS 100 mM)	B6; A50
PBSE + Antibodies + BSA + Tagged MMP-9 (in PB 10 mM)	A51; A52

Experimental Procedure

For the steps 1 (surface modification with PBSE), 2 (antibodies immobilization) and 3 (surface blocking), of the functionalization protocol, it was used the same procedure of Experiment 1.1.

For the step 4 (biomarker detection), MMP-9 was prepared without MNPs tagging according to Methods, Solutions Preparation, MMP-9 (protein)). Everything else was made according the procedure of Experiment 1.1.

All the solutions were prepared with PBS 100mM or PB 10mM according to the samples in which they were applied.

The samples of Experiment 1.6 were analysed using Confocal Raman Spectroscopy and Optical Microscopy.

6.2.2.9. Experiment 1.7

With the results of the Experiment 1.6, the hypothesis of the aggregation caused by sodium chloride was confirmed, since the use of a higher concentration of this salt caused even more evident aggregation. The experiment also showed that the use of PB (10 mM) as the buffer solution did not cause aggregation, for which reason it was chosen for all the forthcoming experiments. However, as the use of PB did not allow to obtain Raman spectra related with the specific detection of MMP-9, the MNPs tagging was again used to identify the surface antibody-antigen interaction. Also, to verify the quality of the antibodies distribution on the modified graphene surface and the quality of the blocking, the functionalization was applied in parallel to gold substrates, mimicking the surface of the most used

material in biosensing [58]. cFn detection was also applied to verify if the antibodies distribution was dependent on their specificity. The controls and samples used are presented in the Table 10.

Table 10: Substrates used in the Experiment 1.7, divided by the modifications done on the substrates.

	Controls	Substrates
Graphene	PBSE + Antibodies + BSA + Tagged MMP-9	A47
	PBSE + Antibodies + BSA + Tagged cFn	A41
Gold	Sulfo-LC-SPDP + Antibodies + BSA + Tagged MMP-9	n/a
	Sulfo-LC-SPDP + Antibodies + BSA + Tagged cFn	

For the functionalization of the gold substrates, the approach is very similar. Only the linker used is different, since the kind of interaction more stable in gold is a thiol bond between the linker and the gold [58]. This way, the linker used for gold had a thiol group to covalently bind to gold and an ester group in the other extremity, very similar to the PBSE one. The linker at use was the one already used by other groups, working on gold biosensors at INL, Sulfo-LC-SPDP.

Experimental Procedure

In the steps 1 (surface modification with PBSE), 2 (antibodies immobilization) and 3 (surface blocking), of the graphene functionalization protocol, it was used the same procedure of Experiment 1.1.

The use of gold substrates created additional steps on the protocol:

5. Gold Substrates Cleaning
 - a. Gold substrates, of 7x7 mm² were rinsed with isopropanol and ultrapure water, and dried with N₂ gun.
6. Gold Surface Modification
 - a. About 30 µL of Sulfo-LC-SPDP at 1 mg.mL⁻¹ were added to all the gold substrates;
 - b. The substrates were kept in a humid atmosphere, incubating, at room temperature, during 2h;
 - c. The gold substrates were then rinsed with PB 10 mM and ultrapure water, and dried with N₂ gun.

For the step 4 (biomarker detection), MMP-9 was prepared with MNPs tagging and applied according to the procedure of Experiment 1.1.

All the solutions were prepared with PB 10mM from this experiment on.

The samples of Experiment 1.7 were analysed using Scanning Electron Microscopy.

6.2.2.10. Experiment 1.8

The results from Experiment 1.7 showed that the blocking agent used, BSA, was not as effective in the functionalized graphene as it was in the functionalized gold. The use of ethanolamine was then proposed, since it is referred as a blocking agent for graphene and graphene-like materials, by several authors [47, 49, 50]. Therefore, the same approach used for Experiment 1.7 (gold vs. graphene) was used in this experiment. In addition, substrates without antibodies were used to test the quality of this new blocking agent. The controls and samples used are presented in the Table 11.

Table 11: Substrates used in the Experiment 1.8, divided by the modifications done on the substrates.

	Controls	Substrates
Graphene	PBSE + Antibodies + Ethanolamine + Tagged MMP-9	A48; B1
	PBSE + Ethanolamine + Tagged MMP-9	A13; A45
Gold	Sulfo-LC-SPDP + Antibodies + Ethanolamine + Tagged MMP-9	n/a
	Sulfo-LC-SPDP + Ethanolamine+ Tagged MMP-9	

Experimental Procedure

The experimental procedure applied for this experiment is equal to the procedure applied in Experiment 1.7, except for the blocking agent used, that changed from BSA (in Experiment 1.7) to Ethanolamine (in Experiment 1.8).

The samples of Experiment 1.8 were analysed using Scanning Electron Microscopy.

6.2.2.11. Experiment 1.9

Although ethanolamine showed to efficiently block graphene in Experiment 1.8, the same did not happen for gold. Due to the composition of the devices to use, the blocking of gold was desirable, so in this experiment a new approach to block gold directly (the blocking agent interacting directly with gold and not via-linker) with Mercaptohexanol (MCH). In parallel graphene substrates with different levels of modification were put in contact with the tagged MMP-9 to confirm if it is really ethanolamine that is blocking the non-specific interactions. The controls and samples used are presented in the Table 12.

Table 12: Substrates used in the Experiment 1.9, divided by the modifications done on the substrates.

	Controls	Substrates
Graphene	Bare graphene + Tagged MMP-9	A55
	PBSE + Tagged MMP-9	A25
	PBSE + Ethanolamine + Tagged MMP-9	A43
Gold	MCH + Tagged MMP-9	n/a
	MCH + Blocked MNPs	
	MCH + Bare MNPs	

Experimental Procedure

1. Gold Substrates Cleaning
 - a. A gold substrate, of $\approx 20 \times 10 \text{ mm}^2$ was rinsed with IPA and ultrapure water, and dried with N_2 gun.
2. Surface Modification
 - a. PBSE 10 mM was added to the graphene substrates referred in Table 12;
 - b. The substrates were kept in a humid atmosphere, incubating, at room temperature, for 2h;
 - c. The graphene substrates were then rinsed with DMF and ultrapure water, and dried with N_2 gun.
3. Surface Blocking
 - a. Ethanolamine 100 mM was added to the substrate referred in Table 12;
 - b. The graphene substrate was kept in a humid atmosphere, incubating, at room temperature, for 40 minutes;
 - c. MCH 20 mM was added to gold substrate, covering the whole surface;
 - d. The gold substrate was kept in a humid atmosphere, incubating, at room temperature, for 1h;
 - e. The substrates were then rinsed with PB 10mM.
4. Biomarker Detection

In this experiment, MMP-9 was tagged with MNPs, using the procedure of Experiment 1.1, but other MNPs solutions were also prepared: bare MNPs and blocked MNPs.

- a. 6 μL of MNPs were diluted in 500 μL of PB-Tween 20 10 mM;
- b. The eppendorf was then placed in the magnetic concentrator (MG) until the solution seemed clean, with the MNPs concentrated in the wall of the eppendorf (≈ 2 minutes);
- c. The solution was discarded, and the MNPs were resuspend in 6 μL of PB-Tween 20 10 mM;
- d. 1 μL of MNPs solution was diluted in 20 μL of PB-Tween 20 10 mM (Solution 1);

- e. 1 μL of MNPs solution was mixed with 100 μL of BSA 5 % and left incubating, 40 minutes, stirring at 100 rpm (Solution 2);
- f. 4 μL of the MNPs solution were added to 240 μL of Anti-MMP-9 biotinylated 50 $\mu\text{g}\cdot\text{mL}^{-1}$ and left incubating for 1h, stirring at 100 rpm (Solution 3);
- g. After this period, the MNPs solutions 2 and 3 were placed on the MG, 2 minutes, and then the solutions were discarded;
- h. The MNPs were resuspend in 20 μL of PB-Tween 20 10 mM for solution 2 and in 100 μL of PB-Tween 20 10 mM for solution 3, and step f. was repeated for the last one;
- i. 100 μL of BSA 5 % were added to the solution 3 eppendorf;
- j. The solution was left incubating, 40 minutes, stirring at 100 rpm;
- k. Steps f. and g. were repeated;
- l. 400 μL of MMP-9 20 $\mu\text{g}\cdot\text{mL}^{-1}$ (in PB-Tween 20 10 mM) were prepared;
- m. 400 μL of MMP-9 20 $\mu\text{g}\cdot\text{mL}^{-1}$ were added to the MNPs solution 3;
- n. The solution was left incubating, 1 h, stirring at 100 rpm;
- o. Steps f. and g. were repeated;
- p. The tagged MMP-9 (Solution 3) was resuspend in 80 μL of PB-Tween 20 10 mM;

The solutions were then ready for interaction with the substrates:

- q. For the gold substrate was applied a spot of 20 μL of each MNPs solution;
- r. For the graphene substrates, 20 μL of tagged MMP-9 (solution 3) was spotted in each one, covering all the surface;
- s. The substrates were left in a humid atmosphere, incubating, 1h, at room temperature;
- t. The substrates were then rinsed with PB-Tween 20 10 mM, PB 10 mM and ultrapure water;
- u. The substrates were then gently dried with N_2 gun and stored in plastic boxes until the measurements.

The samples of Experiment 1.9 were analysed using Scanning Electron Microscopy.

6.2.2.12. Device Fabrication: electrolyte-gated graphene field-effect transistors (EG-GFETs)

For the second part of the project, the fabrication of the EG-GFETs was needed. The process of fabrication was optimized for wafer-scale, allowing the fabrication of many devices in a single process [4]. Briefly, the process started with cleaning up a 200 mm Si wafer (B-doped, $8 - 30 \Omega\cdot\text{cm}^{-1}$, LG Siltron) with 200 nm of thermal SiO_2 , using ultrasonication in acetone, for 5 minutes, followed by rinsing with isopropanol and deionized water, and drying with N_2 gun. The wafer was then sputter-coated with 3 nm of

chromium, as an adhesive layer, and with 30 nm of gold. Optical lithography and ion milling were used to pattern the wafer with 47 dies, and semi-circular source and drain contacts with 75 μm of diameter (equals the channel length) and separated by a gap of 25 μm (equals the channel width). The contacts pads that connect to the external measurement equipment were also patterned in the same operations. After this, an insulating layer of aluminium oxide, 320 nm thick, was patterned by lift-off on the top on the contacts lines, leaving uncovered only the source and drain electrodes, prepared to receive the graphene.

A planar, ring-shaped gold gate, with an internal diameter of 200 μm and separated from the source and drain contacts by 50 μm , was integrated in the transistors array. A 10 nm layer of aluminium oxide was deposited on top of the integrated gate to protect it during the remaining microfabrication process.

The PMMA/graphene films produced by the methods described in the section 6.2.2.1, were manually transferred onto different areas of the patterned wafer, until the desired degree of coverage was achieved. The films were then patterned using optical lithography and oxygen plasma etching, keeping the integrated gates protected with aluminium oxide. The insulating layer of the gates was later removed with diluted photoresist developer, AZ400K 1:4, as etching agent. After all the lithographic steps the wafer was cut in equal rectangular chips by dicing, with the dicing saw DISCO DAD 3350, each containing three EG-GFETs. The chips were then washed in acetone and ethyl acetate, and were dried with N_2 before any measurements.

6.2.2.13. Experiment 2.1

After studying the functionalization and blocking process on graphene it was now possible to understand the events happening in the EG-GFETs. Therefore, the functionalization and detection process was studied in the devices by the changes in electrical characteristics obtained from the transfer curves. Firstly, the devices were measured in all the functionalization steps. Then they were measured after functionalization and exposure to different concentrations of the biomarker, MMP-9. The electrical measurements were made with bare graphene, after modification with PBSE, after antibodies anchoring, after surface blocking and after exposure to MMP-9 in the following concentrations: 0.1 ng.mL^{-1} , 1 ng.mL^{-1} , 10 ng.mL^{-1} and 100 ng.mL^{-1} . All the measures were made with the same buffer used in the functionalization, PB 10 mM.

The devices used and the modifications made to each one are shown in the Table 13.

Table 13: EG-GFETs used in the Experiment 2.1, divided by their origin (wafer and die). The green check marks mean the device went through that functionalization or detection step. The grey columns correspond to non-working devices on the dies used.

Functionalization Steps	Wafer 14						Wafer 17								
	Die 18			Die 13			Die 14			Die 21			Die 22		
	1	2	3	1	2	3	1	2	3	1	2	3	1	2	3
1. Clean	✓	✓		✓	✓			✓	✓	✓	✓	✓	✓	✓	✓
2. PBSE	✓	✓		✓	✓			✓	✓	✓	✓	✓	✓	✓	✓
3. Anti-MMP-9	✓	✓						✓	✓		✓	✓	✓	✓	
4. Ethanolamine	✓	✓		✓	✓			✓	✓	✓	✓	✓	✓	✓	✓
5. MMP-9 (ng/mL)								✓	✓		✓	✓	✓	✓	✓
								(100)	(0.1)		(10)	(1)	(100)	(0.1)	(100)

Experimental Procedure

1. EG-GFETs cleaning

Before any measure was made to the EG-GFETs, they were freshly clean to remove any contaminant from its surface.

- All the devices were immersed in ethyl acetate, for 2h;
- The EG-GFETs were then rinsed with ultrapure water and dried with N₂ gun;
- To obtain the EG-GFETs transfer curves, Keithley 2400 source-meter was used to apply the gate voltage and Keithley 4687 picoammeter was used to measure the drain-source current;
- A drop of 3 μL of PB 10 mM was used to close the circuit for each measure made;
- The transfer curves were obtained for different values of drain-source voltage (V_{SD}), ranging from 0.2 mV to 5 mV;
- The gate-source voltage (V_{GS}) ranged from 0 V to 1 V in every measure;
- After the measures, the devices were rinsed with ultrapure water and dried with N₂ gun to remove any PB residues from the surface.

2. Channel Modification with PBSE

- PBSE 10mM was added to all the devices referred on Table 13, in enough volume to cover all the channel of each EG-GFET;
- The EG-GFETs were kept in a humid atmosphere, incubating, at room temperature, for 2h;
- The EG-GFETs were then rinsed with DMF and ultrapure water, and dried with N₂ gun;

d. The measures were repeated as explained above (EG-GFETs cleaning), for all the working devices.

3. Antibodies Immobilization

- a. Anti-MMP-9 250 $\mu\text{g.mL}^{-1}$ in PB 5 % glycerol 10 mM was spotted, using a microspotter equipment, in the graphene channel of the devices referred on the Table 13;
- b. The EG-GFETs were kept in a humid atmosphere, incubating, at 4 °C, overnight or at room temperature, 2h;
- c. The EG-GFETs were then rinsed with PB 10 mM;
- d. The EG-GFETs that were measured after this step (Wafer 14, Die 18, EG-GFETs 1 and 2) were also rinsed with ultrapure water and gently dried with N₂ gun;
- e. The EG-GFETs referred on step d. were measured as explained above (EG-GFETs cleaning).

NOTE: As in the previous experiments (1.9) gold could not be successfully blocked, there was the necessity to use a microspotter to ensure that the antibodies do not react with the gold gate.

4. Surface Blocking

- a. Ethanolamine 100 mM was added to the referred devices in Table 13, in enough volume to cover all the channel of each EG-GFET;
- b. The EG-GFETs were kept in a humid atmosphere, incubating, at room temperature, for 40 minutes;
- c. The substrates were then rinsed with PB 10 mM;
- d. The EG-GFETs that were measured after this step (Wafer 14, Die 18, EG-GFETs 1 and 2; Wafer 17, Die 13, EG-GFETs 2 and 3; Wafer 17, Die 21, EG-GFET 1) were also rinsed with ultrapure water and gently dried with N₂ gun;
- e. The EG-GFETs referred on step d. were measured as explained above (EG-GFETs cleaning).

5. Biomarker Detection

In this experiment, MMP-9 was not tagged with MNPs, since only the effect of MMP-9 was at study, and not the tagging. The different concentrations prepared were added to different devices.

- a. MMP-9 100 ng.mL^{-1} (in PB-Tween 20 10 mM) was added to the following devices: W17D14GFET2, W17D22GFET1, W17D22GFET3;
- b. MMP-9 10 ng.mL^{-1} (in PB-Tween 20 10 mM) was added to the following devices: W17D21GFET2;
- c. MMP-9 1 ng.mL^{-1} (in PB-Tween 20 10 mM) was added to the following devices: W17D21GFET3;
- d. MMP-9 0.1 ng.mL^{-1} (in PB-Tween 20 10 mM) was added to the following devices: W17D14GFET3, W17D22GFET2;

- e. The EG-GFETs were left in a humid atmosphere, incubating, 1h, at room temperature;
 - f. The substrates were then rinsed with PB-Tween 20 10 mM, PB 10 mM and ultrapure water;
 - g. The EG-GFETs were then gently dried with N₂ gun;
 - h. The EG-GFETs referred on steps b., c. and d. were measured as explained above (EG-GFETs cleaning).
6. Samples Analysis

All the transfer curves obtained were further analysed and treated with the software Origin 9.0.

7. RESULTS

7.1. Experiment 1.1

As explained in section 6.2.2.2 (Experiment 1.1) this first experiment was done to confirm the data from the literature, that reported the successful bio-functionalization of graphene, using PBSE [42, 47, 49, 50]. The obtained samples were analysed with the Nikon SMZ 1500 Stereomicroscope and with the Confocal Raman system Witec Alpha 300R and the software WITec Project Plus for data acquisition. The Stereoscope images were analysed with the software Image J, to estimate the coverage density of the MNPs, and the Raman spectra were analysed with the software WITec Project FOUR+, for computing data, and Microsoft Office Excel 2016 to obtain the characteristics of the spectra (Lorentz fitting of the peaks).

For this experiment the pre-functionalization Raman analysis was not done, reason by which only after the process was concluded it was possible to know the quality and distribution of the graphene used in these samples.

The stereomicroscope images were obtained for 1 sample of each control, as representative samples, as shown in Figure 18.

The stereomicroscope results show a clear difference between the positive control spots (Specific detection) and the negative control spots, and background. Some MNPs residues are seen spread along the substrate, which are driven from the final cleaning step, that cannot remove entirely the non-bound MNPs. Therefore, specific detection is considered when the coverage density of MNPs is much bigger than in the remaining samples. In fact, when analysing the shown sample, C3, with image J, it is obtained a coverage density of 99.4 % for the positive control against 15 % coverage density for the negative control. This gives indication of successful anchoring of the antibodies, which is only possible by the use of the linker molecule, PBSE. This results show that the tagged MMP-9 is specifically recognized

by its specific antibody, Anti-MMP-9, and that it has very little interaction with the non-specific antibodies and blocked background.

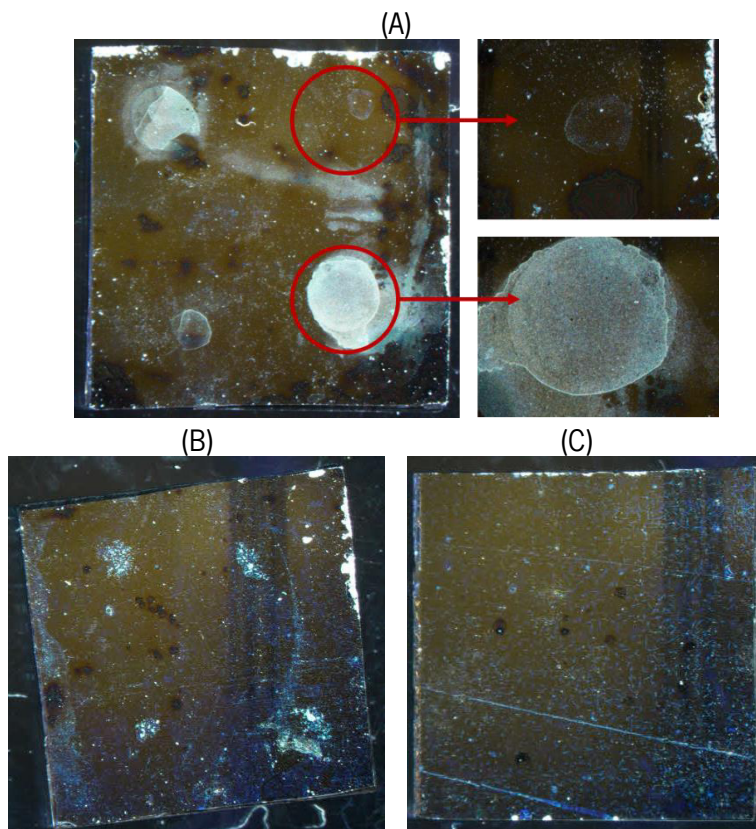


Figure 18: Stereomicroscope results. (A) Picture of the sample C3, after functionalization and MMP-9 detection, showing the difference between the negative (upper inset) and the positive (lower inset) controls. (B) Picture of the sample C7, after the functionalization done until the antibodies anchoring step. (C) Picture of the sample A29, after surface modification with PBSE.

Besides the optical results, Raman spectra were obtained to verify if the surface modification caused any change in the Raman signature of the substrates. Figure 19 shows the representative spectra obtained with the same samples of Figure 18. It is possible to see, that only in the sample where MMP-9 detection took place, there are new peaks besides the graphene ones. This gave indication that the detection of MMP-9 could also be registered by the modification in the Raman spectra of the substrates, since all off the other spectra, including the areas with no detection in the same sample (C3), present only the graphene typical peaks.

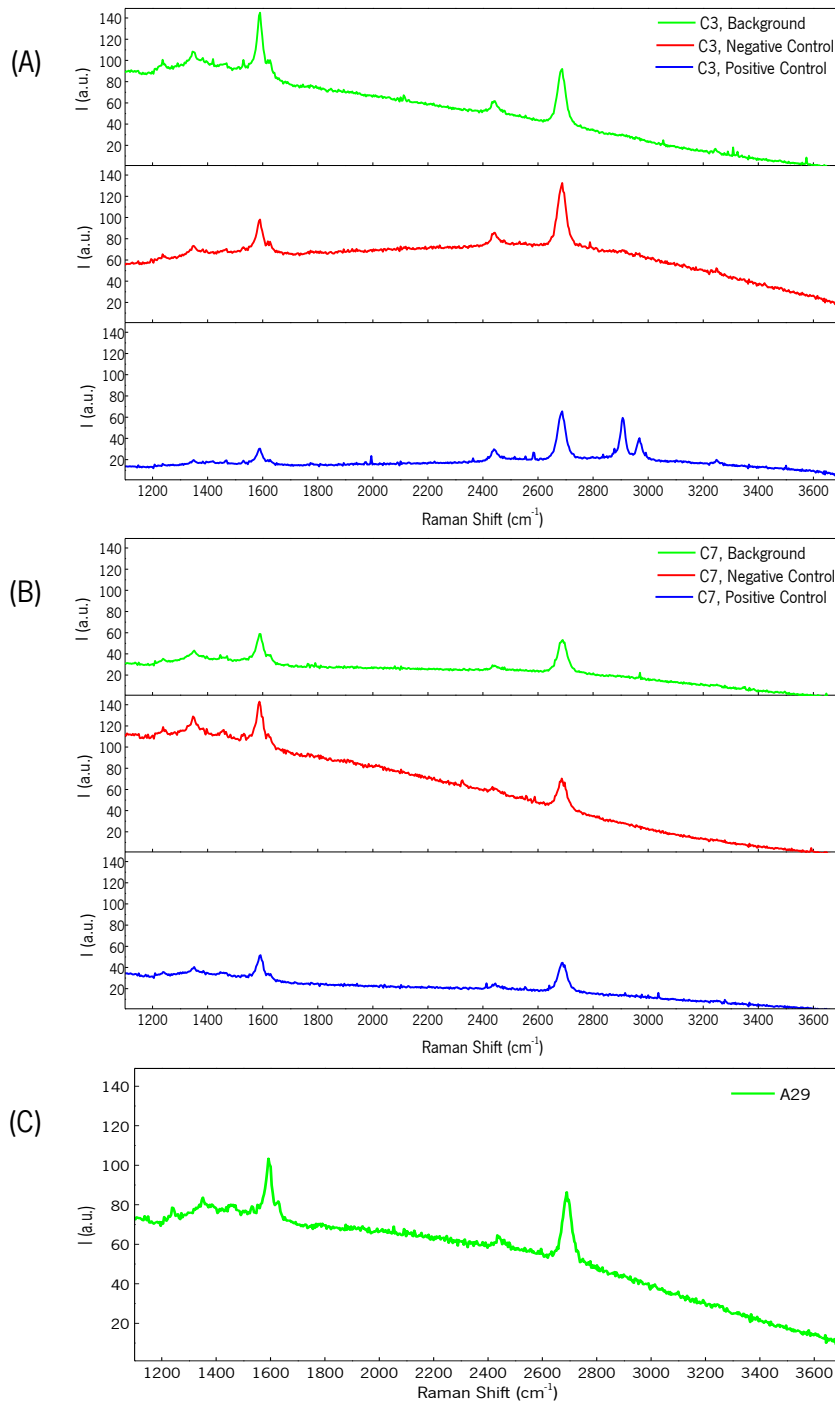


Figure 19: Raman spectra obtained in different regions of the samples from Experiment 1.1.

(A) Raman spectra of sample C3 after functionalization and MMP-9 detection, in the positive control region (blue), negative control region (red) and in the background (green). (B) Raman spectra of sample C7 after antibodies anchoring, in the positive control region (blue), negative control region (red) and in the background (green). (C) Raman spectra of sample A29 after surface modification with PBSE, in a random region. All the spectra are representative, since several spectra were obtained for the same samples in different points.

Analysing the Raman spectra, the graphene most intense vibrational modes are evident, with the G mode at $\approx 1590 \text{ cm}^{-1}$ (first order of in plane vibrational mode) and the 2D mode at $\approx 2690 \text{ cm}^{-1}$, which in a

second order of a different in plane vibrational mode, the D mode that appears at $\approx 1350 \text{ cm}^{-1}$. This D mode is an indication of defects in the graphene network and it cannot be seen in some of the spectra, being only visible in some spectra with very low intensity, indicating low density of defects. The spectra were obtained using a Nd-Yag 532 nm laser, with a 1.5 mW power, a 50x objective and an integration time of 2 s.

In the positive control, of the sample with MMP-9 detection, two new peaks appeared consistently in every sample that had specific detection spots. This peaks appear around $\approx 2908 \text{ cm}^{-1}$ and $\approx 2968 \text{ cm}^{-1}$ with FWHM (full width at half maximum) between 20 cm^{-1} and 25 cm^{-1} (values obtained by fitting the peaks with a Lorentz model, using Microsoft Office Excel).

It is important to notice, that although almost all the samples had a good coverage of graphene, one of the samples that went through functionalization and MMP-9 detection, A59, lacked graphene in one of the supposed positive control spots. Doing a Raman mapping over that region, it was verified that the peaks associated with the detection of MMP-9 were absent, since almost no graphene was present in that region. This information is indicative that the functionalization is highly specific for graphene, and that MMP-9 does not interact in an unspecific way with SiO_2 (which was exposed in this area), as shown by Figure 20.

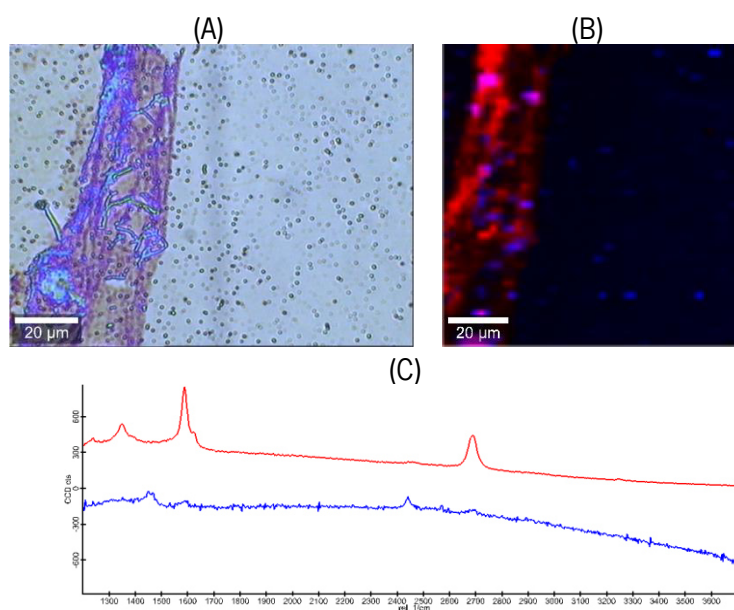


Figure 20: Positive control region of the sample A59 after functionalization and detection of MMP-9. (A) Optical image of the region where graphene is wrinkled, leaving some uncovered substrate. (B) Raman map of the region shown in (A), with red and blue pixels corresponding to the spectra shown in (C). (C) Raman spectra obtained for different points of the region (A). The pixels color in (B) is attributed according to the similarity to the spectra here presented.

To understand what was causing the appearance of the new Raman peaks on the regions of MMP-9 specific detections, samples with each of the components used on the functionalization and detection process were prepared and analysed, as explained in section 6.2.2.2 (Experiment 1.1 – Complementary Data). The measurements were initially made with the liquid solutions. However, the quick drop evaporation and the movement of air bubbles inside the drops created many difficulties in the measurements. Therefore, it was decided to repeat the measures after drying. The drops were spotted on glass and let dry in air. However, during the measurements it was concluded that the filtering of the peaks would be very difficult because many of the substances had peaks in the same region as glass. This way, the process was repeated on Si substrates, since the peaks of this material in the region of interest almost do not appear, making the processing of the signals easier. The measurements were made with the same laser and objective used for the functionalized graphene samples. Only the laser power needed to be modified, with almost all the measures done at 3 mW (except for PBS that was made at 1.5 mW). The spectra obtained are shown in Figure 21.

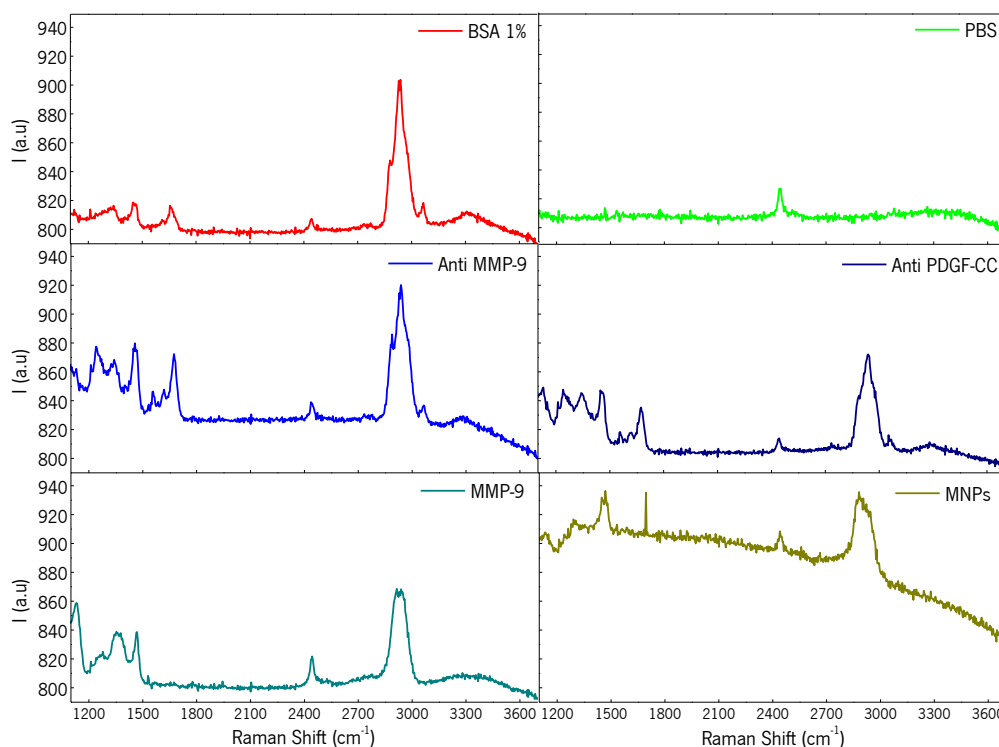


Figure 21: Raman spectra obtained for each substance used in bio-functionalization of graphene. PBS buffer, BSA (blocking agent), Anti-MMP-9 (positive control antibody), Anti-PDGF-CC (negative control antibody), MMP-9 (biomarker) and MNPs (tagging agent).

Although the data from PBSE Raman spectra is not presented, it could not be the origin of those two peaks, since it is present in all the surface (theoretically) and the peaks are specific for the detection regions.

Observing the spectra shown in Figure 21, it is possible to see that almost all the tested compounds have peaks around the region of interest (2900 to 3000 cm^{-1}), due to the rich amine composition of most of them (BSA, Anti-MMP-9, Anti-PDGF-CC and MMP-9). To be able to distinguish between the compounds, the Lorentz fitting was again used. Through this fitting with lorentzian curves it was possible to distinguish the several peaks appearing in that region for the different compounds, since the broad looking peaks that appear in the region of interest are no more than an overlap of peaks. Only after the treatment of the spectra with this method (Figure 22) it was possible to verify that the two peaks match with the Raman signature of the biomarker, MMP-9.

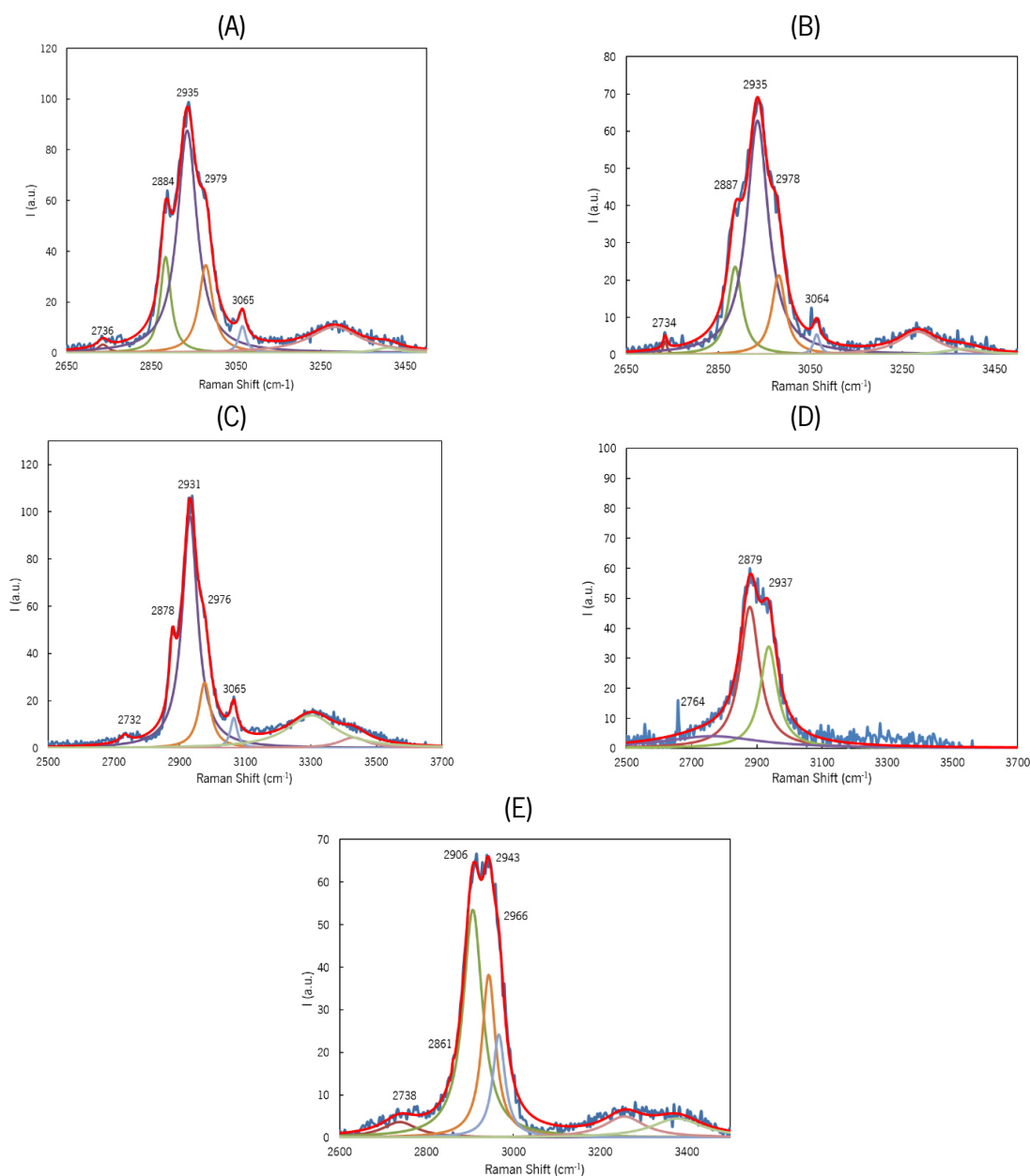


Figure 22: Lorentzian fits done to the Raman spectra of the compounds with signature in the region of interest (2900 – 3000 cm^{-1}). (A) Anti-MMP-9, (B) Anti-PDGF-CC, (C) BSA, (D) MNPs and (E) MMP-9, show the experimental spectra and the fitting obtained, with the Raman peaks signalled.

This means, that the peaks at $\approx 2908 \text{ cm}^{-1}$ and $\approx 2968 \text{ cm}^{-1}$ obtained in the regions of MMP-9 detection, can really correspond to the protein itself. However, doubts remain on the reason for the non-appearance of the $\approx 2943 \text{ cm}^{-1}$ peak on the graphene samples with MMP-9 detection. Also not understood is the different shape of the peaks, as the two peaks were very well defined and separated on the graphene substrate, but not in the protein-on-Si signature.

7.2. Experiment 1.2

To try to answer the doubts that came with the results from the first experiment, the functionalization was further tested on different substrates and the differences between tagging or no-tagging were studied. The parameters at study were those, since it was hypothesized that graphene or the use of MNPs could be the cause for the different signature of the protein. All the samples were analysed with Confocal Raman system Witec Alpha 300R and the data acquisition was made with the software WITec Project Plus, with the same laser and a 3mW power, maintaining the remaining measuring conditions. The optical images shown in Figure 23, show that the MNPs tend to stay on the surface independently from the substrate, meaning there is MNPs adsorption on the substrates, reason by which the amount of MNPs is not directly related with MMP-9 detection. This is confirmed by pictures of the samples without MNPs tagging were only some small aggregates are seen on the surface, and in a very small amount, either on the positive or negative control regions.

The Raman spectra shown in the same Figure (Figure 23), give indication that the appearance of the two distinguishable peaks is not related with graphene, since it appears for both substrates (when done in the agglomerates). Also it cannot be related with the use of MNPs tagging, since this characteristic peaks appear for both tagged (glass) and non-tagged (SiO_2) MMP-9.

This way, it was not possible to conclude what was the cause for the different peaks characteristics seen both in Experiment 1.1 and Experiment 1.2. This problem required a more profound study of the chemistry involved in the functionalization and detection processes, but as this is not the focus of the study, this doubts will remain unanswered for now.

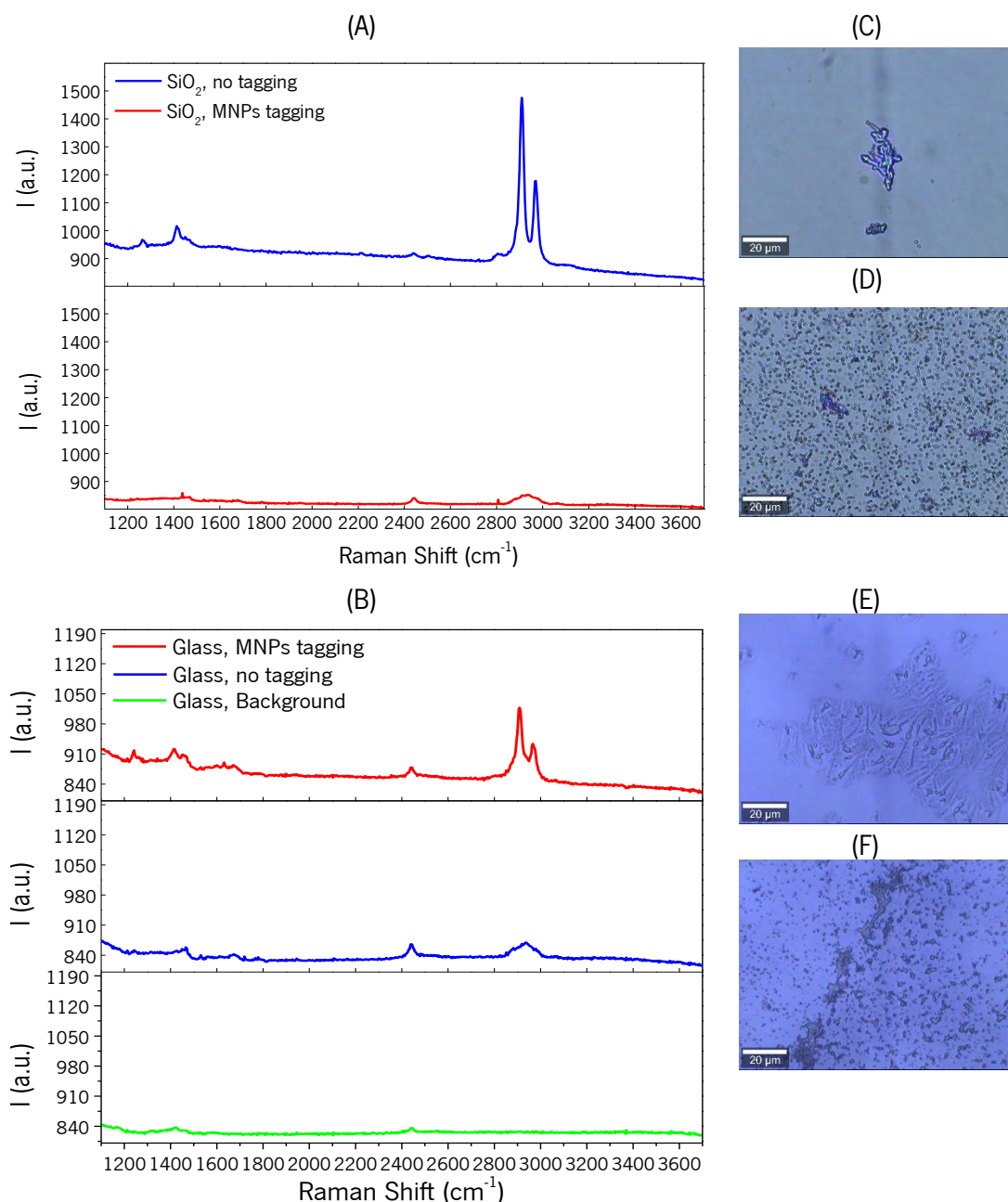


Figure 23: Optical and Raman spectroscopy results from Experiment 1.2. (A) Raman spectra on the SiO_2 substrates after functionalization and MMP-9 detection with (red) and without (blue) MMP-9 tagging with MNPs. (B) Raman spectra on the glass substrates after functionalization and MMP-9 detection with (red) and without (blue) MMP-9 tagging with MNPs, and in the background. (C) Optical image representative of the SiO_2 substrate after functionalization and MMP-9 detection without MNPs tagging. (D) Optical image representative of the SiO_2 substrate after functionalization and MMP-9 detection with MNPs tagging. (E) Optical image representative of the Glass substrate after functionalization and MMP-9 detection without MNPs tagging. (F) Optical image representative of the Glass substrate after functionalization and MMP-9 detection with MNPs tagging.

7.3. Experiment 1.3

As Experiment 1.2 could not clarify the doubts from Experiment 1.1, it was decided to repeat the functionalization in graphene, but this time without MNPs tagging. In this experiment it was used one substrate for each control (PBSE, PBSE + Antibodies, PBSE + Antibodies + BSA, and PBSE + Antibodies + BSA + MMP-9), and the samples were analysed by Confocal Raman Spectroscopy under the same conditions. The main results are shown in Figure 24. After analysing the first two samples (PBSE and PBSE + Antibodies) the results were indicative of possible contamination. In C14 sample (PBSE surface modification) the peaks previously associated with MMP-9 appeared in one region on the sample, but the signal was not stable, indicating that whatever was on the surface was being altered by the laser exposition, which did not happen in the previous experiments. In A22 sample (PBSE surface modification and Antibodies anchoring) the same peaks appeared again in the region of negative control antibodies, result that once again was unexpected since the peaks had been associated with MMP-9 and not with the antibodies.

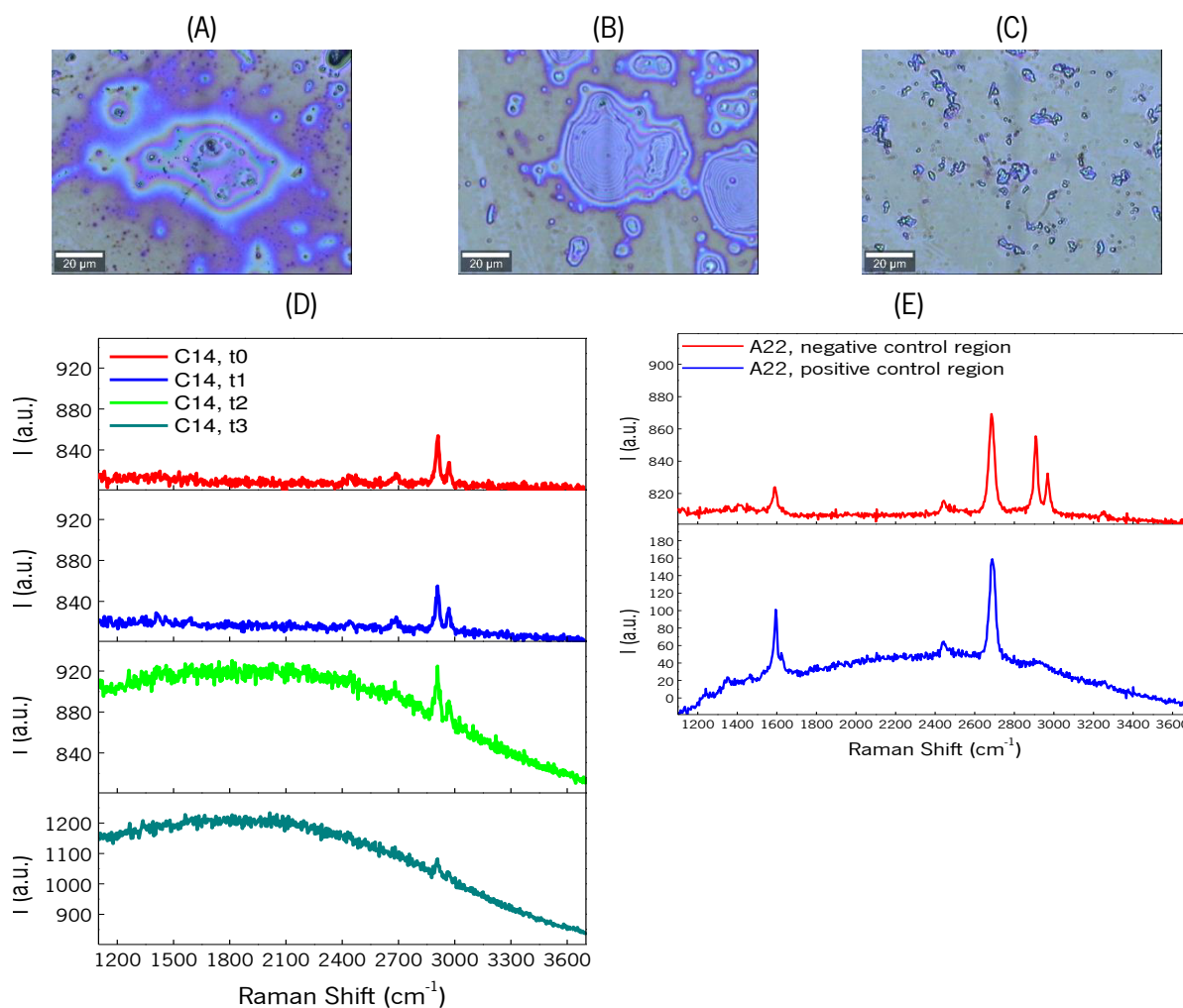


Figure 24: Optical and Raman spectroscopy results from Experiment 1.3. (A) Optical image of one region in C14 sample after PBSE surface modification. (B) Optical image of the negative control region on the sample A22 after the anchoring of antibodies. (C) Optical image of the positive control region on the sample A22 after the anchoring of antibodies. (D) Sequential Raman spectra of the sample C14, on the region shown in (A). (E) Raman spectra of the sample A22 in the negative (B) and positive (C) control regions.

Due to this unexpected results, it was hypothesized that the samples were contaminated during the experimental procedure. It was then needed decided to prepare new samples for new analysis.

7.4. Experiment 1.4

Due to the possible contaminations of the samples in Experiment 1.3, the procedure was repeated using two substrates for each control, to avoid that contaminations could affect all of the experiment. Also, the tips used in the experimental procedure were changed to filtered tips, meaning that any contaminant in the micropipettes could not affect the process anymore. Also, as the obtaining of the Raman spectra was difficult and the signal with a lot of noise (low signal-to-noise ratio), it was decided to do measurements

with AFM to try to see changes in the samples height with the addition of layers. For this end, another protein was used for detection in some samples, cFn, since it is a bigger protein and thus easier to detect with AFM.

For the samples with specific detection of MMP-9, it was observed that most of them had a very dirty appearance, as shown in Figure 25. It was also evident the branched structures on the surface of the samples, indicating the possible formation of agglomerates during the drying of the samples. This branches were even more evident for the samples with cFn, indicating that the protein could really be aggregating on the surface.

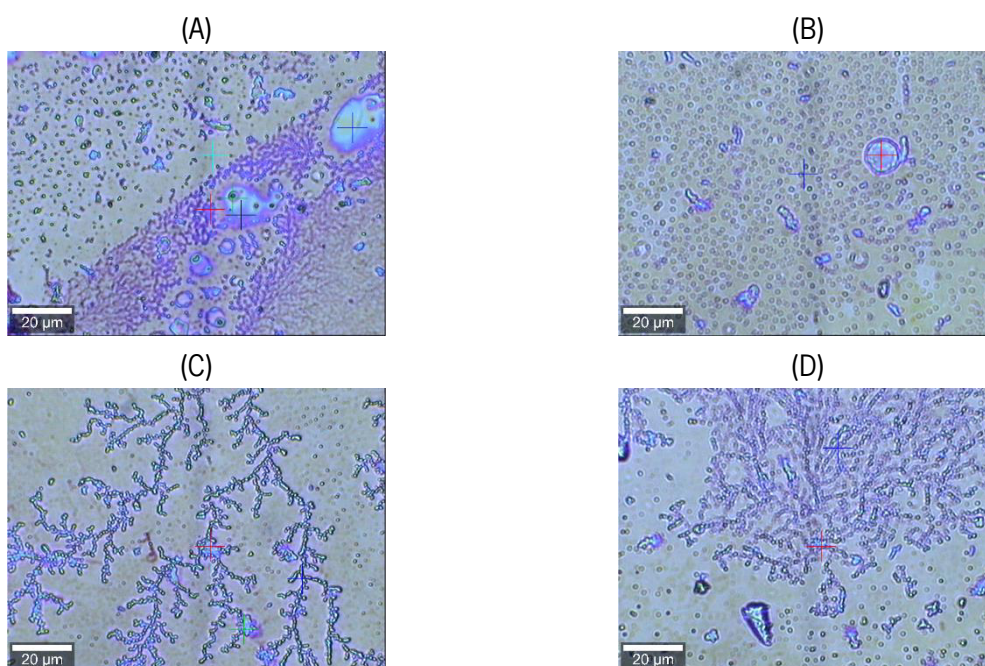


Figure 25: Optical images of the samples after functionalization and detection of MMP-9 (A and B) and cFn (C and D). The formation of branched agglomerates is visible for all the samples. (A) Sample A3, positive control region, after functionalization and detection of MMP-9. (B) Sample A3, negative control region, after functionalization and detection of MMP-9. (C) Sample A33, positive control region, after functionalization and detection of cFn. (D) Sample A33, negative control region, after functionalization and detection of cFn.

The AFM measurements are not presented, because of all the scan rates tested it was not possible to obtain trustworthy data, due to the too soft surface. Instead of insisting on this technique, in later experiments other methods were used.

With this experiment, it was hypothesized that the buffer solution, PBS, could be causing the aggregation in branches during the drying time of the samples, since some buffer residues might remain on the surface, even after the cleaning with ultrapure water.

7.5. Experiment 1.5

To test if PBS was causing the formation of the branched aggregates, graphene substrates were functionalized using a different buffer, PB. As this buffer does not contain the sodium chloride salts, it reduces the possibility of the aggregation. As explained in the section 6.2.2.7 there were used three control samples: bare graphene, graphene with PBSE surface modification, and completely functionalized sample with detection of MMP-9, without tagging. From this experiment on, the negative control antibody was no longer used, since it was already demonstrated that the biomarker does not interact un-specifically with it.

The Raman spectroscopy and optical imaging results in Figure 26, show that mainly show only the graphene signature, even on the sample A11 with the complete functionalization and MMP-9 detection, with exception for the Raman spectrum A11, measure 1 of the same Figure were the peaks are again seen. However, this Spectrum was obtained on the spot seen in picture A of Figure 26, which is not representative of the whole sample, as the second spectrum (A11, measure 2). This gives indication of a more even distribution of the protein along the sample, in monolayer, reason by which it is not detectable with Raman spectroscopy, with exception for some small regions (as shown in Figure 26, (A)). This also gives indication that the Raman peaks obtained in the previous experiments and associated with MMP-9 were only appearing due to the forming of MMP-9 + salt agglomerates, creating multilayers of protein that could be detected.

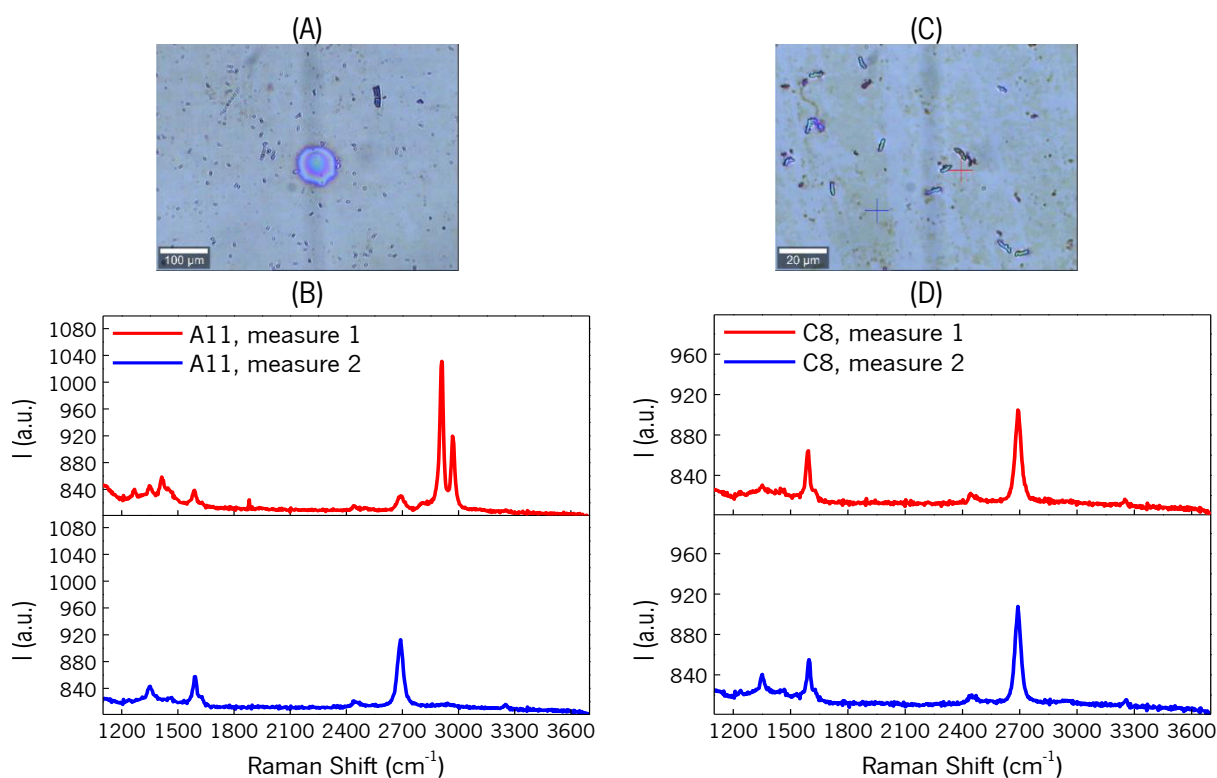


Figure 26: Optical and Raman spectroscopy results from Experiment 1.5. (A) Optical image of a region of sample A11, after functionalization and detection of MMP-9. (B) Raman spectra of two different points in the region shown in (A), inside and outside the visible spot at the center. (C) Optical image of a region of sample C8 after surface modification with PBSE. (D) Raman spectra of two different points in the region shown in (C), with the plots colours matching the plus signals on the optical image.

However, after the experiment, it was realized that the buffer concentration used did not match the concentration of PBS used on the previous experiments, since PB was at a 100mM concentration instead on 10mM.

7.6. Experiment 1.6

Since the buffer used, did not have comparable concentration to the original one, the experiment was repeated but this time using PB 10 mM in half of the samples, to compare with the original PBS concentration, and using PBS 100 mM to compare with the data from Experiment 1.5. The samples were analysed by optical microscopy using the Wide-Field Upright Fluorescence Microscope, Nikon Ni-E. The results, shown in Figure 27, demonstrate the evident agglomeration that happened in the samples treated with the buffer PBS 100 mM, and that is not visible in the samples treated with the buffer PB 10 mM (similarly to what happened with the PB 100 mM samples).

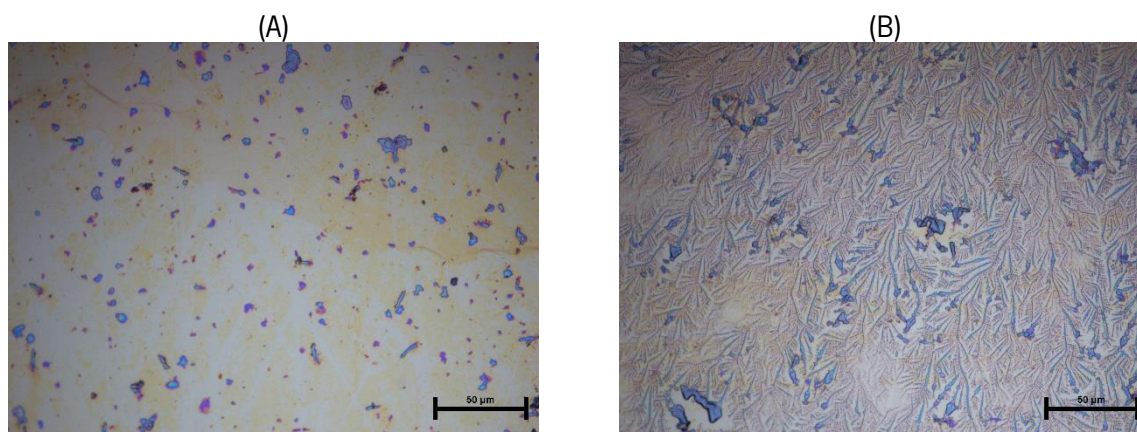


Figure 27: Optical microscopy images of the samples A50 and A52 from Experiment 1.6. (A) Optical image of sample A52 after functionalization and MMP-9 detection with PB 10mM. (B) Optical image of sample A50 after functionalization and MMP-9 detection with PBS 100 mM.

The results of this experiment proved that the effect of the branched-like agglomeration was caused by the presence of residues of sodium chloride arising from the buffer solution, PBS. Also, as it was already shown in Experiment 1.5. with the use of the PB buffer, since there is no agglomeration, Raman spectroscopy is no longer an appropriate way to analyse the samples because the single layer has no visible Raman signal.

7.7. Experiment 1.7

Since Raman could no longer be used for the samples analysis, the use of MNPs tagging became again necessary to identify the regions where the detection of MMP-9 occurs. For this experiment gold substrates were also functionalized and exposed to the tagged MMP-9, so that graphene could be compared to the most used material in biosensing applications [58]. Half of the samples (gold and graphene) were functionalized for the detection of cFn, also tagged with MNPs, to verify if the use of a different target led to a different distribution on the sample.

The samples were then analysed by scanning electron microscopy (SEM) and the software Image J was used to compare the MNPs density. After the respective image was selected, the Threshold on the image was defined by the Otsu method [62], the option 'Analyse Particles' was selected and the summary was displayed with the relative value of particles area, which gives the approximate percentage of MNPs coverage. The SEM results of detection of MMP-9 are shown in Figure 28 and the results of detection of cFn are shown in Figure 29.

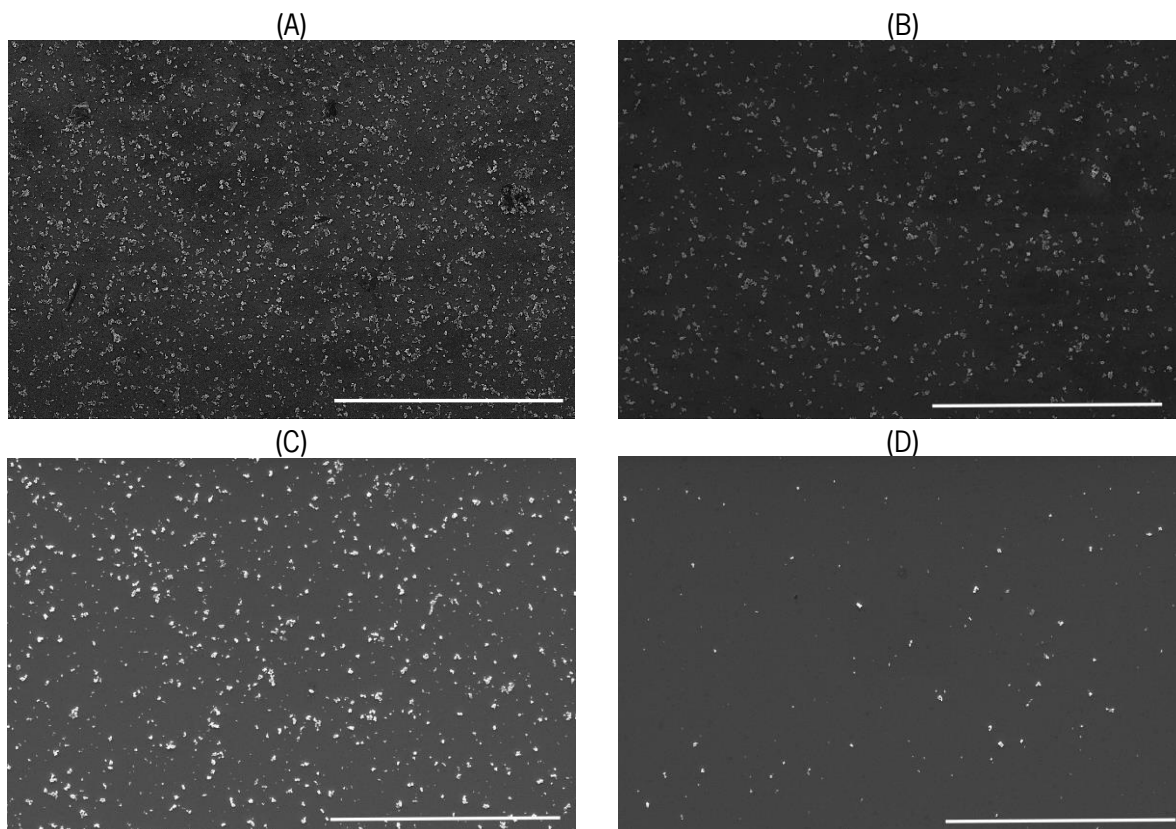


Figure 28: SEM images from samples of Experiment 1.7. (A) SEM image of specific detection region of MMP-9 in the graphene sample. (B) SEM image of the background of the MMP-9 graphene sample. (C) SEM image of specific detection region of MMP-9 in the gold sample. (D) SEM image of the background of the MMP-9 gold sample. The scale bars equal 30 μm . The acquisition was made at a working distance of ≈ 12 mm and at a HV of 5 kV for the gold samples and 15 kV for the graphene samples.

The percentage of coverage by the MNPs obtained with the processing of the samples shown in Figure 28 is presented in the Table 14.

Table 14: Summary of the results of percentage of coverage of the MNPs in the substrates. Results of the samples of the Experiment 1.7, for the specific detection region and for the background.

	Specific Detection region	Background
Graphene	10.03 %	4.499 %
Gold	3.164 %	0.2100 %

Looking at the difference between specific detection and background, both materials get a similar value (difference of ≈ 5.53 % in graphene against a difference of ≈ 2.95 % in gold), meaning that they have a similar distribution of the antibodies which leads to a similar distribution of the tagged MMP-9. However, looking at the percentage of coverage of MNPs in the graphene sample background, it is possible to see that the value is very high when compared with the gold sample background. This gives indication that the blocking agent, BSA, is not blocking the remaining free sites of PBSE effectively.

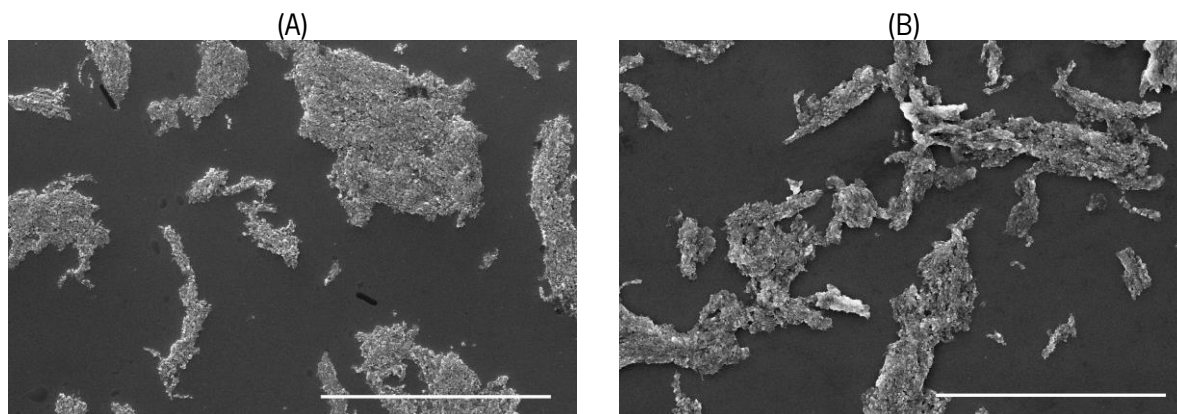


Figure 29: SEM images from samples of Experiment 1.7. (A) SEM image of specific detection region of cFn in the gold sample. (B) SEM image of specific detection region of cFn in the graphene sample. The scale bars equal 30 μm . The acquisition was made at a working distance of ≈ 12 mm and at a HV 15 kV.

The SEM images of the samples functionalized and exposed to cFn, show that the MNPs collapsed and aggregated. This was expected since during the preparation of the tagged cFn, the MNPs solution appearance changed after one of the cleaning steps, meaning that possibly the MNPs dried too much in that step and collapsed. This way, it was not possible to take any conclusions from the detection of a different protein with the same approach.

7.8. Experiment 1.8

As the results from Experiment 1.7 indicate that BSA was not effective in blocking the remaining PBSE free sites, allowing unspecific interaction of MMP-9 with the surface, it was necessary to test another blocking approach. As explained in section 6.2.2.10, Experiment 1.8, ethanolamine was tested with this end. Again, gold substrates were functionalized for comparison of graphene with a typical biosensor surface. The samples were analysed by scanning electron microscopy (SEM) and the software Image J was used to compare the MNPs density. After the respective image was selected, the threshold on the image was defined by the Otsu method [62], the option 'Analyse Particles' was selected and the summary was displayed with the relative value of particles area, which gives the approximate percentage of MNPs coverage. The SEM results of detection of MMP-9 are shown in Figure 30.

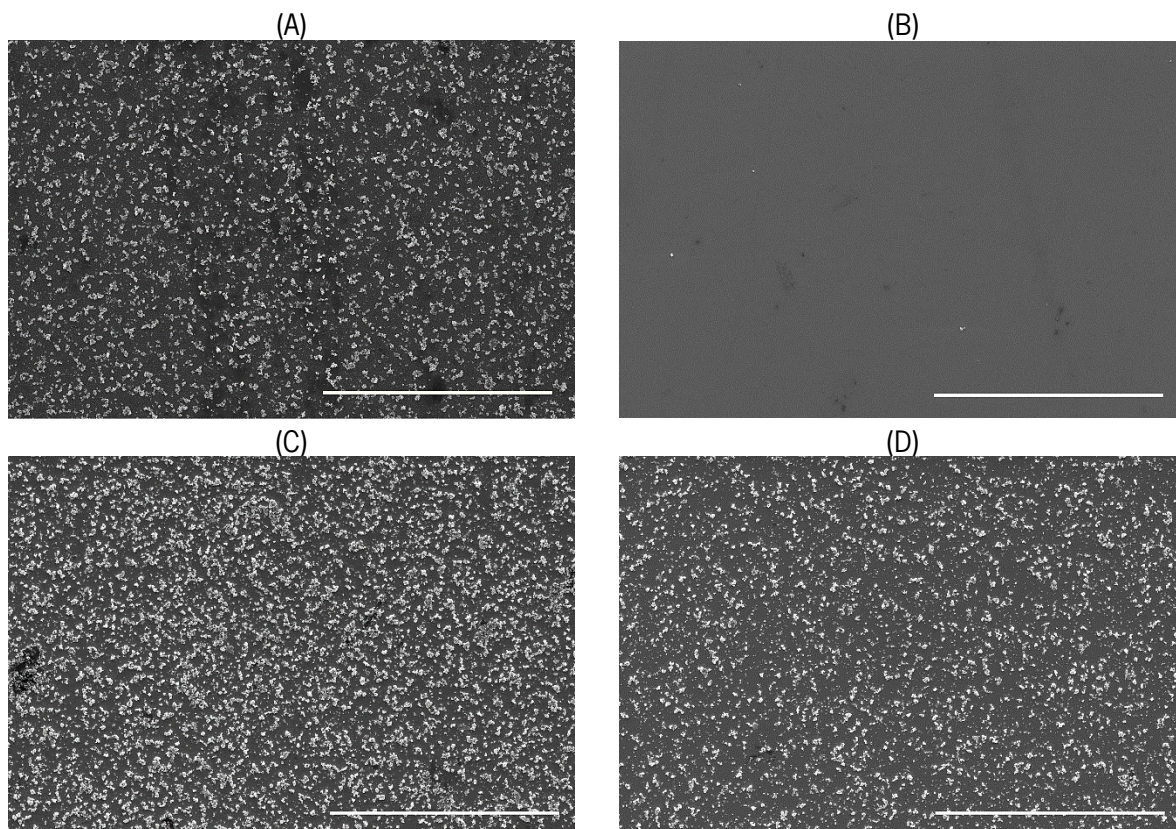


Figure 30: SEM images from samples of Experiment 1.8. (A) SEM image of specific detection region in the graphene sample. (B) SEM image of the background of the graphene sample. (C) SEM image of specific detection region in the gold sample. (D) SEM image of the background of the gold sample. The scale bars equal 30 μm . The acquisition was made at a working distance of ≈ 12 mm and at a HV of 5 kV for the gold samples and 10 kV for the graphene samples.

The percentage of coverage by the MNPs obtained with the processing of the samples shown in Figure 30 is presented in the Table 15.

Table 15: Summary of the results of percentage of coverage of the MNPs in the substrates. Results for the samples of the Experiment 1.8, for the specific detection region and for the background.

	Specific Detection region	Background
Graphene	14.80 %	0.02200 %
Gold	19.85 %	11.24 %

In comparison with the results from the Experiment 1.7, the amount of MNPs in the background of the graphene samples is very low, even lower than what was obtained in gold with the typical BSA blocking. Also the amount of MNPs in the specific detection region is quite similar to the value obtained in the last experiment (14.8 % in this experiment against 10.0 % in Experiment 1.7), showing that the graphene substrates has a very good distribution of the antibodies, creating an area where only specific detection occurs, and there is no space for unspecific reactions to take place. However, for gold it is visible in the

image of Figure 30(D) that the ethanolamine blocking was not effective, since there is a very large amount of MNPs distributed along the gold background. The area percentage of MNPs coverage in this area reaches values near the coverage obtained for specific detection in graphene, showing that the protein, MMP-9 is possibly reacting with the free remaining groups of Sulfo-LC-SPDP. To try to compare gold and graphene, the difference between the coverage percentage in the specific detection area and the background can be analysed. In graphene there is a very large difference between this two regions of the sample (even bigger than what was obtained in Experiment 1.7), with a difference of $\approx 14.8\%$. However, in gold, due to all the unspecific reactions, this difference is smaller, with a difference of $\approx 8.6\%$ between the specific detection region and the background. This is indicative that the use of the PBSE linker in graphene might promote a better distribution of the antibodies in graphene, when compared with Sulfo-LC-SPDP in gold.

Although these results are very good for the graphene functionalization process, they were unexpected for gold. A hypothesis is that ethanolamine, as it is a very small molecule when compared to BSA, can be affected by the charged group bound to the ester group of Sulfo-LC-SPDP (see Figure 31), creating difficulties in the reaction. This would not happen with PBSE, since the ester group is completely exposed (see Figure 31), which facilitates the reaction.

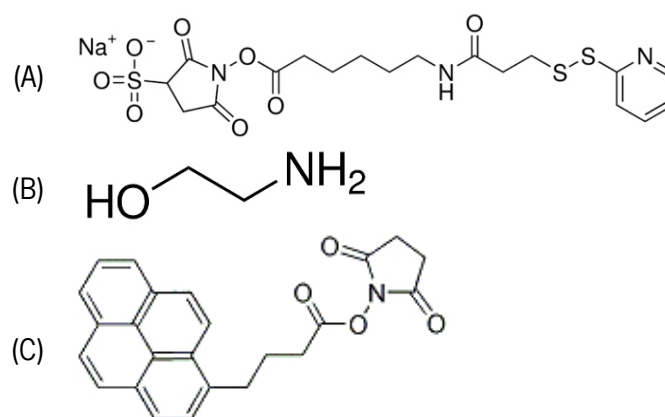


Figure 31: Linkers used for functionalization of gold (A) and graphene (C), and the blocking agent used in Experiment 1.8, ethanolamine (B). (A) Sulfo-LC-SPDP [59], bi-functional linker used for gold functionalization. The thiol group reacts with gold, creating a covalent bond and the ester group on the other end remains free for biomolecules anchoring. (B) Ethanolamine [57], the blocking agent used in this experiment. Its amine group reacts with the ester free group of the linkers, leaving the hydroxyl group free, which does not react with the proteins. (C) PBSE [60], bi-functional linker used for graphene functionalization. The pyrene group interacts in a very stable way with graphene, by a π - π interaction and the ester group on the other end remains free for biomolecules anchoring.

7.9. Experiment 1.9

As the devices to be tested have exposed gold (gate), and the material is biocompatible, there is a tendency for antibodies or protein adsorption in this region of the EG-GFETs. This way, it was necessary to explore an option to block directly any bio-adsorption on gold. Mercaptohexanol (MCH) was proposed as a blocking agent for gold, due to its use for gold blocking in electrochemistry. To test the blocking different MNPs solutions were used, at different stages of MNPs modification (bare, only blocked, with MMP-9). Besides the tests on gold blocking, graphene substrates in different functionalization steps (bare, PBSE, Ethanolamine) were exposed to the tagged MMP-9, to confirm if ethanolamine was really the blocking agent, or if PBSE or bare graphene had already no interaction with MMP-9, making the blocking unnecessary. The samples were analysed by SEM and are shown in Figure 32.

Looking at the SEM images of the gold samples, it is possible to see, that once there are biomolecules attached to the MNPs (Figure 32, B, BSA blocking on the MNPs) the blocking with MCH proves to be inefficient, since there is a large amount of MNPs on the gold samples for the case of MNPs with just BSA and for the MMP-9 tagged with MNPs (complete modification of the MNPs). This might be due to the time of incubation with MCH, that could be not enough, or due to the size of the blocking molecule (in that case, similar compounds with larger chains could be tested).

For the graphene samples, the SEM images show that the graphene is not homogeneously disperse on the surface, with lots of visible defects/borders. The existence of many borders seems to increase unspecific interactions in those regions, maybe due to the different properties of graphene on the borders that react more easily with the compounds around. This indicates that the homogeneity of the graphene sheets on the EG-GFETs is very important to avoid unspecific interactions, and therefore false results. Also, as the homogeneity of the graphene is poor in this sample, it is difficult to compare between samples, where almost all the MNPs got into the borders of graphene.

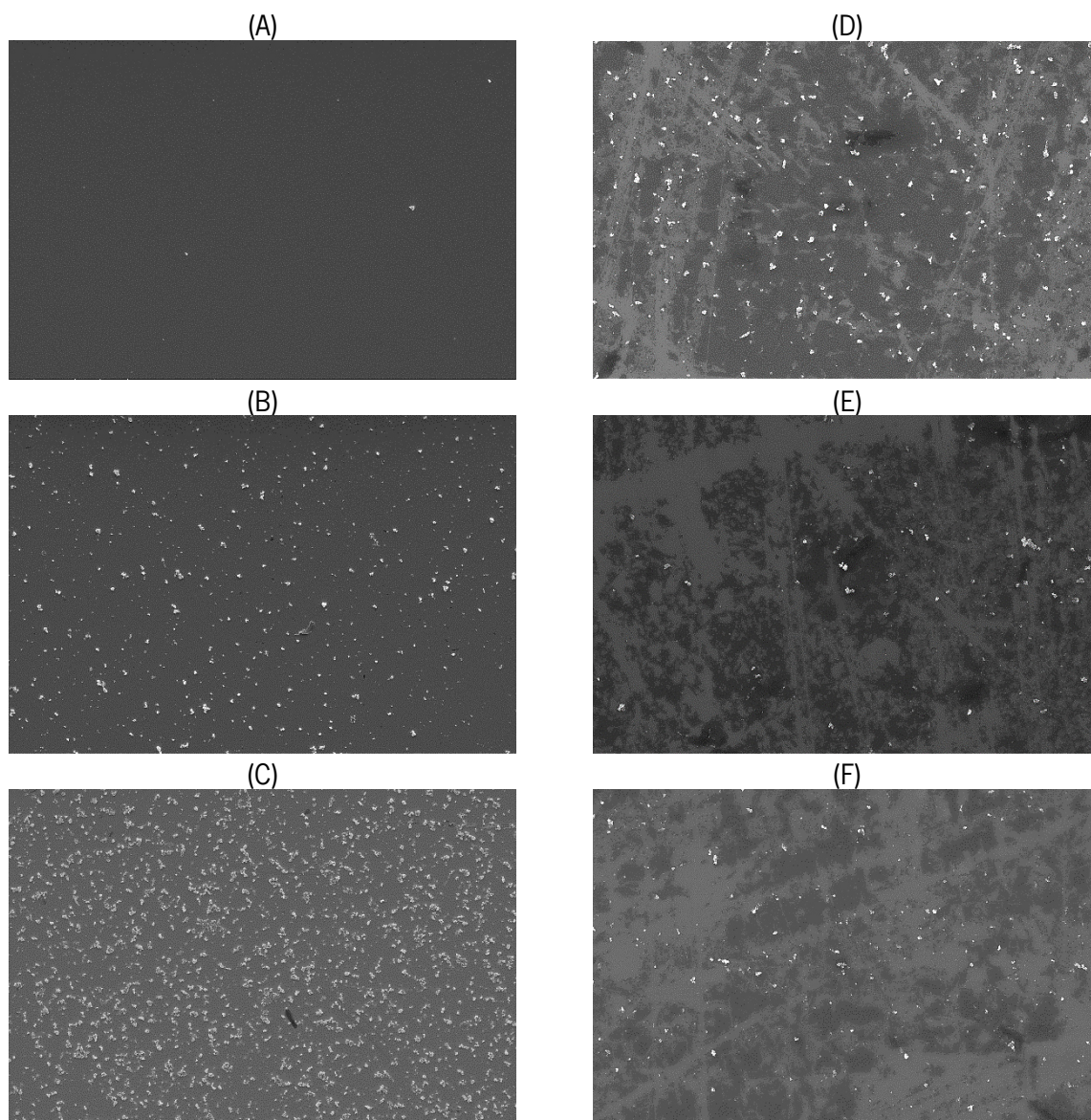


Figure 32: SEM images of the samples from Experiment 1.9. (A) Gold substrate after blocking with MCH and exposition to bare MNPs. (B) Gold substrate after blocking with MCH and exposition to MNPs blocked with BSA. (C) Gold substrate after blocking with MCH and exposition to MMP-9 tagged with MNPs. (D) Graphene substrate after exposition to MMP-9 tagged with MNPs. (E) Graphene substrate after modification with PBSE and exposition to MMP-9 tagged with MNPs. (F) Graphene substrate after modification with PBSE and ethanolamine blocking, and exposition to MMP-9 tagged with MNPs. The scale bars equal 30 μm . The acquisition was made at a working distance of ≈ 12 mm and at a HV of 5 kV for the gold samples and 15 kV for the graphene samples.

7.10. Experiment 2.1

The results from Experiment 1.9 showed that a long way was still needed to improve the approach of direct gold blocking. Therefore, to start the experiments on EG-GFETs it was decided to use a microspotter to add the antibodies to graphene, since in this way, the exposure to antibodies of the gold

gate could be avoided. Neither PBSE nor ethanolamine would, theoretically react with gold since they are not biomolecules (which tend to adsorb in gold) and do not have thiol groups to bind to gold. This way, only the antibodies anchoring needed to be done with the microspotter. However, the addition of MMP-9 to the functionalized devices could not be done with the same equipment, since the time needed to spot would be too long for the stability of MMP-9, since it has a high tendency to aggregate and its behaviour in the presence of glycerol (which needs to be used in the spotted solutions to avoid fast evaporation) was not studied.

To acquire the transfer curves, a Keithley 2400 source-meter was used to apply the gate-source voltage (voltage ramps) and Keithley 4687 picoammeter was used to apply source-drain voltage (constant) and measure the source-drain current. The transfer curves were then analysed with Origin 9.0 (organizing data, tracking Dirac point, average curves, etc.). XYZ-probes with tungsten needles were used to contact the pads of the devices.

After cleaning the devices, they were immediately measured, to obtain the devices characteristics, using PB 10 mM as the electrolytic gate dielectric. For each device, several transfer curves were obtained to allow the study of the signal stability, as shown by the plot of Figure 33. With exception for one of the devices (W14D14, EG-GFET1), all the transfer curves shown were obtained using a Source-Drain voltage of 0.8 mV, and with the Gate-source voltage ramping from 0 V to 1 V, in steps of 0.1 V. In Figure 33, it is possible to see the measuring setup, with the contacts in the gate, source and drain pads, and a drop of PB 10 mM covering the gate, which closes the GFET circuit.

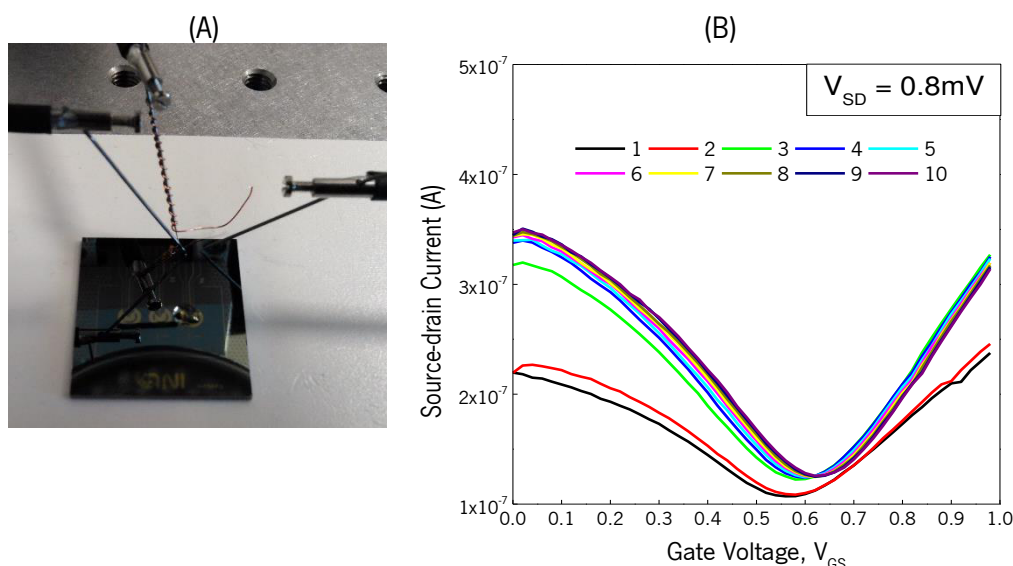


Figure 33: Measuring setup and transfer curves from clean EG-GFETs. (A) Measuring setup used for the EG-GFETs. The contacts are connected to the drain, source and gate pads, and the drop of PB 10 mM closes the circuit of the devices. (B) Transfer curves obtained of the EG-GFET W14D18GFET2, for a $V_{SD} = 0.8$ mV. Ten curves were obtained to see the stability of the EG-GFET signal.

After this first measuring phase, the devices were exposed to PBSE, to modify the graphene channel. The EG-GFETs were then measured again, with the same conditions as before, to check the difference between the bare and the modified graphene. The process was repeated after each functionalization step in two devices (W14D18GFET1 and GFET2) to study the influence of the functionalization procedure on the EG-GFETs characteristics. However, due to a software error, the data relative to the antibodies step of W14D18GFET1 was lost, reason by which only the data referent to the GFET2 is shown. As several transfer curves were taken for each device, in each measurement, the comparison was made between the averages of the transfer curves, with error bars associated to each data point, corresponding to the standard deviation. In this way, a representation of the variability of the transistor response along several gate voltage cycles is obtained. In the case of one or more of the curves showed a big difference from the bulk, it was considered an outlier and was not taken into account for the average. The averaged curves of the EG-GFET W14D18GFET2 for each functionalization step are shown in Figure 34 and the values of charge mobility are shown in the Table 16.

The transfer curves very clearly show the typical ambipolar character of transport in graphene transistors, with a hole branch to the left (lower V_{GS} values), and an electron branch to the right (higher V_{GS} values) of V_{Dirac} . The hole and electron field-effect mobility, μ_h and μ_e , respectively, were obtained from a fit of the transfer curve to a theoretical model of the channel conductivity as a function of carrier concentration that includes the effect of impurities adsorbed at the graphene surface (strong short-range potentials), according to [4].

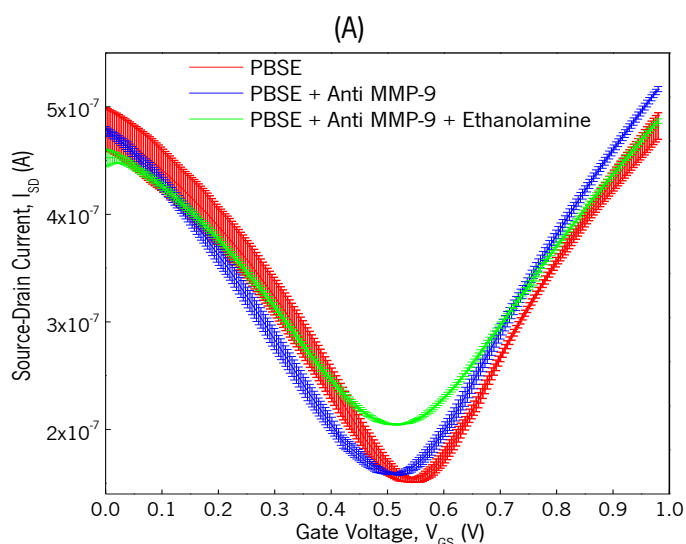


Figure 34: Averaged transfer curves after each functionalization step, with the standard deviation bars, PBSE surface modification (red), antibodies anchoring (blue) and ethanolamine blocking (green).

Table 16: Dirac point and electrical mobility of the device, W14D18GFET2 after each functionalization step. The charge mobility calculation is based on the linear region of the electron (for μ_e) and holes (for μ_h) branches of the transfer curves.

Functionalization steps	V_{Dirac} (V)	μ_h ($\text{cm}^2 \cdot \text{V}^{-1} \cdot \text{cm}^{-1}$)	μ_e ($\text{cm}^2 \cdot \text{V}^{-1} \cdot \text{cm}^{-1}$)
PBSE + Anti MMP-9 + Ethanolamine	0.52	459	519
PBSE + Anti MMP-9	0.52	511	602
PBSE	0.54	535	623

From the data shown, it is noticeable a decrease in the electron and hole mobility with the increasing amount of modifications on the graphene surface, since the hole and electron branches of the transfer curve become less steep. Still, this effect is not large enough to affect significantly the EG-GFETs performance, as the mobility achieved after all the functionalization process is still in the range of normal GFETs [18]. As there were no significant changes in the properties of the device (Dirac point shift was very small), this gave indication that if any big alteration occurred after MMP-9 exposure, it would be derived from its detection. To ensure stability of the antibodies for MMP-9 detection, the devices where MMP-9 was added were measured only until the PBSE step. The results in Figure 35 and Table 17, show the difference between the surface modification with PBSE (after that point it is not expected a significant change in the transfer curve characteristics, according to the previous results, Figure 34) and after exposition to different concentrations of MMP-9, showing an evident large shift of the minimum conductivity point (Dirac point) to lower gate voltages.

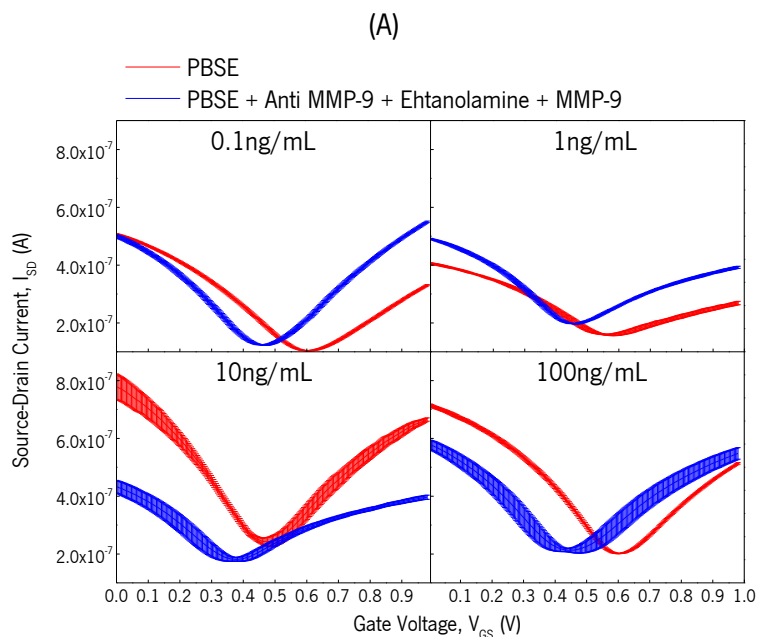


Figure 35: Comparison of the transfer curves obtained after PBSE surface modification and after MMP-9 detection, for each concentration tested. The transfer curves shown, correspond to the following devices: W17D22GFET1 for 0.1 ng.mL⁻¹, W17D21GFET3 for 1 ng.mL⁻¹, W17D21GFET2 for 10 ng.mL⁻¹ and W17D22GFET2 for 100 ng.mL⁻¹. All the transfer curves were obtained with a Source-drain voltage of 0.8 mV.

Table 17: Dirac point and electrical mobility of the averaged transfer curves shown in Figure 35. The charge mobility calculation is based on the linear region of the electron (for μ_e) and holes (for μ_h) branches of the transfer curves.

Device	Functionalization/Detection steps	V_{Dirac}	μ_h (cm ² .V ⁻¹ .cm ⁻¹)	μ_e (cm ² .V ⁻¹ .cm ⁻¹)
W17D21GFET2	PBSE	0.48	1008	751
	MMP-9 10 ng.mL ⁻¹	0.38	582	369
W17D21GFET3	PBSE	0.56	422	208
	MMP-9 1 ng.mL ⁻¹	0.46	611	339
W17D22GFET2	PBSE	0.6	881	657
	MMP-9 100 ng.mL ⁻¹	0.44	748	586
W17D22GFET1	PBSE	0.6	728	538
	MMP-9 0.1 ng.mL ⁻¹	0.46	882	821

Although it is not possible to take any clear conclusions regarding the carrier mobility data (as it increases after detection in some samples, but in others decreases), the evident shift to lower gate voltages indicates that the specific detection of MMP-9 can be electrically detected with this system. The direction of the shift is possibly explained by the isoelectric point value (pI=5.69 [61]) of MMP-9, which is

lower than the $\text{pH} = 7.2$ of PB 10 mM, the buffer used as electrolytic gate for the measurements, meaning that the protein is negatively charged during the measurements, which helps shifting up the Fermi Level of graphene, which leads to the entire transfer curve being translated to lower values of applied V_{GS} .

It is also evident that with increasing concentration, the averaged curves present increasing error, which is due to signal instability for the higher concentrations tested. This could be an effect of protein adsorption on gold, that when exposed to an electric field (during the measurements), suffers electric field assisted changes in conformation, leading to signal instability. Also, when looking at the device W17D22GFET3, which had no antibodies (only ethanolamine blocking, Appendix II), it is possible to observe the same behaviour as in other devices, leading to the indication that due to the high protein concentration, it adsorbed on the gold gate in enough amount to affect the signal in the same way of the specific detection. For the lower concentrations it is unlikely that this happens, since it would be needed a high amount of protein adsorbed on gold to cause the same effect (like on the referred device, that was exposed to MMP-9 100 ng.mL^{-1}).

8. DISCUSSION

The results from the first phase of the project allowed to understand and optimize the functionalization strategy for graphene surfaces, indicating that the material can be successfully functionalized for specific detection of MMP-9. The use of Optical Microscopy, Raman Spectroscopy and Scanning Electron Microscopy, allowed to study not only the distribution of the antibodies in the specific detection regions but also the non-specific interactions in the blocked areas (with BSA or ethanolamine).

The efficiency of non-covalent modification of graphene with PBSE, reported by several authors is confirmed here. For the specific detection different kinds of receptors have been proposed, such as aptamers and antibodies, and all of them show interaction with the linker. However, as aptamers are not available for the detection of a large range of biomarkers (only a few types of aptamers exist), the option of antibodies immobilization was chosen. Also the, monoclonal antibodies used, always show excellent specificity, as it was shown by the use of a negative control antibody in the functionalization experiments. The use of a monoclonal antibody that was specific for other protein, different from MMP-9, resulted in clean, no detection regions, showing that no interaction occurred between the biomarker at study and that antibody (Anti-PDGF-CC).

The Raman studies done on the first experiments allowed to interpret the surface chemistry, i.e, if a monolayer of the target was obtained or if the samples were forming agglomerates. Since biomolecules are

impossible to visualize in Raman it was verified that the signal associated with MMP-9 signature, only appeared in aggregated samples, where is observe some sodium chloride residues on the surface, creating salt-protein agglomerates. The study of each solution used in the functionalization strategy gave rise to new information, not readily available in scientific papers, such as the antibodies and protein signatures. Although the question of the peaks separation had not a clear answer, this technique brought a new light on surface functionalization characteristics, leading to improvements in the functionalization approach.

The blocking applied to the substrates after the antibodies immobilization intended to block any unspecific reactions of MMP-9 with remaining free ester groups of PBSE. Although BSA is a very common blocking agent, even used for graphene [48] the most referred one is ethanolamine [42, 47, 49, 50], which indeed showed to be much more effective than BSA. This might be due to BSA denaturation when reaching the graphene surface, since the material hydrophobic nature could lead to conformational changes in BSA, diminishing the protein effectiveness for blocking.

In fact, as the blocking approaches were studied both in gold and graphene, it was possible to observe that the ethanolamine blocking was more efficient on graphene than BSA was on gold (and, as a side result, that ethanolamine does not work on gold). The MNPs tagging approach was very beneficial to this phase of the project allowing to observe the response of the surface to the modifications in each step, allowing a semi-quantitative analyse of the target bound to the surface. This technique can be further used to optimize the concentrations of the linker, antibodies and ethanolamine.

In the graphene substrates, a higher concentration of MMP-9 was tested in order to saturate the surface and verify if a specific and/or unspecific detection occur. In this way, the distribution of MMP-9 would theoretically be the same as the antibodies distribution. However, for the EG-GFETs, it was intended to study the electrical signal variation with MMP-9 concentration, to reach the goal of detection (biosensing) and understand the dynamic range for this particular marker.

Each step of our functionalization strategy and its effect on the EG-GFETs characteristics showed that there were no significant changes in the devices, as it was also shown by Okamoto et al. [50]. In this way it is possible to say that the changes in the transfer curves of the devices obtained after MMP-9 exposition, are due to the recognition events. For all the devices, the same tendency was observed: after MMP-9 exposition the minimum conductivity point, Dirac point, was shifted to lower gate voltages. This shift might be explained by the effect of the isoelectric point (pI) of the protein at study, as shown by Kim et al. [49] when using a similar system to detect a cancer biomarker, using two buffer solutions: one at a pH higher (7.4) than the protein pI (6.8) and other at a pH lower (6.2) than the protein pI [49]. In that paper, Kim et al. showed that

the use of a buffer at a higher pH than the protein pI leads to a shift to lower gate voltages and the use of a buffer at a lower pH leads to a shift to higher gate voltages [49]. This effect seems to derive from the outer electric charge of the detected species, since when the solution has a pH higher than the protein pI, the protein will be negatively charged (depending on pH of the solution, the protein conformation will change, leading to changes in the exposed charged groups of the protein). In this project, the buffer solution used to prepare MMP-9 and make the electrical measures had a pH of 7.2 whereas the isoelectric point of MMP-9 is 5.69 [61], meaning that MMP-9 was negatively charged during the measurements, causing a shift to lower gate voltages, in accordance with the effect reported by Kim et al. This was also explained in section 7 of this thesis.

The results obtained with the EG-GFETs also showed that increasing the target concentration there was a poor signal stability, leading to higher standard deviations on the averaged transfer curves. Similar results were obtained when the devices were not modified with antibodies (only PBSE and blocking) for specific detection (Appendix II), but were also exposed to a high concentration of MMP-9 (100 ng.mL^{-1}), indicating that for high concentrations there might be significant adsorption of MMP-9 on the gold gate. However, this effect might not be visible for lower concentrations, as very little amount of MMP-9 can adsorb unspecifically on gold, for high concentrations the problem is noticeable. As the goal is to detect specifically in modified graphene, the gold adsorption effect needs to be blocked. In future approaches, this effect needs to be considered and limited, ensuring that only graphene provides an active detection interface. Moreover, the graphene functionalization strategy used for the EG-GFETs shows to be very promising, since the Dirac point shift mentioned is explained by interactions at the graphene interface, and not at the gold interface.

9. CONCLUSIONS

The study of graphene functionalization, allowed to understand the reactions between the functionalizing agents as well as their general distribution on CVD-graphene surfaces. It allowed also to conclude that the use of buffers containing sodium chloride can cause target aggregation, diminishing the detection efficiency as the target could not be uniformly distributed along the specific detection interface. The study of the graphene surface functionalization also allowed to conclude that ethanolamine is a much more efficient blocking agent for PBSE than BSA.

The experiments done on EG-GFETs showed that each functionalization step does not alter significantly the electrical characteristics of the devices, indicating that no defects were introduced to the graphene network during the functionalization process. Also, the electrical response of the EG-GFETs after exposition to MMP-9

indicates the detection of the specific reaction between Anti-MMP-9 and the target, since the observed shift in Dirac point can be explained by the doping caused by the negatively charged protein in graphene.

The results of this project show that functionalized EG-GFETs are very promising route for the biosensing field and are a proof-of-concept in this field. Some points are now open to explore: gold direct blocking (as mentioned during the discussion), the optimization of the concentration of PBSE, antibodies and ethanolamine, and the determination of the dynamic range of the biosensor for MMP-9. The results of this thesis, can also be used for functionalization of graphene surfaces for other specific target bio-recognition strategies.

BIBLIOGRAPHY

- [1] Pumera, M. Graphene in biosensing. *Materials Today*, 14(7-8), 308-315, 2011.
- [2] Yan F., et al. Solution-Gated Graphene Transistors for Chemical and Biological Sensors. *Advanced Healthcare Materials*, 3(3), 313-331, 2014.
- [3] Matsumoto K., et al. Recent advances in functional graphene biosensors. *Journal of Physics D: Applied Physics*, 47, 094005, 2014.
- [4] Vieira N. C. S., et al. Graphene field-effect transistor array with integrated electrolytic gates scaled to 200 mm. *Journal of Physics: Condensed Matter*, 28, 085302, 2016.
- [5] Kim J. Y., et al. Innate inflammatory responses in stroke: mechanisms and potential therapeutic targets. *Current Medicinal Chemistry*, 21(18), 2076-2097, 2014.
- [6] Jickling G. C., et al. Hemorrhagic transformation after ischemic stroke in animals and humans. *Journal of Cerebral Blood Flow & Metabolism*, 34, 185-199, 2014.
- [7] Chaturvedi, M., et al. MMP-9 Inhibition: a Therapeutic Strategy in Ischemic Stroke. *Molecular Neurobiology*, 49, 563-573, 2014.
- [8] Castellanos, M., et al. Plasma Cellular-Fibronectin Concentration Predicts Hemorrhagic Transformation After Thrombolytic Therapy in Acute Ischemic Stroke. *Stroke*, 35(7), 1671-1676, 2004.
- [9] Rodríguez-González, R., et al. Platelet derived growth factor-CC isoform is associated with hemorrhagic transformation in ischemic stroke patients treated with tissue plasminogen activator. *Atherosclerosis*, 226, 165-171, 2013.
- [10] Cinelli, P., et al. Neuroserpin, a Neuroprotective Factor in Focal Ischemic Stroke. *Molecular and Cellular Neuroscience*, 18, 443-457, 2001.
- [11] Foerch, C., et al. Elevated Serum S100B Levels Indicate a Higher Risk of Hemorrhagic Transformation After Thrombolytic Therapy in Acute Stroke. *Stroke*, 38(8), 2491-2495, 2007.
- [12] Cooper, D. R., et al. Experimental Review of Graphene. *ISRN Condensed Matter Physics*, 2012, 501686, 2012.
- [13] Zhan, B., et al. Graphene Field-Effect Transistor and Its Application for Electronic Sensing. *Small*, 10(20), 4042-4065, 2014.

- [14] Cervenka, J., et al. Graphene field effect transistor as a probe of electronic structure and charge transfer at organic molecule-graphene interfaces. *Nanoscale*, 7(4), 1471-1478, 2015.
- [15] Rao, C. N. R., et al. Graphene: The New Two-Dimensional Nanomaterial. *Angewandte Chemie International Edition*, 48, 7752-7777, 2009.
- [16] Novoselov, K. S., et al. Electric Field Effect in Atomically Thin Carbon Films. *Science*, 306, 666-669, 2004.
- [17] Geim, A. K., et al. The rise of graphene. *Nature Materials*, 6, 183-191, 2007.
- [18] Weiss, N. O., et al. Graphene: An Emerging Electronic Material. *Advanced Materials*, 24, 5782-5825, 2012.
- [19] Do, V. N., et al. Graphene and its one-dimensional patterns: from basic properties towards applications. *Advances in Natural Sciences: Nanoscience and Nanotechnology*, 1, 033001, 2010.
- [20] Garcia-Sanchez, D., et al. Imaging Mechanical Vibrations in Suspended Graphene Sheets. *Nano Letters*, 8(5), 1399-1403, 2008.
- [21] Perreault, F., et al. Environmental applications of graphene-based nanomaterials. *Royal Society of Chemistry*, 44(16), 5861-5896, 2015.
- [22] Zhan, N., et al. Layer-by-layer synthesis of large-area graphene films by thermal cracker enhanced gas source molecular beam epitaxy. *Carbon*, 49(6), 2046-2052, 2011.
- [23] Hass, J., et al. The growth and morphology of epitaxial multilayer graphene. *Journal of Physics Condensed Matter*, 20(32), 323202, 2008.
- [24] Berger, C., et al. Ultrathin epitaxial graphite: 2D electron gas properties and a route toward graphene-based nanoelectronics. *Journal of Physical Chemistry B*, 108(52), 19912-19916, 2004.
- [25] Emtsev, K. V., et al. Towards wafer-size graphene layers by atmospheric pressure graphitization of silicon carbide. *Nature Materials*, 8(3), 203-207, 2009.
- [26] Yu, Q., et al. Graphene segregated on Ni surfaces and transferred to insulators. *Applied Physics Letters*, 93(11), 3303, 2008.
- [27] Li, X., et al. Large-area synthesis of high-quality and uniform graphene films on copper foils. *Science*, 324(5932), 1312-1314, 2009.

- [28] Li, X., et al. Graphene films with large domain size by a two-step chemical vapor deposition process. *Nano Letters*, 10(11),4328– 4334, 2010.
- [29] Kosynkin, D. V., et al. Longitudinal unzipping of carbon nanotubes to form graphene nanoribbons, *Nature*, 458(7240), 872–876, 2009.
- [30] Larisika, M., et al. An improved synthesis route to graphene for molecular sensor applications. *Materials Chemistry and Physics*, 136, 304-308, 2012.
- [31] Kim, K. S., et al. Large-scale pattern growth of graphene films for stretchable transparent electrodes. *Nature*, 457, 706-710, 2009.
- [32] Bae, S., et al. Roll-to-roll production of 30-inch graphene films for transparent electrodes. *Nature Nanotechnology*, 5, 574-578, 2010.
- [33] Han, T., et al. Extremely efficient flexible organic light-emitting diodes with modified graphene anode. *Nature Photonics*, 6, 105-110, 2012.
- [34] Kim, K., et al. Ultrathin Organic Solar Cells with Graphene Doped by Ferroelectric Polarization. *ACS Applied Materials and Interfaces*, 6(5), 3299-3304, 2014.
- [35] Torrisi, F., et al. Electrifying inks with 2D materials. *Nature Nanotechnology*, 9, 738-739, 2014.
- [36] Liu, J., et al. Charging graphene for energy. *Nature Nanotechnology*, 9, 739-741, 2014.
- [37] Böhm, S., et al. Graphene against corrosion. *Nature Nanotechnology*, 9, 741-742, 2014.
- [38] Dubey, N., et al. Graphene: A Versatile Carbon-Based Material for Bone Tissue Engineering. *Stem Cells International*, 2015, 804213, 2015.
- [39] Kostarelos, K., et al. Graphene devices for life. *Nature Nanotechnology*, 9, 744-745, 2014.
- [40] Chang, H., et al. Graphene Fluorescence Resonance Energy Transfer Aptasensor for the Thrombin Detection. *Analytical Chemistry*, 82(6), 2341-2346, 2010.
- [41] He, S., et al. A Graphene Nanoprobe for Rapid, Sensitive, and Multicolor Fluorescent DNA Analysis. *Advanced Functional Materials*, 20(3), 453-459, 2010.
- [42] Viswanathan, S., et al. Graphene–protein field effect biosensors: glucose sensing. *Materials Today*, 18(9), 513-522, 2015.

- [43] Dong, X., et al. Electrical Detection of DNA Hybridization with Single-Base Specificity Using Transistors Based on CVD-Grown Graphene Sheets. *Advanced Materials*, 22, 1649-1653, 2010.
- [44] Cohen-Karni, T., et al. Graphene and Nanowire Transistors for Cellular Interfaces and Electrical Recording. *Nano Letters*, 10, 1098-1102, 2010.
- [45] Hess, L. H., et al. Graphene Transistor Arrays for Recording Action Potentials from Electrogenic Cells. *Advanced Materials*, 23, 5045-5049, 2011.
- [46] Lerner, M. B., et al. Scalable Production of Highly Sensitive Nanosensors Based on Graphene Functionalized with a Designed G Protein-Coupled Receptor. *Nano Letters*, 14, 2709-2714, 2014.
- [47] Ohno, Y., et al. Label-Free Biosensors Based on Aptamer-Modified Graphene Field-Effect Transistors. *Journal of the American Chemical Society*, 132, 18012-18013, 2010.
- [48] Mao, S., et al. Highly Sensitive Protein Sensor Based on Thermally-Reduced Graphene Oxide Field-Effect Transistor. *Nano Research*, 4(10), 921-930, 2011.
- [49] Kim, D., et al. Reduced graphene oxide field-effect transistor for label-free femtomolar protein detection. *Biosensors and Bioelectronics*, 41, 621-626, 2013.
- [50] Okamoto, S., et al. Immunosensors Based on Graphene Field-Effect Transistors Fabricated Using Antigen-Binding Fragment. *Japanese Journal of Applied Physics*, 51, 06FD08, 2012.
- [51] Stine, R., et al. Fabrication, Optimization, and Use of Graphene Field Effect Sensors. *Analytical Chemistry*, 85, 509-521, 2013.
- [52] Heller, I., et al. Identifying the Mechanism of Biosensing with Carbon Nanotube Transistors. *Nano Letters*, 8(2), 591-595, 2008.
- [53] Pandya, R. S., et al. Central Nervous System Agents for Ischemic Stroke: Neuroprotection Mechanisms. *Central Nervous System Agents in Medicinal Chemistry*, 11(2), 81-97, 2011.
- [54] Kawamura, K., et al. Effects of Angiopoietin-1 on Hemorrhagic Transformation and Cerebral Edema after Tissue Plasminogen Activator Treatment for Ischemic Stroke in Rats. *Plos One*, 9(6), 98639, 2014.
- [55] Jickling, G. C., et al. Blood Biomarkers of Ischemic Stroke. *Neurotherapeutics*, 8, 349-360, 2011.
- [56] Sabnis, R. W. Handbook of Fluorescent Dyes and Probes. 1st ed. Hoboken, New Jersey: John Wiley & Sons, Inc., 2015.

- [57] Sigma-Aldrich. Sigmaaldrichcom. Retrieved 14 July 2016, from <http://www.sigmaaldrich.com/catalog/product/sial/e9508?lang=pt>, 2016.
- [58] Prats-Alfonso E., et al. Functionalization of gold surfaces: recent developments and applications. *Journal of Materials Science*, 46, 7643-7648, 2011.
- [59] Thermo Fisher Scientific. Thermofishercom. Retrieved 14 July 2016, from <https://www.thermofisher.com/order/catalog/product/21650>, 2016.
- [60] Sigma-aldrich. Sigmaaldrichcom. Retrieved 14 July 2016, from <http://www.sigmaaldrich.com/catalog/product/sial/457078?lang=pt>, 2016.
- [61] Jaiswal, A., et al. Comparative analysis of human matrix metalloproteinases: Emerging therapeutic targets in diseases. *Bioinformatics*, 6(1), 23-30, 2011.
- [62] Liu, D., et al. Otsu method and K-means., *Ninth International Conference on Hybrid Intelligent Systems*, 1, 344 – 349, 2009.

APPENDIX I

Experiment 1.1 – Complementary Calculus, MNPs proportions

Antibodies – MNPs

- 1 MNP = 500 streptavidin molecules
- 1 Streptavidin molecule = 4 binding sites.
- Assuming each molecule has 2 binding sites available (and the remaining are bound to the MNP), then there are 1000 sites available for each MNP.
- Assuming each Antibody occupies 1 binding site, 1000 antibodies are needed for each MNP.

Knowing the stock solution of MNPs has $4,9 \times 10^8$ NPs. μL^{-1} :

Antibody	MNPs
1000	1
X	4.9×10^8

Meaning that, 4.9×10^{11} Antibodies are needed to cover all the MNPs for each μL of particles.

Considering an antibodies solution of $50 \mu\text{g}/\text{mL}$ prepared in a volume of $30 \mu\text{L}$ and that has a M.W. of 103.88 kDa (Anti-MMP-9), then the Antibodies mass will be $1.04 \mu\text{g}$ and there will be $103.88 \times 10^9 \mu\text{g} \cdot \text{mol}^{-1}$ of antibodies.

mol	μg
1	103.88×10^9
X	1.04

Meaning that there are approximately 1×10^{-11} mol of antibodies in a $50 \mu\text{g} \cdot \text{mL}^{-1}$ Anti-MMP-9 solution.

Knowing that $1 \text{ mol} = 6.022 \times 10^{23}$ entities (Avogadro constant), and that the solution of Anti-MMP-9 has $30 \mu\text{L}$, then there are 6.022×10^{12} Antibodies in solution, which largely exceeds the amount needed.

Therefore, the concentration used for the calculation can be used for the MNPs preparation.

Biomarker – MNPs

The biomarker solution must be prepared at a higher concentration than what will be captured by the MNPs so that they become saturated. Assuming a solution of MMP-9 at $20 \mu\text{g} \cdot \text{mL}^{-1}$ and a volume of $30 \mu\text{L}$, the mass of protein in solution is $0.6 \mu\text{g}$. Considering the M.W. of MMP-9, 92 kDa ($= 92 \times 10^9 \mu\text{g} \cdot \text{mol}^{-1}$), there are 6.5×10^{-12} mol of protein, which translates to 3.9×10^{12} proteins in solution.

Considering the amount of antibodies needed to cover completely 1 μL of MNPs and that 1 antibody binds to 1 protein, the amount of proteins in the 30 μL of the 20 $\mu\text{g}\cdot\text{mL}^{-1}$ solution also exceeds the saturation, as wanted.

Therefore, the concentrations at work are enough to saturate the MNPs surface. The proportion of antibodies to MNPs was kept as in the calculation (1 μL of MNPs to 30 μL of Antibodies at 50 $\mu\text{g}\cdot\text{mL}^{-1}$), but the proportion for MMP-9 was increased to ensure the saturation of the MNPs (1 μL of MNPs to 100 μL of MMP-9 at 20 $\mu\text{g}\cdot\text{mL}^{-1}$).

APPENDIX II

Experiment 2.1 – Complementary Results

1. After cleaning

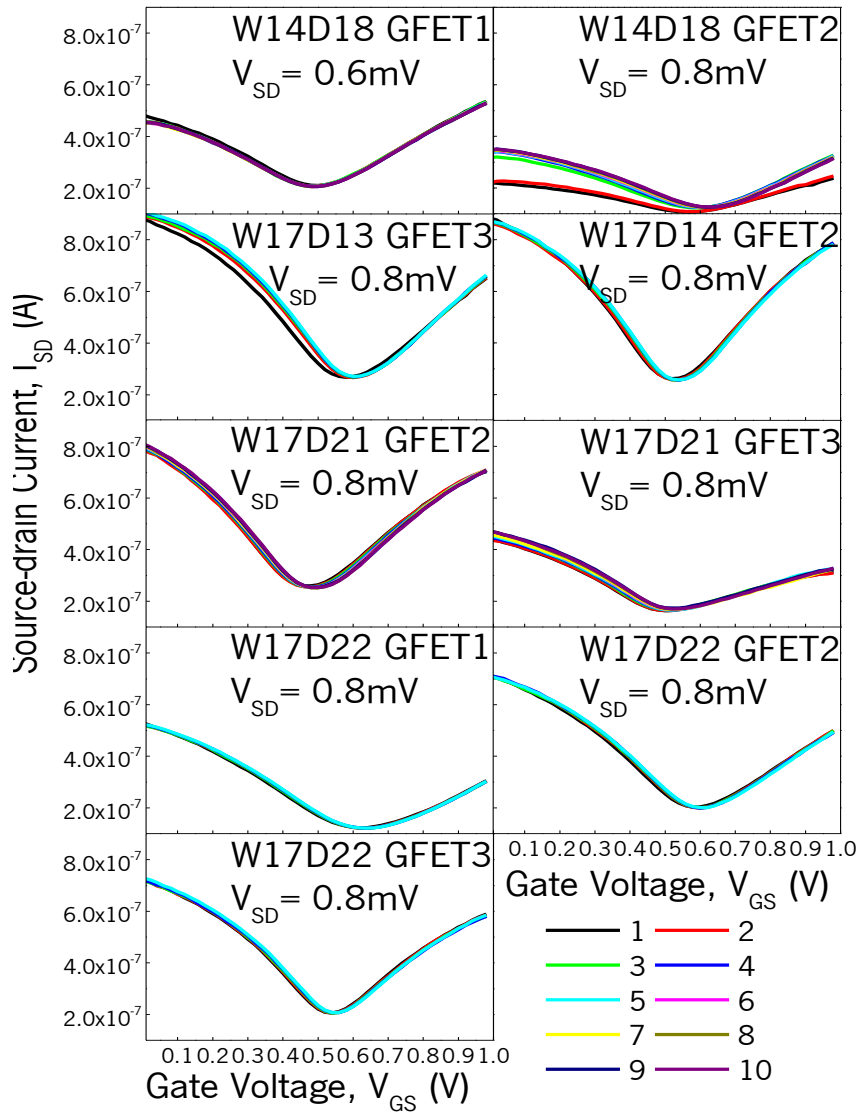


Figure 36: Transfer curves obtained for each EG-GFET after the cleaning process. Some devices are not presented, since they stopped working at some point of the modification or some data was lost (due to the software error already mentioned).

From the transfer curves obtained after cleaning it was possible to analyse the devices stability. As for each measure, five to ten transfer curves were taken for each device, the comparison between steps was only possible by making the average of the curves measured for each step.

2. After functionalization and detection

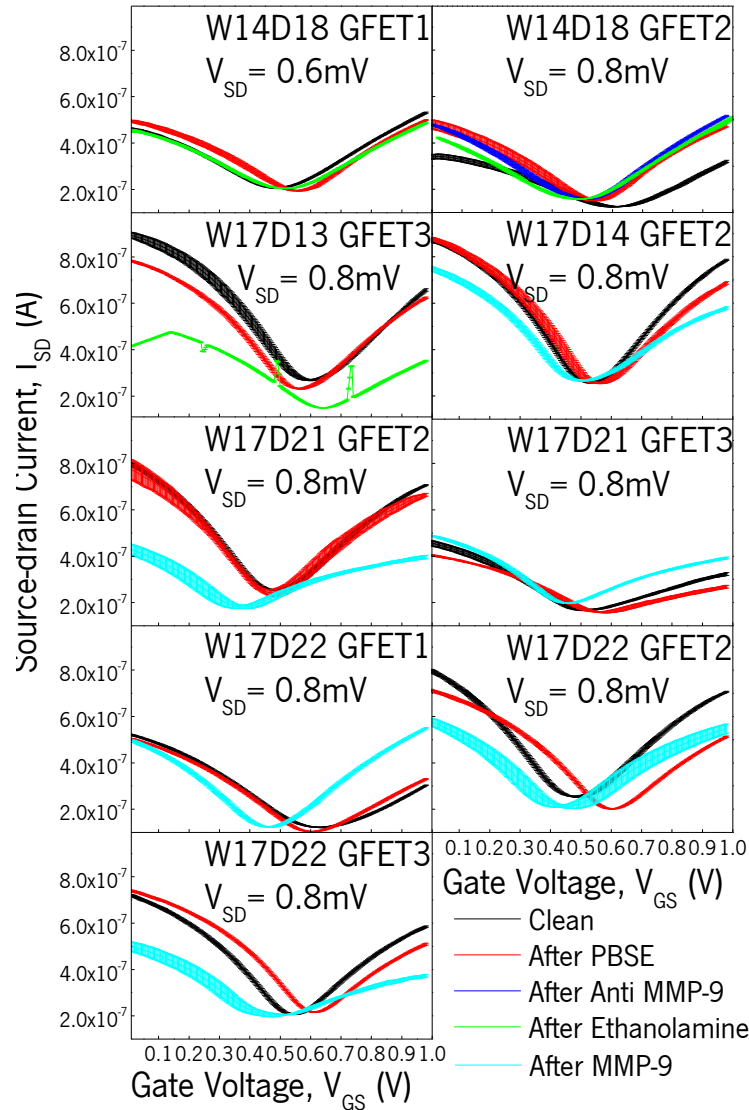


Figure 37: Transfer curves obtained for each EG-GFET after each functionalization/detection step. The EG-GFETs that were exposed to MMP-9, were measured only after cleaning, PBSE surface modification and after exposure to MMP-9. The devices were exposed to MMP-9 at different concentrations: MMP-9 0.1 ng.mL⁻¹ was used on the devices W17D14GFET2 and W17D22GFET1, MMP-9 1 ng.mL⁻¹ was used on the device W17D21GFET3, MMP-9 10 ng.mL⁻¹ was used on the device W17D21GFET2, and MMP-9 100 ng.mL⁻¹ was used on the devices W17D14GFET3 (the device stopped working during the last measuring sequence) W17D22GFET3 and W17D22GFET3 (without antibodies, unspecific detection control).